Tubuloglomerular Feedback Synchronization Occurs Across the Nephrovascular Network

by

Tayyaba Zehra

A thesis submitted in partial fulfillment of the requirements for the degree of

Master of Science

Department of Medicine
University of Alberta

Abstract

Renal autoregulation, comprised of the myogenic response (MR) and the kidney-specific tubuloglomerular feedback (TGF), maintains steady perfusion to the kidneys despite blood pressure fluctuations. The emphasis of this work is on TGF, the dynamics of which generate autonomous oscillations that synchronize extensively across the kidney. Synchronization occurs through endothelial gap junctions formed by connexin40 (Cx40) proteins which allow a nephrovascular unit (NVU), consisting of the nephron, glomerulus, afferent arteriole and efferent arteriole, to communicate electrically over long distances upstream to other NVUs via the vascular tree. Clusters of NVUs form dynamic small-world networks across the kidney, meaning that NVUs are tightly connected to each other in one cluster, but clusters are loosely interconnected to each other. Synchronization, or coupling, between NVUs spatiotemporally optimizes blood flow distribution to ensure that NVUs receive appropriate perfusion to match the energy-intensive and oxygen-dependent reabsorption of sodium.

Many patients with diabetes mellitus or hypertension have chronic kidney disease (CKD) secondary to their conditions. In Canada, recent estimates suggest that 4 million people suffer from CKD; this is associated with a health burden upwards of $40 billion per year [1]. Loss of synchronization impairs autoregulation and is implicated in the progression of kidney disease, but synchronization has not been studied in pathophysiological models. We hypothesized that improving synchronization may preserve renal function by improving network behavior.

To advance our understanding of the nephrovascular network's role in physiology with clinical relevance, we explored the impact of manipulating TGF signaling on synchronization in our first aim. In healthy male Lewis rats (n = 6), we inhibited the sensor component of the TGF to study synchronization and network behavior using acute administration of the loop diuretic

furosemide. The sodium glucose cotransporter-2 (SGLT2) inhibitor dapagliflozin was acutely administered in healthy rats (n = 6) to enhance TGF signaling by increasing sodium chloride delivery to the macula densa cells in the distal tubule.

In the second aim, we tested the impact of renal disease on TGF synchronization and network behavior using the remnant kidney model of experimental CKD to gain greater insight into the nephrovascular network's role in pathophysiology. Male Lewis rats were subjected to $5/6^{th}$ nephrectomy or sham-operations and were assessed after 1 week (n = 4) or 6 weeks (n = 6) (n = 7, 1 week shams; n = 7, 6 week shams).

Our third aim was to determine whether the SGLT2 inhibitor dapagliflozin would enhance synchronization in the pathophysiological context of experimental CKD. We used male Lewis rats that were subjected to $5/6^{th}$ nephrectomy to create a remnant kidney for 6 weeks (n = 6) or sham operations (n = 6). After 6 weeks had elapsed, animals were acutely administered dapagliflozin.

In all three aims, laser speckle contrast imaging (LSCI) was used to assess renal cortical perfusion and determine the strength and variability in the synchronization of TGF and MR, the decay in TGF synchronization over distance, and the spatiotemporal heterogeneity of cortical perfusion.

Our results demonstrate furosemide induced a rapid decay in TGF synchronization over long distances, whereas dapagliflozin improved entrainment of regions across the renal surface in intact rats. Disruption of the nephrovascular network in the remnant kidney at 1 week enhanced MR synchronization, and at 6 weeks TGF synchronization and the maximum distance over which synchronization occurs was diminished. Breaking the network impaired the communication pathway necessary for TGF signals to travel because the remnant kidney at both

1 and 6 weeks induced a rapid decay in the spread of the TGF signal, reduced synchronization amongst kidney regions and induced heterogeneity in cortical perfusion. Intervention with dapagliflozin improved the strength of TGF synchronization and reduced the magnitude of its decay with distance, suggesting these changes may underlie SGLT2 inhibition's renoprotective effects. These findings suggest that TGF is best regarded as a distributed network process that regulates the microcirculation by synchronized adjustments in vascular resistance amongst communicating NVUs so that all elements in the network effectively respond to blood pressure perturbations. The implications of these findings includes a greater understanding of nephrovascular network regulation that can be enhanced by intervention to restore coordinated vascular responses among NVUs with better oxygenation/perfusion matching and prevention of renal injury as a consequence.

Preface

This thesis is an original work by Tayyaba Zehra. The research project, of which this thesis is a part, received research ethics approval from the University of Alberta Research Ethics Board, project title 'Renal venous pressure, renal function and experimental heart failure.' NO: AUP 00000836, Date: Oct. 20, 2014 to present.

The research conducted for this thesis was done with the assistance of Dr. Shereen Hamza, who provided technical support for the experiments. Dr. Heather More created the data analysis codes, mentioned in chapter 3, that were used to analyze and interpret the data and also provided extensive trouble-shooting assistance with analysis. Wenqing Zhuang contributed to analytical methodology development mentioned in chapter 3. Dr. Branko Braam and Dr. William A. Cupples were the supervisory authors and were involved with concept formation and manuscript revision. I was responsible for data collection, analysis and manuscript composition.

The literature review in chapter 2 has been submitted for publication as 'Tayyaba Zehra, Branko Braam, William A. Cupples. Tubuloglomerular Feedback Synchronization in Nephrovascular Networks" to the *Journal of the American Society of Nephrology* on April 8th, 2020. The work presented in this thesis in chapters 1, 3, 4 and 5 will be submitted for publication.

All chapters 1 through 5 of this thesis are my original work.

Acknowledgements

I would like to express my most sincere gratitude to my supervisors and mentors, Dr. Branko Braam and Dr. William A. Cupples, for their endless encouragement, guidance and friendship.

I would like to acknowledge Dr. Shereen Hamza and Dr. Xiaohua Huang for their tremendous expertise and for their patience in passing on their expert abilities and knowledge to me, without which I could not carry out this work. I am extremely grateful to Dr. Heather More for her incredible coding ability and for going above and beyond to help every step of the way, and to Wenqing Zhuang for her untiring help and expert skills.

Thanks to the members of my supervisory committee, Dr. Scott Thomson, Dr. Barbara Ballermann, Dr. William A. Cupples and Dr. Branko Braam, for their invaluable insights and support.

Finally, I am grateful to the Department of Medicine, University of Alberta, for the opportunity to pursue my graduate studies. The Division of Nephrology in the Faculty of Medicine and Dentistry supported Dr. Braam's Kidney Health Translational Research Chair which made this study possible.

Table of Contents

List of Tables

List of Figures

List of Symbols, Nomenclature and Abbreviations

A	magnitude of decay of synchronization
AKI	acute kidney injury
ANG II	angiotensin II
ASL	arterial spin labelling
ATPase	adenosine triphosphatase
BOLD	blood oxygen level dependent
BSA	bovine serum albumin
CBX	carbenoxolone
CKD	chronic kidney disease
Cx	connexin
CRA	cortical radial artery
$CV_{f,MR}$	coefficient of spatial variation of dominant MR frequency
$CV_{f,TGF(S)}$	coefficient of variation of dominant TGF frequency from spatial speckle
$CV_{f,TGF(T)}$	coefficient of variation of dominant TGF frequency from temporal speckle
$CV_{PC,MR}$	coefficient of variation of PC in MR frequency band
$CV_{PC,TGF(S)}$	coefficient of variation of PC in TGF frequency band from spatial speckle
$CV_{PC,TGF(T)}$	coefficient of variation of PC in TGF frequency band from temporal speckle
$CV_{spatial(S)}$	spatial coefficient of variation from spatial speckle
$CV_{spatial(T)}$	spatial coefficient of variation from temporal speckle

$CV_{temporal(S)}$	temporal coefficient of variation from spatial speckle
$CV_{temporal(T)}$	temporal coefficient of variation from temporal speckle
DAPI	4′,6-diamidino-2-phenylindole, nucleus stain
EC	endothelial cell
FFT	fast Fourier transform
FITC	fluorescein isothiocyanate
f_{MR}	dominant MR operating frequency
$f_{TGF(S)}$	dominant TGF operating frequency from spatial speckle
$f_{TGF(T)}$	dominant TGF operating frequency from temporal speckle
GFR	glomerular filtration rate
IF	immunofluorescence
K^+	potassium
k_1	initial rapid decay of synchronization
k_2	second slower decay of synchronization
KO	knock-out
LiCl	lithium chloride
L-NAME	N(ω)-nitro-L-arginine methyl ester
LSCI	laser speckle contrast imaging
MAP	mean arterial pressure
MEGJ	myoendothelial gap junction
MR	myogenic response
MRI	magnetic resonance imaging
MSE	mean squared error

Na^+	sodium
Na-K-ATPase	sodium-potassium-ATPase
NKCC1	sodium-potassium-chloride cotransporter 1
NKCC2	sodium-potassium-chloride cotransporter 2
NVU	nephrovascular unit
P_{BC}	hydrostatic pressure in Bowman's capsule
PC	phase coherence
PC_{MR}	phase coherence associated with myogenic response
$PC_{TGF(S)}$	phase coherence associated with tubuloglomerular feedback from spatial speckle
$PC_{TGF(T)}$	phase coherence associated with tubuloglomerular feedback from temporal speckle
PCT	proximal convoluted tubule
P_{GC}	glomerular capillary hydrostatic pressure
RBF	renal blood flow
RK	remnant kidney
RVC	renal vascular conductance
RVR	renal vascular resistance (inverse of RVC)
SGLT2	sodium glucose cotransporter 2
TGF	tubuloglomerular feedback
μCT	microcomputed tomography
VCR	vascular conducted response
VSMC	vascular smooth muscle cell

CHAPTER 1: INTRODUCTION

1.1 Background

Like other organs in the body, the kidneys stabilize perfusion to protect from fluctuations in function and glomerular injury. This is achieved through autoregulation of blood flow through the myogenic response (MR) and tubuloglomerular feedback (TGF). TGF is a negative feedback mechanism by which afferent arteriolar resistance is adjusted in response to the concentration of distal tubular sodium chloride sensed at the macula densa by the Na-K-2Cl cotransporter (NKCC2).

Unlike other organs in the body, the kidney presents some unique features. Renal blood flow (RBF) and glomerular filtration rate (GFR) dictate the kidneys oxygen metabolism by determining the filtered load of Na^+; its reabsorption uses the Na^+-K^+-ATPase pump in the proximal convoluted tubule (PCT) which is energy intensive and oxygen-dependent. In addition, the organization of the renal arterial tree is highly irregular; tubular flow is separate from postglomerular (efferent blood flow) and oxygen delivery for 90% of NVUs in the kidney, with the exception of those in the superficial cortex, comes from 3-5 other glomeruli on average [2,3]. In other words, one PCT travels through several postglomerular capillary beds. The renal microcirculation is arranged so that perfusion in one nephrovascular unit (NVU: a nephron, its glomerulus, afferent arteriole and efferent arteriole), which dictates its metabolic demand, adjusts to optimize oxygen delivery by blood flow to other NVUs to prevent ischemia. This is achieved by synchronized autoregulation which allows communication over long distances upstream in the renal vasculature so that every branch downstream can adjust and coordinate resistance to receive appropriate perfusion [4].

Renal autoregulation is a distributed process; communication between otherwise isolated NVUs are synchronized across the kidney to optimize perfusion across space and time. This is in

contrast to the classical view that each NVU individually autoregulates in response to altered blood pressure so that the whole kidney response would be the average of a massively parallel array of units. Synchronization is achieved by the autonomous oscillations of TGF activity that transmit upstream to neighbouring NVUs and arteries as an electrical signal, or vascular conducted response (VCR), using endothelial gap junctions comprised of connexin40 (Cx40). Because all afferent arterioles have their own autonomous oscillations, groups of them are likely to interact. When two or more oscillating systems interact or "couple", they can entrain at a common frequency leading to clusters of synchronized, communicating NVUs [5].

Synchronized clusters of NVUs seem to be arranged within dynamic, small-world networks [6]. This means that NVUs are tightly connected with each other in a module and have strong communication and synchronization with each other, but modules of NVUs are loosely connected with other modules across the kidney. Small-world networks have functional consequences, discussed in chapter 2, but there are scant studies looking at the modularity in the kidney [7]. Innovations in technology to probe renal cortical perfusion, namely the use of laser speckle contrast imaging (LSCI), allow greater insight into the modularity of the nephrovascular network and distributed regulation.

Previous studies using LSCI observed that blocking the transmission of VCRs between NVUs by gap junction inhibition resulted in loss of TGF synchronization and impaired autoregulation [8]. However, nephrovascular network behavior and TGF synchronization have not been studied in pathophysiological models such as chronic kidney disease (CKD). Improving network function and synchronization may lead to preservation of kidney function, thus preventing progression to CKD secondary to hypertension and diabetes mellitus.

1.2 Objectives of Thesis

In the first aim, this thesis examined the impact of inhibiting and enhancing the TGF mechanism on synchronization. Furosemide, a loop diuretic, acts on the NKCC2 cotransporter which is selectively expressed in the apical membrane of cells in the thick ascending limb of the loop of Henle. Inhibition of NKCC2 results in diuresis when sodium chloride uptake is inhibited. In addition, NKCC2 stimulation by chloride uptake is the first step in sensing whether TGF needs to be activated. We also manipulated TGF to enhance it by means of the sodium glucose cotransporter-2 (SGLT2) inhibitor dapagliflozin. Dapagliflozin inhibits the SGLT2 protein found in the proximal tubule. This prevents sodium-coupled glucose uptake in the early part of the tubule and increases the amount of salt arriving to the NKCC2 proteins, where TGF is activated. By increasing salt delivery to the macula densa, TGF signaling is strengthened. We hypothesized that inhibiting TGF by acutely administering furosemide would impair synchronization and network behavior, whereas dapagliflozin would improve synchronization.

Poor TGF synchronization and impaired oxygenation/perfusion matching are key features of progressive renal disease, but this has not been studied in pathophysiological models. In the second aim, this thesis explored the impairment of synchronization using the remnant kidney model of experimental CKD and analyzing the differences in the early remnant kidney at 1 week, and more progressed remnant kidney at 6 weeks. We hypothesized that TGF synchronization will be diminished after both 1 and 6 weeks after inducing CKD, but the structural changes that occur after 6 weeks, such as development of lesions, will further impair TGF synchronization between NVUs.

In the third aim, we investigated the impact of an acute intervention that is known to be cardioprotective and renoprotective, namely SGLT2 blockade, in rats with a remnant kidney for

6 weeks. This also allowed us to probe another mechanism by which SGLT2 inhibition imparts renoprotection. Dapagliflozin in this pathophysiological setting was hypothesized to improve network behavior by strengthening TGF.

In all three aims, LSCI was used to assess renal cortical perfusion to assess the strength and variability in synchronization of TGF and MR, to assess how synchronization of TGF decays over distance in the kidney, and to assess the heterogeneity in cortical perfusion.

CHAPTER 2: LITERATURE REVIEW

Tubuloglomerular Feedback Synchronization in Nephrovascular Networks[1]

Tayyaba Zehra[1], William A. Cupples[2], Branko Braam[1,2]

Running title: Synchronization in nephron networks

Key words: tubuloglomerular feedback, nephrovascular network, microvasculature, distributed autoregulation, synchronization, oxygenation-perfusion, modular networks.

[1] This literature review has been submitted for publication in the *Journal of the American Society of Nephrology* as "Zehra et al. Tubuloglomerular Feedback Synchronization in Nephrovascular Networks".

Abstract

To perform their functions, the kidneys maintain stable blood perfusion in the face of fluctuations in systemic blood pressure. This is done through autoregulation of blood flow by the generic myogenic response (MR) and the kidney-specific tubuloglomerular feedback (TGF) mechanism. The central theme of this paper is that, to achieve autoregulation, nephrons do not work as single units to manage their individual blood flows, but rather communicate electrically over long distances to other nephrons via the vascular tree. Accordingly, we define the nephrovascular unit (NVU) to be a structure consisting of the nephron, glomerulus, afferent arteriole and efferent arteriole. We discuss features that require and enable distributed autoregulation mediated by TGF across the kidney. These features include the highly variable topology of the renal vasculature that creates variability in circulation and the potential for mismatch between tubular oxygen demand and delivery, the self-sustained oscillations in each NVU arising from the autoregulatory mechanisms, and the presence of extensive gap junctions formed by connexins and their electrical properties that enable long distance conduction of TGF signals. Further, we examine methods of assessing synchronization as well as pathological situations that disrupt the nephrovascular network. The existence of TGF synchronization across the renal microvascular network enables an understanding of how NVUs optimize oxygenation-perfusion matching while preventing transmission of high systemic pressure to the glomeruli which could lead to progressive glomerular and vascular injury.

Definitions

Coupling: The process of two oscillating systems interacting and adjusting their frequencies.

Entrainment: When two oscillating systems with similar oscillatory periods are somehow connected to each other (for instance, two or more NVUs branching from a common artery), the oscillating motions of each system, even if extremely subtle, will transmit to the other system(s) through the shared structure. This weak interaction allows the systems to "feel" each other's motions and couple, so that they adjust their frequencies and begin oscillating with the same period.

Myogenic response (MR): Autoregulatory mechanism where contraction of the vascular smooth muscle layer constricts the blood vessel in response to elevated intravascular pressure, and conversely dilates the vessel when intravascular pressure is lowered.

Nephrovascular unit (NVU): Structure consisting of the nephron, glomerulus, afferent arteriole and efferent arteriole

Nephrovascular network: A dynamic, functional group of interacting NVUs that exist in space and have interactions that regulate vascular resistance

Oscillations: Pertaining to MR and TGF, oscillations refer to the rhythmic movement of each of these mechanisms that is generated by their dynamic activity. MR and TGF oscillations are self-sustained, or autonomous, which means that their periodic motion is maintained by a source of power that does not have any corresponding periodicity and when perturbed, returns to its original trajectory.

Synchronization: Oscillating systems that are coupled with each other can become synchronized, also known as becoming phase-locked, and are resistant to perturbations.

Tubuloglomerular feedback (TGF): Autoregulatory negative feedback mechanism that links changes in glomerular filtration rate to the concentration of salt in the tubule fluid at the macula densa.

Introduction

The intrinsic mechanisms matching blood flow to metabolic demand have been recognized in many organs. In the kidney, autoregulation stabilizes renal blood flow (RBF) and glomerular filtration rate (GFR) despite naturally occurring variations in blood pressure. To satisfy the functional and metabolic needs of the tissue, the kidneys self-regulate their blood flow by altering preglomerular vascular resistance through two components, the ubiquitous myogenic response (MR) and the kidney-specific tubuloglomerular feedback (TGF) response. TGF is a mechanism in which luminal sodium chloride concentration is sensed at the macula densa and a signal is relayed to the afferent arteriole to alter preglomerular resistance to restore distal tubular sodium chloride concentration. The current review focusses on the TGF mechanism.

Historically and even today, it is considered that the nephron, which supplies TGF, and its afferent and efferent arterioles, is responsible for the autoregulation of its own blood flow so that whole kidney autoregulation is the sum of all nephrons, i.e. the average of a massively parallel array of units. However, it is difficult to reconcile this idea with the variability in preglomerular resistance presented by the renal vascular organization. It is equally difficult to reconcile this idea with known post-glomerular-vascular-tubular relationships. Hence, we define the nephron and its afferent and efferent arterioles as the minimum structure, or "nephrovascular unit" (NVU), capable of autoregulation.

We argue that groups of NVUs, synchronized with each other in a network, represent an accurate depiction of the distributed nature of autoregulation within the kidney. The following arguments are consistent with our proposition. The anatomical irregularity of the renal arterial tree requires that microcirculation must be arranged so that perfusion in one NVU, which dictates its metabolic demand, adjusts to optimize oxygen delivery to other NVUs. Other aspects

include the self-sustained oscillations of TGF within each NVU, generation by TGF of an electrical signal and its transmission to upstream vascular segments using endothelial gap junctions formed by connexin (Cx) proteins. Interaction of these signals at vascular branch points allows NVUs to self-organize into synchronized ensembles. Synchronization of TGF effectively optimizes resistance and provides smoothing of blood flow in time and space. Functional and structural disruptions to the network may lead to structural offenses to the network which exacerbates the functional disruption; this pathophysiological process may be responsible for renal injury.

These arguments align to produce our line of thinking that NVUs are synchronized in functional networks by interactions among their oscillatory TGF responses. This review aims to examine the evidence that NVUs are coupled. Furthermore, we explore methods of assessing perfusion in NVUs and to detect nephrovascular networks in the kidney.

Renal arterial organization supports distributed renal autoregulation

The kidneys are distinct from other organs because RBF determines GFR and thus metabolic demand generated by the oxygen-intensive proximal tubular reabsorption of sodium. The challenges for the kidneys are i) to ensure tightly regulated glomerular capillary pressure (P_{GC}) and GFR in the face of fluctuating blood pressure, and ii) to ensure that metabolic demand in one NVU does not become mismatched from oxygen delivery which is supplied by other NVUs [3,9]. For 90% of NVUs, oxygenation-perfusion matching is an active process enabled by synchronization of TGF; the renal microvasculature forms a macroscopic network that supports communication to coordinate the behaviour of NVUs and optimize perfusion.

There are distinct features of the renal vasculature that enable synchronization between NVUs to achieve distributed autoregulation (Fig. 1). Renal arteries of larger diameters (> 40 μm) contain one or a few layers of vascular smooth muscle cells (VSMCs) which makes them thinner-walled than skeletal muscle arteries of equivalent diameters [10]. Thinner walls in the mid-sized cortical radial arteries (CRA) and arcuate arteries means a lower capacitative load. Along with endothelial gap junctions, this enables longer transmission of electrical signals along the vessels. Smaller renal vessels (< 40 μm) have relatively thicker walls as well as a high wall to lumen ratio [11], consistent with the known distal pressure drop in preglomerular circulation where there is a greater involvement in modulating resistance. These features facilitate ascending communication along the arterial tree.

The organization of the renal arterial tree, based on μCT of a renal cast, demonstrates irregular vascular topology resulting in pre-glomerular resistance that varies markedly among glomeruli [12,13]. In addition to being present at terminal branches, a quarter of afferent arterioles originate from non-terminal arteries that continue to branch into additional arteries; a quarter arise from unpaired, lower-order single vessels that terminate in pairs of afferent arterioles, and the remaining half are present in pairs, triplets and quadruplets at the tops of vascular trees and at branching points of vessels, shown in rats and in humans [14,15]. This structural variability creates the risk of hypertensive injury or inadequate perfusion to glomeruli. Autoregulation has to operate on a scale larger than a single NVU to modulate vascular resistance regionally so that P_{GC} is tightly distributed. Coordinated behaviour of NVUs through synchronization allows integration of communication over long distances upstream in the renal vasculature so that every branch downstream can adjust its resistance to maintain appropriate perfusion.

There exists an anatomical separation of post-glomerular (efferent arteriolar) blood flow from tubular flow. Beeuwkes et al described the separation between efferent arterioles and tubules in a series of papers that studied multiple species [2]. Only in the superficial cortex does an efferent arteriole perfuse its own PCT; this is about 10% of all PCTs in the kidney. Most efferent arterioles perfuse other PCTs, and on average these PCTs travels through three capillary beds. This has been shown in dogs and humans [2,3]. Since the bulk of renal oxygen consumption occurs in the PCT it is crucial to match oxygen delivery to metabolic demand. A mechanism operating at the level of a single NVU to maintain adequate P_{GC} and perfusion for its own tubule would be inconsistent with vascular anatomy. Instead, separation between the post-glomerular vasculature and the tubules strongly suggests a mechanism where each NVU anatomically contributes to the distribution of flow among groups of NVUs (Fig. 2) [2]. This ensures homogenous perfusion of multiple glomeruli so that post-glomerular blood flow is matched with tubular reabsorption of sodium.

The complexity of the renal microvasculature suggests the requirement for a distributed mechanism that regulates perfusion on a large scale. TGF-induced synchronization is the most likely solution to the challenges posed by the irregular anatomical arrangement of the renal microvasculature, particularly the fact that a single PCT is perfused by several efferent arterioles.

TGF generates self-sustained oscillations within NVUs

TGF (and MR) activity generates autonomous oscillations of proximal tubular pressure, proximal tubular flow, and single nephron blood flow within individual NVUs [16,17]. Oscillations in intratubular pressure were observed as early as 1983 by Leyssac and Baumbach in halothane-

anaesthetized Sprague-Dawley rats [18]. These oscillations subsequently entrain and synchronize between clusters of NVUs, permitting their interaction, demonstrated first by Holstein-Rathlou [17].

Autonomous oscillations originate from the high gain and the delay in the negative feedback loop of the TGF mechanism. Transmission of fluctuations in glomerular capillary pressure, which change GFR, and tubular fluid from the Bowman's space to the macula densa creates a 20 s delay [19]. Further delays occur due to the time it takes for the TGF mediator to be released from the macula densa and to elicit vasoconstriction of the afferent arteriole. Pressure and flow oscillations at efferent arterioles are noted to be in phase with proximal tubular pressure and flow oscillations, thus arising from changes in preglomerular vasculature resistance that transmit down to the postglomerular vasculature [17,18].

The self-sustained oscillations of TGF and MR each reflect operation of nonlinear systems [5,20]. MR and TGF interact since they act on the same target, afferent arteriolar VSMCs. In rat kidneys, TGF oscillates at a frequency of 0.015 – 0.06 Hz and MR at 0.09-0.3 Hz. When two oscillating systems interact or "couple", they adjust their rhythms and start to oscillate with a common frequency to become synchronized. A hallmark of entrainment or synchronization is that when interrupted, the oscillators spontaneously recouple [21]. MR certainly generates oscillations, but extensive, sustained synchronization of MR is not common and when interrupted, the oscillations tend to diminish [8]. MR, with its higher frequency, stabilizes local fluctuations in flow resulting from blood pressure fluctuations under the influence of TGF [22]. TGF, with its lower frequency, modulates the amplitude and frequency of MR to stabilize larger fluctuations of blood pressure and thereby stabilizes sodium chloride delivery to the macula

densa [23]. Several studies have confirmed this concept of TGF and MR interacting within individual NVUs in the rat kidney [23–27].

In sum, measurable self-sustained oscillations occur in both MR and TGF due to the delays, high gain and non-linear properties of the systems, and MR and TGF oscillations interact.

Vascular conducted responses enable communication in the arterial tree

TGF is a property of individual NVUs; increased sodium chloride concentration reaching the macula densa activates TGF to initiate afferent arteriolar constriction. The mediator is thought to be adenosine and possibly ATP but may also be an electrical signal traversing the extraglomerular mesangium which initiates depolarization in VSMCs of the afferent arteriole [28,29]. This depolarization is a non-regenerative electrical signal that travels upstream towards neighbouring afferent arterioles and into the CRA via axial endothelial gap junctions. Although every NVU adjusts its own perfusion, upstream electrical communication optimizes regional perfusion by information exchange at branch points. There are two important components to this system: connexins and vascular conducted responses (VCRs).

Connexins: Gap junctions formed by multiple transmembrane Cx proteins create axial and radial communication pathways enabling TGF signal transmission by passage of current and various small molecules. Cx40 is the predominant isoform in gap junctions between endothelial cells (EC) and forms the axial communication pathway (Fig. 1). Studies with Cx40 knockout (KO) mice demonstrate impaired RBF autoregulation, an inability to regulate afferent arteriolar resistance, and a significant decrease in propagated vasomotion in intact skeletal muscle microcirculation [30–32]. Cx37 is also detected in the renal endothelium but its function is unclear

[29,33–35]. Cx expression between VSMCs is not fully understood but a few studies demonstrate Cx45 and possibly Cx43 [29,30,36,37]. Further, using Cx45 to replace Cx40 in a Cx40 KO model rescues the renin-dependent hypertension observed in the mice, but not the poor autoregulation [30].

In addition to homocellular gap junctions, heterocellular myoendothelial gap junctions (MEGJ) constitute the radial communication pathway that connect ECs to VSMCs (Fig. 1) [38]. At MEGJ sites, the EC physically contacts the VSMC by club-shaped cellular protrusions through the internal elastic lamina [38–40]. The Cx isoforms in MEGJs are not fully elucidated; Cx37, Cx40 and Cx43 have been found in myoendothelial connections across various vascular beds. Cx37 in MEGJs seems central in controlling the spreading gap junctional calcium signal [41,42]. Cx37, Cx40, and Cx43 are also found in the extraglomerular mesangium which suggests they may play a role in signal transmission between the macula densa and the afferent arteriole [29]. Both Cx37 and Cx40 have been observed between ECs and renin secreting cells which are transformed VSMCs located at the distal portion of the afferent arterioles [42,43].

Although not immediately relevant for autoregulation, proper Cx40 function plays a role in renin regulation. Renin release by renin secreting cells is of critical importance for blood pressure regulation and extracellular fluid volume homeostasis [44]. Whereas mice without Cx43 and Cx45 are not viable, Cx37 KO mice are normotensive and Cx40 KO mice are hypertensive [44]. However, endothelial-specific deletion of Cx40 does not result in hypertension [45]. Cx40 is strongly expressed in renin secreting cells and seems to be necessary for their proper localization by perhaps exerting a scaffolding function required for this process. It is also required for a coordinated response among renin secreting cells. Cx40 KO mice have loss of gap junctional coupling between renin secreting cells and aberrant localization of renin secreting cells from the

smooth muscle layer to the extraglomerular mesangium, glomerular tuft and periglomerular interstitium [46,47]. This ectopic localization of renin secreting cells in Cx40 KO mice results in renin release that is no longer reduced by increased blood pressure or angiotensin II, leading to hypertension [31,44].

Vascular conducted responses: TGF-mediated depolarization initiates a VCR, a non-regenerative electrical signal, which can travel over 1500 μm to neighbouring afferent arterioles and upstream into the CRA [48–50]. VCRs can be induced by hyperpolarizing (vasodilating) and depolarizing (vasoconstricting) currents. The main physiological distinction between the kidney and other tissue beds is that the functional input to the kidney, RBF, also delivers the metabolic load that must be matched with perfusion. Matching metabolic load with perfusion is likely achieved by regulating RBF and GFR ~~in parallel~~ through afferent vasoconstriction and therefore, we focus our discussion on propagating preglomerular vasoconstriction.

In mesenteric and cerebral tissue beds, VCRs typically transmit hyperpolarizing ionic currents which are reasonably understood [51]. There are only two in vivo studies of VCR in the kidney. Both show transmission of depolarizing currents using KCl microapplication and direct electrical stimulation of renal vessels which achieved approximately 50% local constriction, however ionic currents underlying this are not well understood [49,50]. VCR membrane potentials have been measured using electrodes in ECs and VSMCs and propagate at a velocity of at least 1 mm/s [50]. The propagation of calcium waves is too slow (0.1 mm/s) compared to the transmission speed of membrane potentials in VCR, ruling out a role for calcium in the propagation [52]. Presumably, VCRs result from the passive electrotonic spread of depolarization which is initiated by the macula densa upon TGF activation and spreads upstream from the

extraglomerular mesangium through ECs [40,53]. The transformation of transient electrical events into conducting voltage responses is thus enabled by gap junctions.

The longitudinal conduction of VCRs along the endothelium is aided by structural features and electrical properties of ECs. ECs are oriented axially and their extensive axial coupling by Cx40 results in a low input resistance and a low impedance pathway (1.5 to 3 mΩ) and also prevents charge accumulation in the endothelium [51]. On the other hand, VSMCs are oriented circumferentially and have much higher input resistance than ECs (90 mΩ) which makes the VSMC layer an unlikely VCR conduction pathway.

Computational modelling studies of VCRs show EC-initiated conduction and parallel changes in membrane voltage occurring in VSMCs [54,55]. The biophysics of this have been discussed elsewhere in detail [51,56]. Radial communication between ECs and VSMCs through MEGJs allows current from ECs to reach VSMCs [55–57] MEGJs are localized distally in the smallest arterioles, with less expression in the CRA, and little to none in the arcuate and larger arteries [38,39,58,59]. In the absence of MEGJs, current leakage out of the endothelium is greatly reduced, thus enabling long-distance EC-EC transmission. VCR transmission is optimal when approximately one-third of VSMCs have active MEGJs because that amount of current injection into ECs is enough to elicit quasi parallel changes in the VSMC layer while minimizing current loss from the endothelium [56]. The presence of glycocalyx on the surface of endothelial cells may also serve as an insulator at the luminal side of the endothelium [60].

The limiting factor for VCR conduction along the endothelium is current loss into VSMCs. Multiple layers of smooth muscle in the renal arteries would absorb enough current to stop a VCR in a very short distance [56]. Current transmission is optimized by limited VSMC-

VSMC coupling. An absence of VSMC-VSMC coupling would lead to erratic VCRs because a MEGJ would only depolarize one VSMC. On the other hand, a very high coupling between VSMCs which would create a conduction pathway, albeit short-lived, of electrical signalling along the smooth muscle layer. Limited coupling between VSMCs minimizes current drain from ECs into VSMCs while smoothing out local variations in membrane voltage of VSMCs so that they all achieve similar levels of activation [61].

Taken together, gap junctions allow depolarizing TGF signals to transmit into upstream arteries. The axially oriented endothelial cells provide the 'electrical cable' for VCR transmission, while the radially oriented MEGJs permit quasi parallel current changes in the smooth muscle layer to enable optimal transmission. Cx40 is not only required for appropriate renin release, but it is indispensable for VCR transmission.

TGF-oscillations are responsible for synchronization of groups of NVUs

Entrainment of self-sustained oscillations in TGF of each NVU leads to clusters within the larger network. Clusters vary in the number of NVUs that comprise them and are dynamic [20].

There is ample evidence of synchronization amongst NVUs. Holstein-Rathlou et al and Yip et al identified pairs of nephrons with synchronized tubular pressure oscillations using micropuncture [16,17]. Kallskog and Marsh used micropuncture and observed that increasing perfusion in one nephron reduced stop-flow pressure in that nephron and in the adjacent coupled nephron, indicating an interaction [21]. Chen et al detected interactions between two nephrons at distances as far as 1.5 mm along the vasculature in rat kidneys [48].

TGF-initiated VCRs from multiple afferent arterioles interact at branching points of the vascular tree. Holstein-Rathlou demonstrated interactions between nephrons sharing the same CRA: 29 of 33 nephron pairs whose afferent arterioles originated from the same CRA had identical frequency and phase of oscillations [17]. Yip et al measured tubular pressure oscillations simultaneously in two or three nephrons and found synchronization in pairs of nephrons that branched from a common CRA, as determined by vascular casts. When one of the tubules was perfused with furosemide, the amplitude of tubular pressure oscillations diminished similarly in the coupled nephron whereas no changes occurred in the oscillations of a non-coupled nephron [16]. This is consistent with the idea that the afferent arteriole and CRA are involved in oscillating changes of vascular resistance and that NVUs are coupled through the vasculature [62,63]. Modelling studies of nephrovascular networks also support the necessity of upstream vascular communication between NVUs in the arterial tree because it contributes to spatial and temporal smoothing of blood flow [4].

The first study assessing TGF-oscillations on a large scale assessed coupling of TGF dynamics in over 50 efferent arterioles simultaneously [27]. Laser speckle contrast imaging (LSCI, discussed in a later section) was used to image the surface of the kidney. The study used hierarchical clustering which gives insight into the modularity, or clusters, of the network. This revealed the time-varying nature in the synchronization of oscillations in clusters of 2-3 nephrons across the renal surface that were not always nearest neighbours. The data were interpreted to show synchronization that was consistent with the dimensions of cortical lobules.

Evidence supporting that synchronization occurs in regions larger than the dimension of cortical lobules comes from experiments using nitric oxide synthase inhibition. Mitrou et al segmented an imaged region with dimensions corresponding to 50-60 lobules into synchronized

clusters [7]. The imaged region was treated as a flow field and phase coherence was assessed between every possible pair of pixels in the image. Phase coherence is a value bounded between 0 and 1 and uses constant phase differences of time-varying TGF dynamics of pixel pairs to give a robust measurement of synchronization [64]. Strong synchronization exists between the elements within a cluster, with looser synchronization between clusters; this differential pattern of synchronization is referred to as a "small-world" network. TGF showed significant clustering under control conditions with strong synchronization between pixel pairs as far as 5 mm from each other.

To summarize, all afferent arterioles have autonomous oscillations arising from autoregulatory dynamics. When VCRs from afferent arterioles reach each other, groups of these signals interact to become synchronized. Recent studies using laser speckle imaging show synchronization that occurs in large regions across the kidney.

Modularity of the nephrovascular network

The nephrovascular network has major physiological contributions to optimizing resistance to maintain adequate blood flow to glomeruli and P_{GC} and for oxygenation-perfusion matching on a large scale. Spatiotemporal variations occur across the network in the sizes and connections of synchronized clusters of NVUs. These dynamics arise because of the modular organization of the network and have implications for network function. Few data address the functional and regulatory consequences of this dynamic network.

Modularity is a common feature of biological systems, especially neuronal networks, and is a small-world network [6,65] In a system that is organized randomly, or in other words,

considered to be “global” because of a lack of modularity, any perturbation experienced by a node in the system will spread throughout the network in an uncontained fashion [66]. Every element in the network will feel the effect of the perturbation. On the other hand, a network could be perfectly modular, where nodes are tightly connected to each other within a module, and loose connections exist between modules. If a perturbation is experienced by a node in one module, it will be contained within that group of nodes because of their strong interconnections. The effect of the perturbation will not dissipate towards other modules where it could be detrimental to their function.

A real-life system, such as the nephrovascular network, most likely falls somewhere on the spectrum between a global and modular network. Indeed, using N(ω)-nitro-L-arginine methyl ester (L-NAME) as a tool to manipulate blood flow dynamics reveals increased modularity, an indicator of the group characteristics of a network. L-NAME results in small, highly synchronized clusters that are loosely interconnected with each other [7]. The clusters increasingly show small-world dynamics with less pronounced coupling between clusters.

Small-world networks have functional implications. For one, they are fault-tolerant [6]. If one cluster is impaired or lost, that change will have little effect on the remaining clusters because of the looser connections between them. Second, modularity facilitates the integration and spreading of electrical signals because of the higher density of connections in a cluster resulting in easier activation within that region [65,67]. Third, this type of network allows the maintenance of balance between network activity dissipating too quickly but also from becoming pathologically large. It limits global spreading of perturbations or activity while sustaining local changes. Fourth, it facilitates the flexibility of the network as it can be combined or divided while stability is maintained [65]. Last, it optimizes perfusion across space and time by allowing

adjustments in the resistance of upstream vasculature that feeds a cluster of glomeruli in response to fluctuations while minimally affecting other clusters.

In summary, the behavior of the network shows small-world dynamics which has consequences for kidney function because it is fault-tolerant, aids in the integration of electrical signals without letting network activity dissipate or spread globally, has flexibility and optimizes perfusion spatiotemporally.

Is the function of the nephrovascular network disturbed in disease states?

Disrupted network dynamics impair distributed autoregulation and increase susceptibility to ischemia of the renal parenchyma which is also a critical feature in the pathophysiology of diabetic nephropathy, acute kidney injury (AKI) and progression to chronic kidney disease (CKD). Network function can be disrupted firstly by microvascular dysfunction such as endothelial or gap junctional changes which grossly impair transmission of electrical signals. Second, it can be impaired by proximal tubular dysregulation that reduces sodium chloride delivery to the macula densa within the loop; and third, by damage to NVUs. Such functional disruptions to the communication network may cause structural damage to elements of the network that worsens the functional disturbances, aggravating this cycle (Fig. 4). It is important to preface this discussion with the fact that network contributions have only been sporadically investigated in pathophysiological models.

Microvascular dysfunction is present in most forms of AKI. For instance, sepsis is characterized by reduced density of functional capillaries, increased heterogeneity in blood flow and hypoxia [68]. Luminal narrowing, increased wall-to-lumen ratio and microvascular rarefaction

are induced by hypertension and may diminish signal transmission along the endothelium (Fig. 3) [69]. Hypertension-associated thickening of the VSMC layer may change conduction efficiency because of increased current drain from ECs. These processes could increase the susceptibility of the glomeruli to hypo- and hypertensive damage and to ischemic damage. In our studies, we infused the gap junction inhibitor Carbenoxolone (CBX) to study its impact on disrupting communication in the nephrovascular network [8]. CBX increased spatial and temporal heterogeneity in cortical perfusion, reduced the strength and extent of synchronization of TGF, and impaired whole kidney autoregulation.

Inappropriate TGF activity is observed in early diabetic kidney disease. High proximal sodium reabsorption coupled to glucose reabsorption reduces the concentration of sodium chloride arriving at the macula densa, leading to TGF-mediated hyperfiltration. Our own studies investigated the effects of early diabetes mellitus on nephrovascular network behaviour, demonstrating increased spatial heterogeneity in perfusion and impaired autoregulation [70].

Structural damage to the network, like tubular loss, failing NVUs (focal segmental glomerulosclerosis) or complete loss of NVUs (global glomerulosclerosis), can occur in CKD (Fig. 3). Since TGF signal transmission is non-regenerative, NVU loss would result in a reduced amount of signal generated and a greater average distance between signal generators (NVUs) in the network is exacerbated by hypertrophy in CKD that further separates nodes. Increased separation means reduced TGF signals travelling from one node to the next and reduced communication effectiveness. Hyperfiltration in diabetes increases the likelihood of intraglomerular hypertension leading to glomerular injury, resulting in loss of NVUs from the network and a further increase in single nephron GFR in the remaining NVUs. This has two consequences: the remaining NVUs have a higher oxygen demand while a disrupted network has

lower capacity to match oxygen supply to demand in the remaining NVUs (Fig. 4). Because of the loss of nodes where signals from multiple afferent arterioles are able to interact, the resistance upstream of multiple NVUs will be less optimized to match oxygen delivery to demand in all tubules.

In conclusion, loss of nodes from the network and increased distance between nodes, microvascular injury which leads to impaired gap junction communication, and reduced TGF signals will impair synchronization and overall autoregulation. A comprehensive understanding of how pathophysiological conditions such as endothelial dysfunction, hypertension, diabetes, and kidney disease impacts the behaviour of the nephrovascular network and synchronization warrants further study.

Methods to assess nephrovascular synchronization

Several techniques to study renal network function are now available to assess the effectiveness of autoregulatory mechanisms (Table 1).

The ability to visualize the anatomical structure of the microvasculature provides a tool to phenotype renal diseases and determine changes to glomerular number and vessels. Micron-scale computed tomography (μCT) can produce high resolution (voxel size ≤ 20 μm^3) images of the vascular network of the whole kidney and is relatively low cost with a high scanning efficiency; details of μCT are reviewed by Clark et al [71]. A constraint of μCT for the purposes of studying renal microvascular anatomy is that the available algorithms for segmentation of the renal vasculature, which refers to the extraction of three-dimensional features from two-dimensional

images, are limited for use in the renal cortex [72]. Segmenting images is therefore done manually and requires a vast amount of patience, time and skill with correspondingly small sample sizes.

Micropuncture enables study of TGF oscillations and coupling between pairs of superficial NVUs [16,21,49]. TGF can be studied by varying late proximal flow and measuring single nephron GFR, P_{GC} or stop-flow pressure, for instance. See Lorenz for details [73]. Micropuncture was crucial for early studies that demonstrated nephron-nephron interactions and synchronization. A significant limitation to micropuncture is that it is an inherently high-resolution technique, is very difficult to perform, and can only assess 2-3 nephrons simultaneously, precluding the ability to make dynamic measurements about TGF-induced synchronization for multiple NVUs.

LSCI is a non-invasive, full-field technique used to assess the vasculature that offers high spatial and temporal resolution and has been instrumental in experimental and clinical neurological [74,75], dermatological [76] and retinal imaging applications [77]. Detailed information regarding LSCI is discussed by Postnov et al, Vaz et al and Allen et al [78–80]. LSCI generates a speckle, an interference pattern produced when laser light reflects or scatters from the field of view. The motion of red blood cells at the surface is the significant contributor to the interference pattern and reduces speckle contrast, which is interpreted by the imager as a change in local surface motion. Efferent arterioles approach the renal surface where they branch into "star" vessels (branches of efferent arterioles visible on the surface of the kidney) – these are the main source of speckle signals [64]. LSCI requires a similar preparation as micropuncture.

LSCI gives information about microvascular hemodynamics and captures real-time images to assess tissue perfusion. It can provide insight into clustering of nephrons and synchronization in those clusters mediated by TGF. The first study that successfully measured

TGF-induced synchronization dynamics in over 50 nephrons simultaneously used LSCI to image the surface of the rat kidney [27]. Scully et al presented a method of segmenting LSCI-obtained images into synchronized clusters by phase coherence, also known as phase-locked value [64]. Phase coherence reflects the stability of the phase difference between two oscillators, or pairs of pixels of the image in this case. Mitrou et al reported consistent results using LSCI regarding clustering after L-NAME, but also quantified the strength of MR and TGF synchronization in the clusters using graph analysis of phase coherence [7,81]

Drawbacks to LSCI include that it can only examine blood flow in the surface of the cortex because the illumination is dispersed across the surface rather than concentrated into the surface [82,83]. Advantages of LSCI include that it has a high spatial and temporal resolution, capturing information in real-time. It is also capable of discerning frequencies arising from cardiovascular, respiratory, baroreflex and renal autoregulatory systems [83].

The techniques discussed above share a common limitation that they cannot be used in humans. Non-invasive measurement of intrarenal oxygenation and perfusion in humans (and rodents) can be made with Blood Oxygen Dependent (BOLD) MRI and Arterial Spin Labeling (ASL) MRI. Although BOLD-MRI is a low spatial resolution technique, it has high temporal resolution (sampling rate 1-3 s per image) and can image the full kidney without the need for contrast agents with a high scanning efficiency [84]. ASL-MRI provides assessment of tissue perfusion [85]. ASL-MRI has a low spatial and temporal resolution (sampling rate 3-8 s per image) compared to BOLD MRI [84,86]. The temporal resolution of these two techniques has to be able to resolve the frequency bands corresponding to MR and TGF oscillations. BOLD-MRI and ASL-MRI can be used simultaneously to virtually "map" tissue oxygenation and perfusion and determine if hemodynamic heterogeneity exists [87,88].

Various techniques with the ability to make measurements from the level of a single NVU to large-scale cortical perfusion exist. The use of LSCI is hugely innovative for the latter purpose and can provide crucial insight into network dynamics. For now, methods to assess renal perfusion in humans are limited to BOLD and ASL MRI.

Conclusion

This review has discussed the newly emerging concept of distributed autoregulation from anatomical and physiological standpoints. Autonomous oscillations of TGF facilitate the entrainment and synchronization of multiple oscillating NVUs, and gap junction mediated communication provide the highway on which the TGF-induced VCRs can travel. Electrical communication (i.e. VCRs) results in information processing at every arterial branch point within the radius of TGF depolarization. This optimizes partly shared resistance upstream for a cluster of glomeruli, resulting in smoothing of the resistance differences in all of the NVUs within that cluster so that the differences in glomerular blood flow and P_{GC} are minimized. Oxygenation-perfusion matching is an inevitable consequence of glomerular blood flow optimization (Fig. 2).

We have discussed that instead of autoregulation being the averaged response of single nephrons, it may actually be the coordinated behaviour of many nephrons working together to optimize perfusion. This view of synchronized network behaviour represents a paradigm shift that has a high impact on the understanding of disease; interventions that could enhance synchronization and thereby oxygenation-perfusion matching might be able to prevent progression of diseases like AKI, CKD and diabetic nephropathy.

Perspectives

The emerging paradigm shift regarding renal autoregulation and synchronization of NVUs has enormous potential to change the view renal disease management and treatment is considered. First, it may offer a new way to appreciate the mechanisms behind disease onset and progression. Second, it leads to the question of how network function can be restored in the setting of renal disease using interventions that restore coordinated responses among NVUs. The health burden of AKI, CKD and diabetic nephropathy mandates the need to better understand their dysregulation and prevent progression to the point of renal replacement therapies. Strengthening the nephrovascular network, by means of strengthening TGF's electrical signals to enhance the robustness of interactions among NVUs or by increasing the responsiveness of the TGF system, could mitigate further renal injury in these situations. The effect of these strategies is to improve coordinated behavior of NVUs, thereby augmenting network regulation, the inevitable consequence of which is oxygenation-perfusion matching in the renal parenchyma. This concept has the potential to inform strategies used to treat renal disease. For instance, sodium glucose contransporter-2 (SGLT2) inhibitors block the SGLT2 protein in the PCT leading to increased luminal sodium at the macula densa which is sensed by TGF. SGLT2 inhibitors are renowned for their beneficial effects in diabetes. Based on an understanding of TGF, the beneficial effects of SGLT2 inhibitors may actually come from the reduced consumption of oxygen at the PCT that occurs after SGLT2 inhibition and preserved integrity of the nephrovascular network. Using this new lens to view disease progression and improving synchronization to improve oxygenation-perfusion matching have a vast potential to inform the management of kidney disease.

Table 2.1. Comparison of microvascular and perfusion imaging techniques.

Technique	Information Obtained	Resolution	Advantages	Disadvantages
μCT	3D models of tissue	Voxel size ≤ 20 μm^3	High spatial resolution	Requires contrast agents, radiation exposure, invasive
Micropuncture	Single nephron GFR, P_{GC}	One or two superficial nephrons	Single/dual nephron resolution provides quality information about NVU physiology	Cannot measure dynamics of more than two nephrons simultaneously, invasive
LSCI	Perfusion	Best at 300 μm	High spatial and temporal resolution, real-time data capture, full-field, non-invasive	Only images surface perfusion, cannot use for human kidneys
BOLD-MRI	Oxygenation	Spatial: 3.4 × 3.4 × 4 mm^3 voxel size Temporal: sampling rate 1-3 s/image	Full-field, non-invasive, used in humans, no contrast agent needed	Low spatial resolution
ASL-MRI	Perfusion	Spatial: 3.4 × 3.4 × 4 mm^3 voxel size Temporal: sampling rate 3-8 s/image	Full-field, non-invasive, used in humans, no contrast agent needed	Low spatial and temporal resolution, reduced sensitivity

μCT, microcomputed tomography; LSCI, laser speckle contrast imaging; BOLD-MRI, blood oxygen level-dependent magnetic resonance imaging; ASL-MRI, arterial spin labelling magnetic resonance imaging.

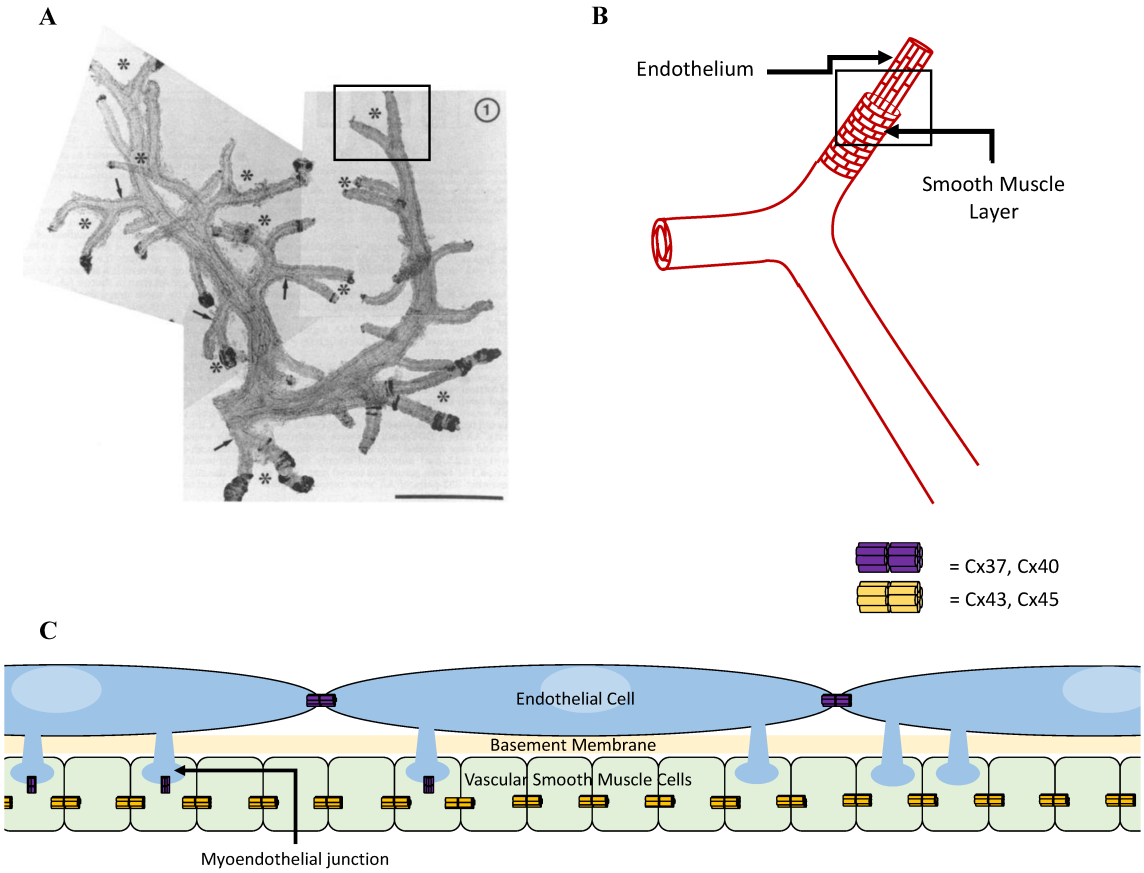

Figure 2.1. The renal arterial tree and its components. A) shows the high variability in the arterial organization, superimposed upon a composite low-power micrograph of two cortical radial arteries (CRA) and their afferent arterioles. B) shows the axially oriented cells of the endothelium and radially oriented smooth muscle cell layer. C) shows myoendothelial junctions (MEJs) protruding from endothelial cells (EC) towards the vascular smooth muscle cells (VSMC). It also illustrates the presence of myoendothelial gap junctions (MEGJs) comprised of connexins (Cx) present at MEJs. Gap junctions enables depolarizing tubuloglomerular feedback (TGF) signals to transmit upstream the afferent arteriole to neighbouring afferent arterioles and into the larger artery, where similar signals from other afferent arterioles can interact to regulate vascular resistance. Fig.1A reproduced from Casellas et al. Anatomic pairing of afferent arterioles and renin cell distribution in rat kidneys. *Am J Physiol.* 1994;267:F931-36.

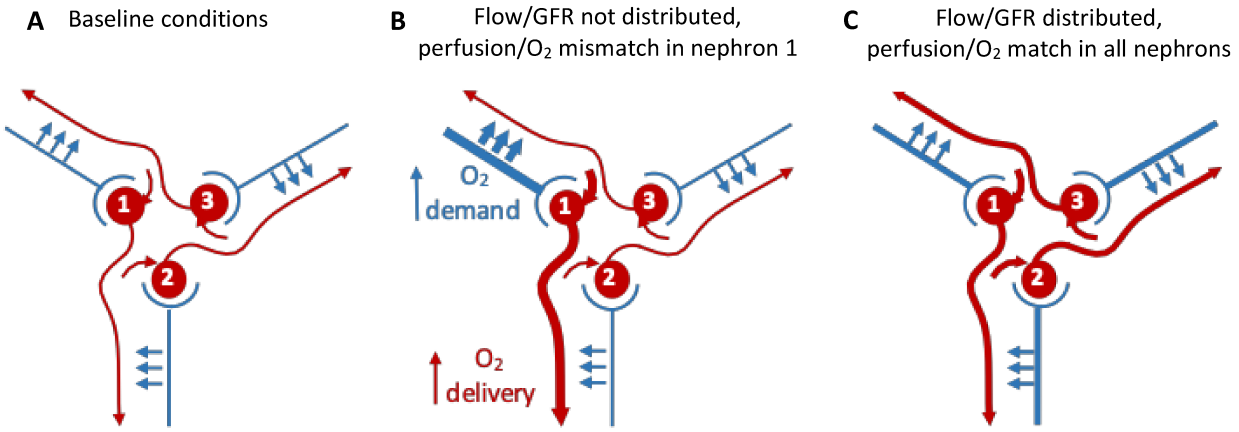

Figure 2.2. Consequences of local vs distributed blood flow. In this simplified diagram, three glomeruli receive blood from their respective afferent arteriole. Efferent blood flow and tubular flows from the glomeruli are separated so that each tubule receives its blood supply from another glomerulus; in vivo it may be up to 5 other glomeruli. If flow and filtered Na^+ increase in NVU 1, reabsorption will generate a greater oxygen demand. If autoregulation is local, a mismatch between oxygen supply and demand would occur. NVU 1 needs to communicate with NVU 3, whose efferent vessel perfuses its tubule. This communication occurs through TGF-induced synchronization and leads to distributed autoregulation; the resistance upstream every glomerulus is regulated partly by itself and partly by signals coming from all the other NVUs in the arterial tree.

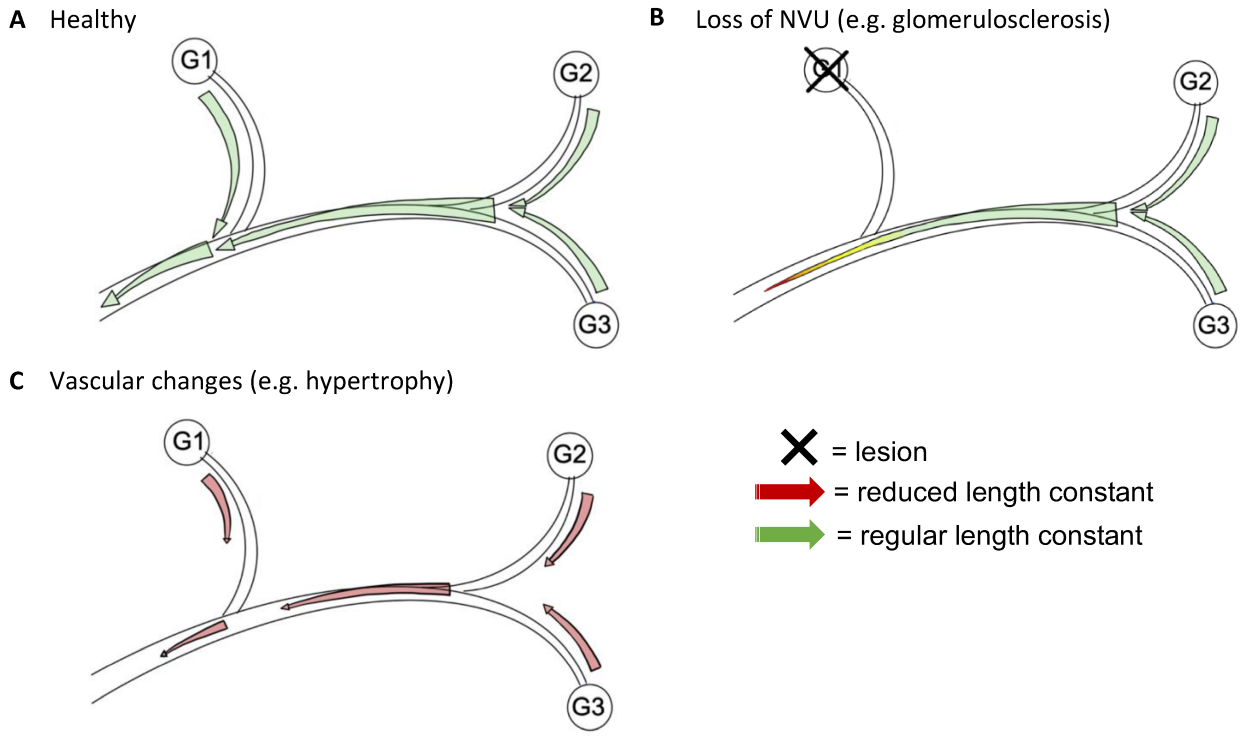

Figure 2.3. TGF signal ascending into the artery and pathological situations that impair transmission. A) shows upstream transmission of the TGF signal from each glomerulus, where it can interact with other TGF signals and affect autoregulation in other NVUs as they continue upstream. B) In situations of glomerular or vascular lesions, the NVU completely "drops out" of the nephrovascular network. The TGF signal from G2 and G3 will have a shorter interaction radius without the addition of the signal from G1. C) changes to the vessel such as hypertrophy of the smooth muscle layer in hypertension also shorten the interaction radius and result in reduced length constant, meaning the signal does not transmit as far. Thickness of the arrows represents the magnitude of the TGF signal. Not shown here for the sake of simplicity is that TGF signals also travel upstream to neighbouring afferent arterioles where the signals can interact as well.

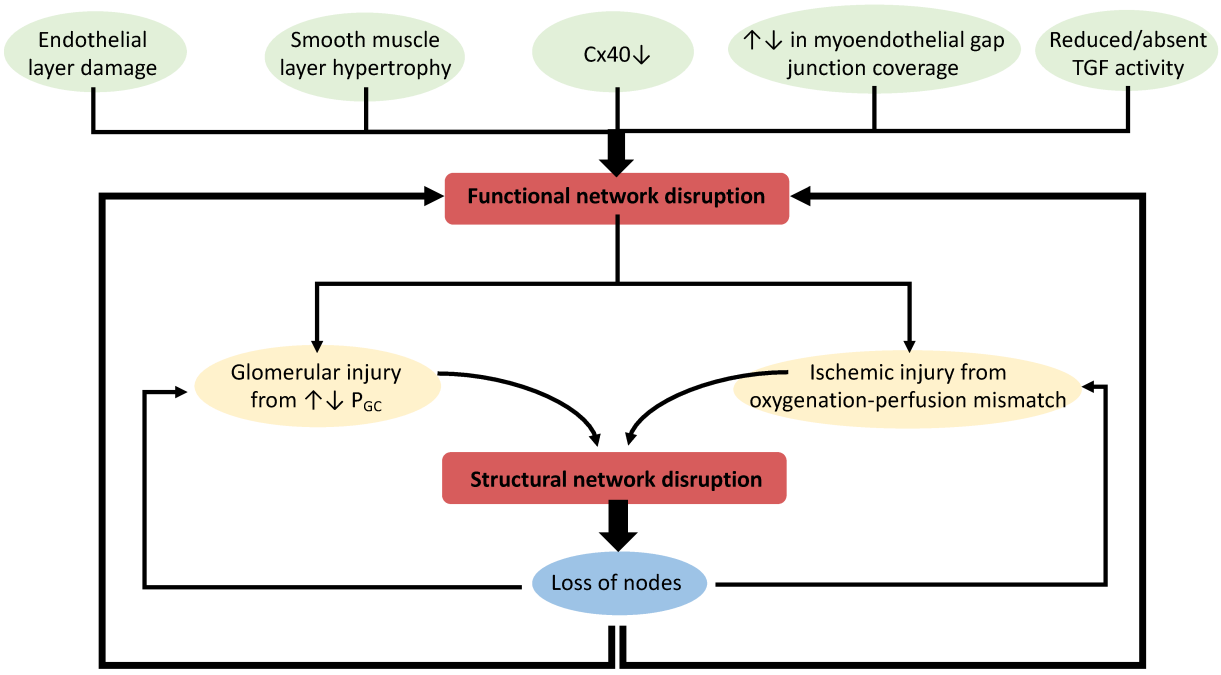

Figure 2.3. Pathophysiological changes in the nephrovascular network. Functional disturbances to the nephrovascular network contribute to failing or loss of nodes from the network. These derailments include microvascular alteration or damage, decreased Cx40, changes in MEGJs, and reduced or absent TGF signals, increase susceptibility of glomerular injury from unregulated P_{GC} and ischemic injury from oxygenation-perfusion mismatches. As the network starts to fall apart and lose elements, the likelihood of glomerular and ischemic injury increases and functional network disruptions worsens, exacerbating structural disruption.

CHAPTER 3: METHODOLOGY

Methods

All experiments received prior approval by the Animal Care Committee of the University of Alberta and were conducted in accordance with the guidelines of the Canadian Council on Animal Care. Male Lewis rats (350-450 g) (Charles River, St. Constant, QC, Canada) were housed in a temperature- and humidity-controlled environment with a 12:12 h light-dark cycle. All rats received regular rat chow and water ad libitum (Canadian Laboratory Diets, Leduc, AB, Canada).

Aim 1: TGF manipulation with furosemide and dapagliflozin

Intact rats (n = 6) to be given furosemide were prepared for acute terminal procedures, as described below. Another group of intact rats to be given dapagliflozin (n = 6) were prepared similarly; this group of rats is the same one used in Aim 3.

Four out of ten animals in the furosemide group were excluded from analysis because of low blood pressure by the end of the experiment, leaving six animals for full analysis. Three out of nine animals were excluded from the dapagliflozin group because of low blood pressure, leaving six for the full analysis.

Aim 2: TGF synchronization in the remnant kidney

Male Lewis rats were randomly assigned to the following groups: remnant kidney (RK) 1-week (n = 4), RK 6-weeks (n = 6), and their sham-operated 1-week (n = 7) and 6-weeks (n = 7) counterparts serving as controls. 5/6th nephrectomies were performed to create the remnant kidney model of CKD. After 1 or 6 weeks, all rats were subjected to acute procedures.

Four out of nine animals were excluded from RK 1wk because of low blood pressure. Seventeen animals were part of the RK 6wk group but all except six were excluded because of low blood pressure or technical difficulties in experimental preparation such as the inability to obtain urine samples. Ten animals were in the sham 1wk group with three being excluded for low blood pressure, and similarly eleven animals were in the sham 6wk group with four excluded from analysis for having low blood pressure.

Aim 3: TGF synchronization in the remnant kidney after dapagliflozin intervention

Male Lewis rats were randomly assigned to the following groups: RK (n = 6) and their sham-operated (n = 6) counterparts. $5/6^{th}$ nephrectomies were performed to create the remnant kidney model of CKD. The sham controls in this group are the same animals in the dapagliflozin group used in Aim 1. After 6 weeks, all rats were subjected to acute procedures during which they were acutely administered dapagliflozin.

Three out of nine animals were excluded from both the sham group and RK because of low blood pressure, leaving six for the full analysis. One animal in the RK group had a large decrease in blood pressure in the first 25 min and stable blood pressure thereafter, so the first 25 mins were excluded from analysis.

$5/6^{th}$ nephrectomy procedure

Each rat received buprenorphine (0.02 mg/kg) and meloxicam (2 mg/kg) subcutaneously before anesthesia. Anesthesia was induced with 4% isoflurane in inspired air (45% O_2). After induction, the rat was transferred to a surgical table heated with gel pads. Ophthalmic ointment (OptixCare, CLC MEDICA, Ontario, Canada) was applied to the rat's eyes. Hair from the right

flank was removed by shaving, and the surgical field was cleansed with alternating applications of 10% povidone iodine (Prepodyne, West Penetone Inc., Canada) and 70% ethanol. Under aseptic conditions, the right kidney was exposed following a flank incision and two 4-0 silk sutures (Braintree Scientific, Braintree, MA, USA) were tied around the renal vessels, with enough gap between each to make a cut to perform a total nephrectomy. After suturing the incision close (3-0 Chromic Gut, Ethicon, NJ, USA), antiseptic ointment was applied over the suture site. A second dose of meloxicam (2 mg/kg) was given 24 h after the procedure.

One week after the total right nephrectomy, the same procedure was repeated to perform the partial left nephrectomy. After exposing the left kidney, the upper and lower poles were cut and Surgifoam (Ethicon US, LLC) and pressure were applied on the cut ends to facilitate blood clotting. The remaining kidney was placed back into the abdomen and the incision was closed. Sham-operated animals were subjected to exploratory surgery only.

One week after the partial left nephrectomy, all rats were switched to a high salt diet formulated with 6% NaCl (Canadian Laboratory Diets, Leduc, AB, Canada) ad libitum and given free access to water until their acute procedure.

Acute procedure

All rats were subjected to the acute procedure as follows. Rats were given buprenorphine (0.02 mg/kg) subcutaneously 20 min before anesthesia. Anesthesia was induced in an induction chamber precharged with room air, and isoflurane was introduced up to 4% in inspired air (45% O_2). Once the animal reached surgical plane, it was transferred to a heated surgical table equipped with a thermo-feedback system to maintain rectal temperature at 37°C (Vestavia Scientific, Birmingham, AL, USA). Anesthesia was maintained through a nose cone and the

isoflurane dosage was gradually reduced in 0.5% increments to 2% for the duration of the surgery. Hair from the neck, abdomen and left groin was removed by shaving, and the surgical field was cleansed with alternating applications of 10% povidone iodine and 70% ethanol. After verifying surgical plane with the toe-pinch reflex, a midline incision was made on the neck to expose the trachea. The rat was intubated via tracheotomy (PE 240, VWR, Alberta, Canada) and the tracheal tube was fitted to the nose cone and secured with Parafilm to prevent escape of isoflurane.

The left femoral vein was cannulated (Silastic tubing, 0.51 mm ID, 0.94 mm OD; Dow Corning, Midland, MI) for intravenous infusion of 5% bovine serum albumin (BSA) (A7906; Sigma, Oakville, ON) with 250 µg/min FITC inulin (Sigma) and 50 mM LiCl (Sigma) in 0.9% NaCl at 1.5 mL/h. The left femoral artery was cannulated (PE-50; BD Intramedic) for direct recording of mean arterial pressure and heart rate. The left kidney was exposed by a midline laparotomy, freed from surrounding fat and placed in a plastic kidney cup mounted to the surgical table. The kidney was embedded in silicone stopcock grease (Dow Corning, Midland, MI) to minimize motion. The left renal artery was stripped and a transit time ultrasound flow probe (Transonic, Ithaca, NY) was placed around it for direct measurement of RBF. The flow probe was secured in place with acoustic coupling gel (SurgiLube, Transonic Systems, Ithaca, NY, USA). The left ureter and bladder were catheterized for urine collection (PE-10; BD Intramedic). Except during data acquisition, the surface of the kidney was covered with Parafilm to prevent drying and was periodically moistened with normal saline. Anesthesia was reduced to the lowest dose (1.5%) that prevented responses to toe pinching, the intravenous infusion solution was switched to a mixture of 1% BSA with 250 µg/min FITC inulin and 50 mM LiCl in 0.9% NaCl at 1.5 mL/h during equilibration, and the animal was allowed to stabilize for 40 min.

Following equilibration, the kidney surface was cleaned with normal saline. The Moor FLPI LSCI (Moor Instruments, Axminster, UK) was positioned ~18 cm above the surface of the kidney. The instrument was modified by the manufacturer to have twice the optical zoom of the standard mode, permitting a small field of view (3.5 x 5 mm). In rats with the RK, there was enough kidney tissue remaining to position the LSCI on top. The imager was used for spatial and temporal calculation of laser speckle for each experiment; the spatial mode analyzes a small group of pixels (5x5) within a single frame, acquiring 113 x 152-pixel images at 25 Hz whereas the temporal mode analyzes single pixels over 25 frames, acquiring 760 x 568-pixel images at 1 Hz. The advantage of the temporal speckle is that the information is captured at high resolution, but it cannot be used to detect MR in rats because the process of averaging each pixel aliases heart rate into the MR frequency. Before beginning recordings, a 4 mm hair was placed on the kidney surface to determine pixel size and assist with focusing the LSCI camera. Approximately one-third of the dorsal surface was imaged. Previous work has shown that record lengths of 30 – 50 cycles of oscillation (1500 s) are needed to investigate TGF synchronization [64]. Based on this we used a record length of 25 min for each spatial and temporal record and made two sets of each recording per experiment.

Furosemide administration. After the baseline spatial and temporal records were made with the LSCI, a bolus of furosemide (5 mg/kg) was administered via the left femoral vein. Following the bolus, the animal was switched to 1% BSA with 5 mg/kg/hr furosemide, 250 µg/min FITC inulin and 50 mM LiCl in 0.9% NaCl. The infusion rate was determined over a 25 min period of equilibration following administration of the bolus by determining the volume of urine produced and was set to 5 mL/h. Recording with LSCI commenced again with two 25 min records in spatial and temporal averaging modes obtained.

Dapagliflozin administration. After the baseline spatial and temporal records were made with the LSCI, a bolus of dapagliflozin (1 mg/kg) was administered to the rat through the femoral vein followed by a switch to an intravenous infusion of 1% BSA with 1 mg/kg/hr dapagliflozin, 250 μg/min FITC inulin and 50 mM LiCl in 0.9% NaCl. The infusion rate was determined over a 25 min period of equilibration by determining the volume of urine produced and was set at 2 mL/h. After equilibration, spatial and temporal records were made again.

A baseline arterial blood sample (400 μL) was taken and urine collection commenced. Following each LSCI record, timed urine samples were collected every 30 min for a total of 4 samples. Arterial blood samples were collected every 60 min for a total of 3 samples. At the end of each experiment, the left kidney was excised and immediately prepared for immunofluorescence and also snap-frozen and stored in -80°C to use for western blots.

Data analysis

Blood pressure and renal blood flow data was collected and stored on a PC using PowerLab Data Acquisition System (8/30; ADInstruments, Dunedin, NZ) and LabChart 6 Software. These data were reconfigured to be compatible with Matlab to allow cross-correlation with LSCI data.

This experiment reports MR values calculated from spatial records, and TGF values from both spatial speckle and temporal speckle for comparison, denoted by (S) and (T) in subscripts next to the variable names, respectively. Briefly, changes in synchronization among regions on the renal surface were determined by three measurements: 1) the strength and variability of synchronization of MR and TGF, 2) the decay of TGF synchronization with distance, and 3) heterogeneity in cortical perfusion.

Each spatial record was filtered with a Gaussian filter and then down-sampled by a factor of 4, yielding a 21 x 31-pixel image for each frame. Temporal records were similarly filtered with a Gaussian filter and then down-sampled by a factor of 20, yielding a 21 x 31-pixel image. Each pixel's timeseries was then normalized so that they had a standard deviation of 1. The MR (0.09 – 0.3 Hz) and TGF (0.015 – 0.07 Hz) frequency of each pixel timeseries was isolated by a bandpass forward-backward elliptic filter to avoid phase-shift, and the records were temporally downsampled.

1) *Strength and variability of synchronization of MR and TGF*

The strength of the phase synchronization of MR and TGF were determined by calculating phase coherence (PC). The Hilbert transform of each pixel timeseries was used to calculate the instantaneous phase. Synchronization was assessed by a pairwise comparison between all possible pairs of imaged pixels to calculate PC,

$$PC_{jk} = \left| \frac{1}{N} \sum_{m=1}^{N} e^{i(\phi_j - \phi_k)} \right|$$

where PC_{jk} is the phase coherence between two pixels *j* and *k*, where N is the number of points in the original data, and ϕ_j and ϕ_k are the instantaneous phases of pixels *j* and *k*, respectively. It is the mean of the exponential difference between the instantaneous phases of two pixels over time. PC is a value between 0 and 1, where PC = 0 means no relationship exists between two pixels, and PC = 1 indicates complete 1:1 phase locking [64].

To determine what values of PC could be considered significant, a surrogate data approach was used and PC was computer over an entire 1500 s record. Surrogates with random phases but unchanged power spectra were generated by using Fourier Fast Transform (FFT) of the timeseries which gives the power spectrum, then phases of the FFT were randomly shuffled

without altering the amplitude spectrum, and the FFT of the phase-randomized spectrum was inversed. For each pixel pair, surrogates were generated by applying FFT to each trial 50 times and computing PC between the original timeseries of one pixel and the randomized values of the second pixel's time series, giving a total of 100 randomized PC values to estimate significance. The significance threshold was set as the mean ± two standard deviations of the surrogate PC data for that pixel pair. Pixel pairs with PC less than the threshold were considered to be nonsignificant and excluded from further analyses. Increased mean PC reflects stronger synchronization, whereas decreased PC indicates weaker synchronization. In addition to average PC (PC_{MR} and PC_{TGF}), coefficients of variation of PC ($CV_{PC,MR}$ and $CV_{PC,TGF}$) were calculated which indicate variability in synchronization.

To visualize the group characteristics of TGF synchronization, the renal surface was reconstructed using graph analysis [6,89]. In this graph, each downsampled pixel was treated as a node and was connected to other nodes when significant PC existed between that pair of pixels; this connection is known as an edge. An increase in the number of significant edges as well as longer edge lengths indicate increased and long-distance synchronization between kidney regions. We limited our analysis to edges with $PC > 0.6$ based on previous studies that found edges with $PC \leq 0.5$ in the absence of autoregulation [8,70], and excluded lengths of 1 and $\sqrt{2}$ because pixels immediately adjacent are expected to have high PC that would inflate the overall analysis.

2) *Decay of TGF synchronization with distance*

We tried several non-linear regression models to fit the relationship between PC and edge length, using exponential decay, double exponential, piece-wise linear, and sum of exponentials

fits. We found that piece-wise linear and sum of exponentials best represented our data (lowest MSE, most even distribution of residuals). We chose sum of exponentials over piece-wise linear because the exponential decay terms were more readily interpretable in the physiological context of synchronization,

$$PC = Ae^{\frac{length}{-k_1}} + e^{\frac{length}{-k_2}} - A$$

where A is the magnitude of the decay of PC over edge length, e is the base of natural logarithms, and k_1 and k_2 are length constants. We constrained the fit to PC = 1 at edge length = 0 based on the assumption that two nodes that are very close together (shorter edge length) will have greater synchronization and a PC value close to 1. We calculated the maximum distance that TGF synchronization occurs over in the kidney ($length_{max}$) by calculating the x-intercept of the equation to determine what length PC = 0 when synchronization has become absent.

3) *Heterogeneity in cortical perfusion*

Dominant operating frequencies of MR and TGF (f_{MR} and f_{TGF}) were calculated for each pixel as the frequency at which power was highest in the MR (0.09– 0.3 Hz) and TGF (0.015–0.06 Hz) frequency ranges. Spatial heterogeneity of each operating frequency was determined as the coefficient of variation of frequency in the entire image ($CV_{f,MR}$ and $CV_{f,TGF}$), which indicates the degree of frequency coupling on the kidney surface. Increased heterogeneity suggests that fewer regions of the kidney are entrained with each other.

The spatiotemporal heterogeneity of cortical perfusion was determined by calculating the coefficient of variation of the LSCI speckle of all pixels in every frame ($CV_{spatial}$) and then determining the temporal coefficient of variation ($CV_{temporal}$)

$$CV_{temporal} = \frac{stdev(CV_{spatial})}{mean(CV_{spatial})} \times 100\%$$

Increased $CV_{spatial}$ indicates that the heterogeneity of blood flow on the renal surface is increased. Increased $CV_{temporal}$ indicates increased epochs of $CV_{spatial}$, or in other words that spatial $CV_{spatial}$ fluctuates over time.

Assessment of Cx40 expression

Immunofluorescence. Immediately after the acute procedure, the left kidneys were excised and prepared for immunofluorescence (IF). A frontal cut of the kidney tissue was placed in 30% sucrose for 24 hr, mounted in OCT and stored in a freezer at -80°C. The block was sectioned into slices about 10 μm in thickness. The slice was fixed with ice-cold acetone and blocked in 10% normal donkey serum in PBS-T-1% BSA solution for 1-2 hrs. The primary antibodies that were used, Cx40 polyclonal antibody (Thermo Fisher Scientific REF: 36-4900) and CD31 monoclonal antibody (Thermo Fisher REF: MA1-81051), were diluted 1:200 in blocking solution and used to incubate the kidney tissue overnight. The secondary antibodies used, donkey - Alexa Fluor® 568 dye (Thermo Fisher Scientific REF: A10042) and anti-mouse - Alexa Fluor® 647 dye (Thermo Fisher Scientific REF: A31571) were diluted 1:600 and 1:1000 respectively, blot with the kidney tissue for one hour, and followed by the 0.1 μg/mL DAPI staining for 5 min. The slice was then mounted with Prolong Gold antifade reagent (Thermo Fisher Scientific: REF: P36934).

The stained slide was detected with Quorum Wave FX spinning disc confocal system (Quorum technology). The positive staining of CD31 and Cx40 were acquired in Cy5 (690/50) and Cy3 (595/50) using Perkin Elmer's Volocity. The pre-glomerular arterioles were determined

by CD31 positive signals and by the smooth muscle layer around the endothelium. The Cx40 intensity on these arterioles was calculated using Volocity 6.3.1 software.

Statistical analysis

Hemodynamic variables for all experiments were analyzed using Two Way repeated-measures (RM) ANOVA to account for the effect of group and time. Student-Newman-Keuls was used as the post hoc test. The differences between variables calculated from LSCI analysis for Aim 1 were analyzed with Two Way RM ANOVA, with the two factors being period (baseline vs. intervention) and group (furosemide vs. dapagliflozin). Similarly, LSCI data from Aim 3 was analyzed with Two Way RM ANOVA, with period (baseline vs. intervention) and group (sham controls vs. remnant kidney) factors. LSCI data for Aim 2 was analyzed with One Way RM ANOVA with the factor being group. Western blot data was analyzed with One Way ANOVA. These statistical tests were performed on groups of 4-7 individuals, therefore it is difficult to assume that these data approach a normal distribution even if a statistical test cannot reject the null hypothesis that it is non-normal. Data analysis was performed in Matlab (r2019a, The Mathworks, Natick, MA) and statistical tests were performed in SigmaPlot (v14). Data are shown as mean ± SEM , and $p < 0.05$ was considered statistically significant.

CHAPTER 4: RESULTS

Results

Urine excretion.

Figure 4.1 shows GFR and urine flow data, which is summarized in Table 4.1, during baseline and after furosemide or dapagliflozin administration in intact rats. GFR increased after furosemide and decreased after dapagliflozin administration, and urine flow was increased after interventions in both groups.

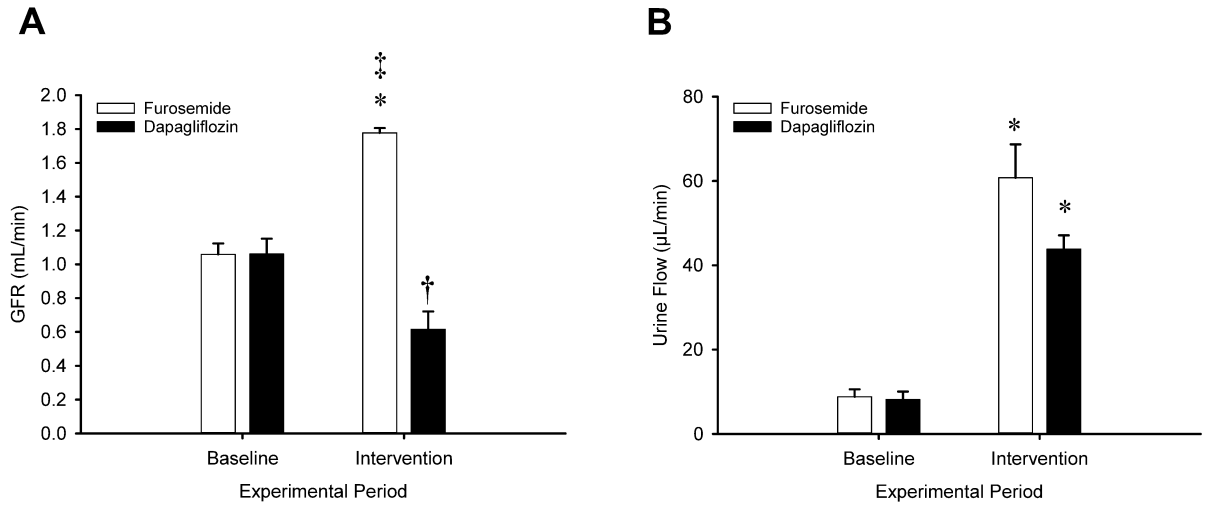

Figure 4.1. Changes in glomerular filtration rate (GFR) and urine flow after furosemide and dapagliflozin interventions. Furosemide increased GFR and urine flow (*$p < 0.001$ in both cases), whereas dapagliflozin decreased GFR (†$p = 0.008$) and increased urine flow (*$p < 0.001$). GFR was higher after furosemide than dapagliflozin at intervention (‡$p < 0.001$) (Two Way RM ANOVA). Data are shown as mean ± SEM; n = 6 furosemide; n = 6 dapagliflozin.

Table 4.1. Glomerular filtration rate (GFR) and urine flow data after furosemide and dapagliflozin administration.

	Furosemide		Dapagliflozin	
	Baseline	Intervention	Baseline	Intervention
GFR, mL/min	1.06 ± 0.06	1.78 ± 0.03†	1.06 ± 0.09	0.62 ± 0.11*
Urine flow, µL/min	9 ± 2	61 ± 8†	8 ± 2	44 ± 3†

Values are presented as mean ± SEM; n = 6 furosemide; n = 6 dapagliflozin. Shown are urinary excretion data obtained from healthy rats given furosemide or dapagliflozin. MAP, mean blood pressure; RBF, renal blood flow; RVC, renal vascular conductance; HR, heart rate; GFR, glomerular filtration rate. *p = 0.049, †p < 0.001 (Two Way RM ANOVA).

Figure 4.2 shows GFR and urine flow data for RK 1wk, RK 6wk and their sham controls, which is summarized in Table 4.2. RK 6wk had significantly lower GFR compared to all groups.

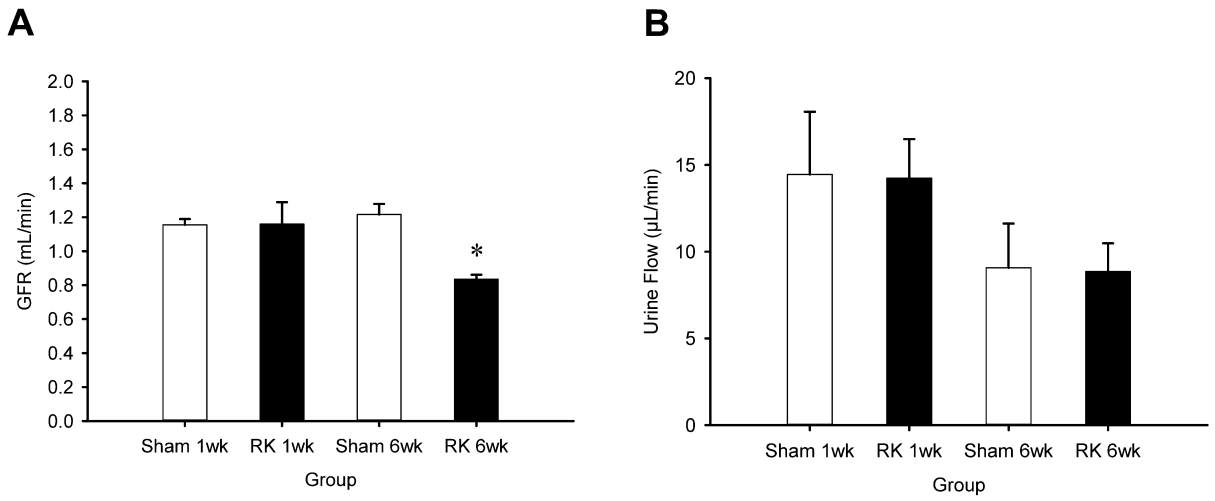

Figure 4.2. Changes in glomerular filtration rate (GFR) and urine flow in RK 1wk, RK 6wk and sham controls. RK 6wk had lower GFR compared to RK 1wk and sham counterparts (*p < 0.001) (Two Way RM ANOVA). Data are shown as mean ± SEM; n = 7 sham 1wk; n = 4 RK 1wk; n = 7 sham 6wk; n = 6 RK 6wk.

Table 4.2. Glomerular filtration rate (GFR) and urine flow data from RK 1wk, RK 6wk and sham controls.

	Sham 1wk	RK 1wk	Sham 6wk	RK 6wk
GFR, mL/min	1.16 ± 0.03	1.16 ± 0.13	1.22 ± 0.06	0.84 ± 0.03*
Urine flow, μL/min	14 ± 4	14 ± 2	9 ± 3	9 ± 2

Values are presented as mean ± SEM; n = 7 sham 1wk; n = 4 RK 1wk; n = 7 sham 6wk; n = 6 RK 6wk. Shown are hemodynamic and urinary excretion data obtained from rats with remnant kidneys for 1 week or 6 weeks and their respective sham controls. RK, remnant kidney; SRK, sham remnant kidney; MAP, mean blood pressure; RBF, renal blood flow; RVC, renal vascular conductance; HR, heart rate; GFR, glomerular filtration rate. *$p < 0.001$ (Two Way RM ANOVA).

Analysis of GFR and urine flow data in Figure 4.3, which is summarized in Table 4.3, show that both RK and sham controls had comparable GFR during baseline. After dapagliflozin, GFR decreased significantly in both groups. Urine flow similarly show comparable values at baseline with a significant increase after dapagliflozin in both groups. RK and sham groups did not have significantly different GFR and urine flow at baseline and after dapagliflozin.

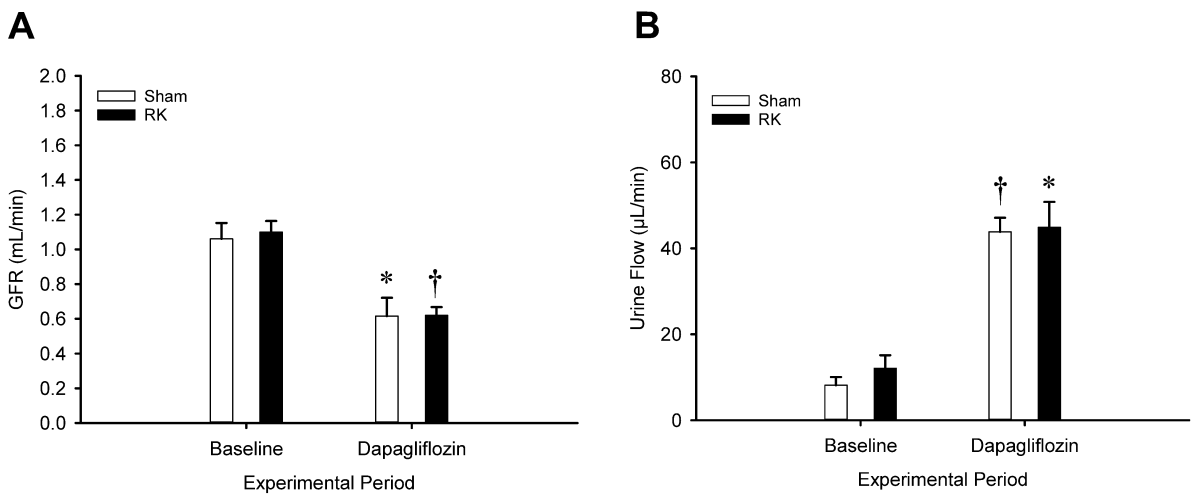

Figure 4.3. Changes in glomerular filtration rate (GFR) and urine flow in RK and sham controls administered dapagliflozin. Dapagliflozin comparably *A:* decreased GFR in sham controls (*p = 0.008) and RK (†$p < 0.001$), and *B:* increased urine flow in shams controls (†$p < 0.001$) and RK (*p = 0.003) (Two Way RM ANOVA). Data are shown as mean ± SEM; n = 6 sham controls; n = 6 RK.

Table 4.3. Glomerular filtration rate (GFR) and urine flow data from RK and sham controls administered dapagliflozin.

	Sham Controls		RK	
	Baseline	Dapagliflozin	Baseline	Dapagliflozin
GFR, mL/min	1.06 ± 0.09	0.62 ± 0.11*	1.10 ± 0.06	0.62 ± 0.05†
Urine flow, µL/min	8 ± 2	44 ± 3†	12 ± 3	45 ± 6*

Values are presented as mean ± SEM; n = 6 sham; n = 6 RK. Shown are hemodynamic and urinary excretion data from rats with RK for 6 weeks and their sham controls given dapagliflozin. RK, remnant kidney; MAP, mean blood pressure; RBF, renal blood flow; RVC, renal vascular conductance; HR, heart rate; GFR, glomerular filtration rate. *p = 0.05, †p = 0.001 (Two Way RM ANOVA).

Strength and variability of synchronization.

Table 4.4 summarizes variables that assess the strength and heterogeneity of synchronization of MR and TGF after furosemide and dapagliflozin. The strength of synchronization was quantified with phase coherence (PC) and by the number and length of significant edges (PC > 0.6) (Figure 4.4). Neither mechanism was significantly affected by either furosemide or dapagliflozin. The variability in synchronization was assessed by the variation in PC associated with MR and TGF. CV_{PC} associated with both MR and TGF were unchanged after furosemide and dapagliflozin.

Table 4.4. Assessment of the strength and heterogeneity in synchronization after acute furosemide and dapagliflozin administration.

	Furosemide		Dapagliflozin	
	Baseline	Intervention	Baseline	Intervention
MR				
PC_{MR}	0.37 ± 0.03	0.29 ± 0.02	0.39 ± 0.05	0.37 ± 0.03
$CV_{PC,MR}$, %	20.0 ± 2.1	23.0 ± 2.5	21.2 ± 4.6	20.3 ± 4.3
#Edges for high PC (>0.6)	3764 ± 742	939 ± 281	9344 ± 6094	5558 ± 2932
Length, high PC, mm	0.09 ± 0.01	0.08 ± 0.00	0.11 ± 0.03	0.10 ± 0.02
TGF (Spatial speckle)				
$PC_{TGF(S)}$	0.72 ± 0.03	0.67 ± 0.03	0.66 ± 0.02	0.68 ± 0.01
$CV_{PC,TGF(S)}$, %	12.2 ± 2.0	12.7 ± 2.3	12.3 ± 1.3	12.2 ± 1.2
#Edges for high PC (>0.6)	179132 ± 16897	155739 ± 21068	160138 ± 18245	163579 ± 16499
Length, high PC, mm	0.48 ± 0.01	0.45 ± 0.03	0.45 ± 0.03	0.47 ± 0.01
TGF (Temporal speckle)				
$PC_{TGF(T)}$	0.70 ± 0.04	0.70 ± 0.05	0.74 ± 0.02	0.72 ± 0.03
$CV_{PC,TGF(T)}$, %	15.2 ± 2.2	12.3 ± 2.2	10.0 ± 1.5	12.6 ± 1.9
#Edges for high PC (>0.6)	154647 ± 23160	167838 ± 29001	194836 ± 11563	176273 ± 12707
Length, high PC, mm	0.51 ± 0.03	0.52 ± 0.05	0.57 ± 0.02	0.54 ± 0.03

Values are presented as mean ± SEM; n = 6 furosemide; n = 6 dapagliflozin. Shown is a summary of cluster and graph analysis to assess the strength and variability of synchronization after furosemide and dapagliflozin interventions. MR, myogenic response; TGF, tubuloglomerular feedback; PC, phase coherence; PC_{MR} and PC_{TGF}, mean PC of edges in MR and TGF frequency bands; $CV_{PC,MR}$ and $CV_{PC,TGF}$, coefficients of variation of PC in MR and TGF frequency bands; length, mean length of edges detected in the field of view; S, spatial speckle; T, temporal speckle. There were no changes after the interventions were administered (Two Way RM ANOVA).

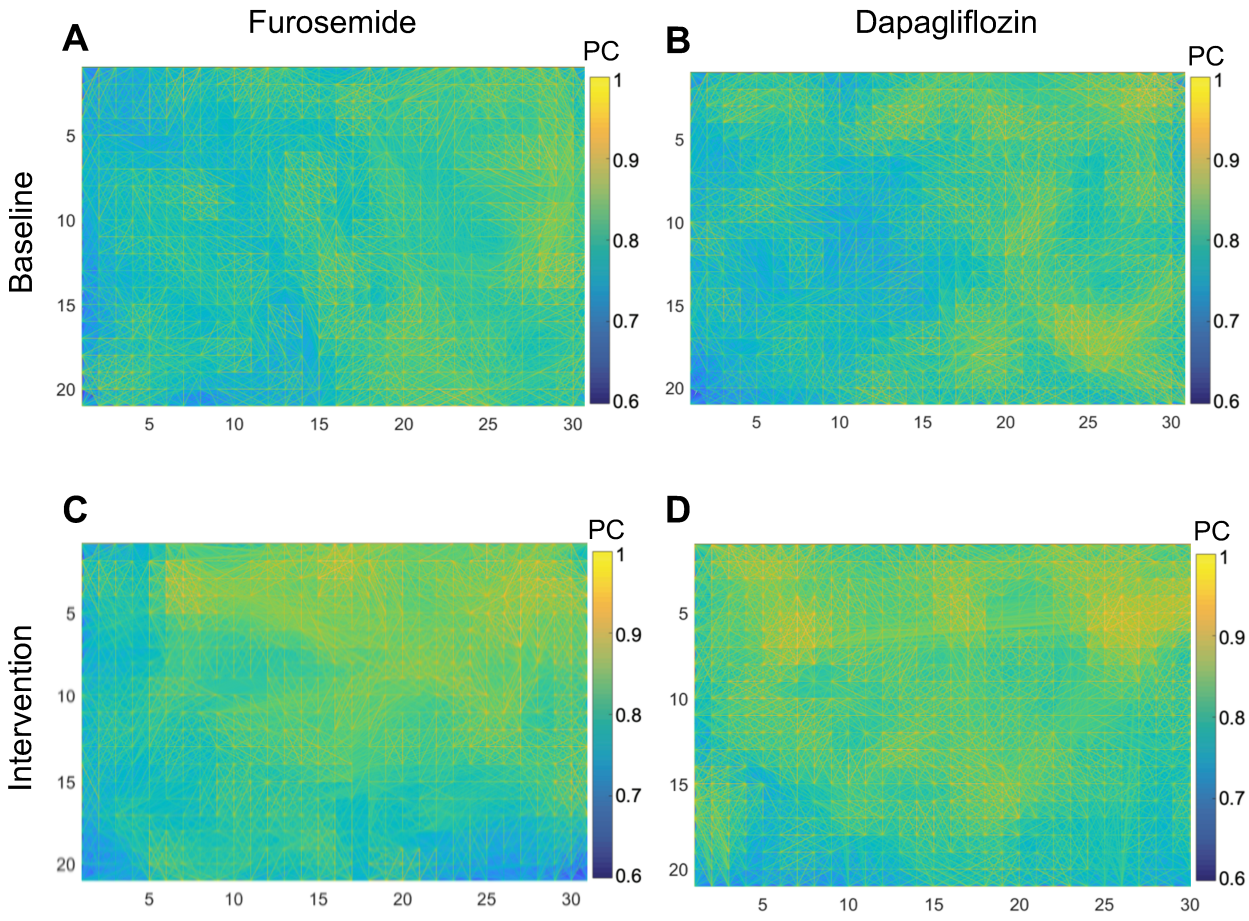

Figure 4.4. Graph representation of the phase coherence of tubuloglomerular feedback (PC_{TGF}) synchronization at the kidney surface after acute furosemide and dapagliflozin interventions. These results are from spatial speckle from individual rats. LSCI pixels are depicted as nodes (orange dots); each node is connected to every other node with an edge that has significant PC. The color of the edge corresponds to the strength of PC between the pair of connected nodes. In this rat, furosemide intervention did not alter $PC_{TGF(S)}$ (0.69 to 0.71), $CV_{PC,TGF(S)}$ (8.9% to 10%), or the number of TGF edges (195304 to 2019125). Dapagliflozin did not alter $PC_{TGF(S)}$ (0.67 to 0.71), $CV_{PC,TGF(S)}$ (11% to 9%), or the number of TGF edges (172655 to 199091).

Table 4.5 summarizes the strength and heterogeneity of synchronization in the remnant kidney. The strength of MR synchronization was increased in the early remnant kidney, as shown by high values of PC_{MR}, and CV_{MR} was decreased which reflects increased homogeneity in MR synchronization. The number of MR edges were also significantly higher, suggesting increased extent of MR synchronization. In the remnant kidney at 6 weeks, TGF synchronization was significantly diminished which is denoted by decreased $PC_{TGF,}$ while MR synchronization was unaffected (Figure 4.5). The number of TGF edges decreased in RK 6wk and TGF edge lengths from temporal speckle decreased, indicating reduced strength and extent of distribution of TGF synchronization.

Table 4.5. Assessment of the strength and heterogeneity in synchronization in RK 1wk, RK 6wk and sham controls.

	Sham 1wk	RK 1wk	Sham 6wk	RK 6wk
MR				
PC_{MR}	0.32 ± 0.02	0.54 ± 0.03*	0.32 ± 0.03	0.28 ± 0.02
$CV_{PC,MR}$, %	22.1 ± 2.3	8.6 ± 1.1†	23.4 ± 2.5	25.6 ± 1.8
#Edges for high PC (>0.6)	2698 ± 730	56254 ± 31698†	2375 ± 662	1225 ± 456
Length, high PC, mm	0.09 ± 0.01	0.22 ± 0.06†	0.09 ± 0.00	0.09 ± 0.00
TGF (Spatial speckle)				
$PC_{TGF(S)}$	0.66 ± 0.03	0.64 ± 0.06	0.70 ± 0.02	0.56 ± 0.03‡
$CV_{PC,TGF(S)}$, %	14.0 ± 1.8	13.1 ± 2.4	12.8 ± 1.2	17.5 ± 1.5
#Edges for high PC (>0.6)	127148 ± 19315	124198 ± 32197	165547 ± 10937	84831 ± 19155‡
Length, high PC, mm	0.44 ± 0.03	0.37 ± 0.05	0.48 ± 0.01	0.36 ± 0.04‡
TGF (Temporal speckle)				
$PC_{TGF(T)}$	0.68 ± 0.03	0.62 ± 0.06	0.64 ± 0.02	0.26 ± 0.02§
$CV_{PC,TGF(T)}$, %	13.9 ± 1.5	14.2 ± 2.3	11.1 ± 1.5	15.6 ± 1.5
#Edges for high PC (>0.6)	141052 ± 16488	116266 ± 32559	183601 ± 8283	129230 ± 16574‡
Length, high PC, mm	0.31 ± 0.05	0.39 ± 0.07	0.56 ± 0.01	0.50 ± 0.03

Values are presented as mean ± SEM; n = 7 sham 1wk; n = 4 RK 1wk; n = 7 sham 6wk; n = 6 RK 6wk. Shown is a summary of cluster and graph analysis to assess the strength and variability of synchronization. RK, remnant kidney; MR, myogenic response; TGF, tubuloglomerular feedback; PC, phase coherence; PC_{MR} and PC_{TGF}, average PC of edges in MR and TGF frequency bands; $CV_{PC,MR}$ and $CV_{PC,TGF}$, coefficients of variation of PC in MR and TGF frequency bands; length, mean length of edges detected in the field of view; S, spatial speckle; T, temporal speckle. RK 1wk increased PC_{MR} (*$p < 0.001$), decreased $CV_{PC,MR}$ ($p = 0.002$), increased the number of MR edges ($p = 0.013$), and increased MR edge length ($p = 0.001$), (†$p < 0.05$). RK 6wk decreased $PC_{TGF(S)}$ compared to sham controls (‡$p < 0.05$) and $PC_{TGF(T)}$ compared to RK 1wk and sham controls (§$p < 0.001$). The number of TGF edges from spatial and temporal speckle were significantly lower in RK 6wk compared to sham controls (‡$p < 0.05$). TGF edge length from spatial speckle was lower in RK 6wk than sham controls (‡$p < 0.05$). PC, #edges and length associated with TGF for RK 6wk were significantly different between spatial and temporal speckle ($p < 0.01$) (One Way RM ANOVA).

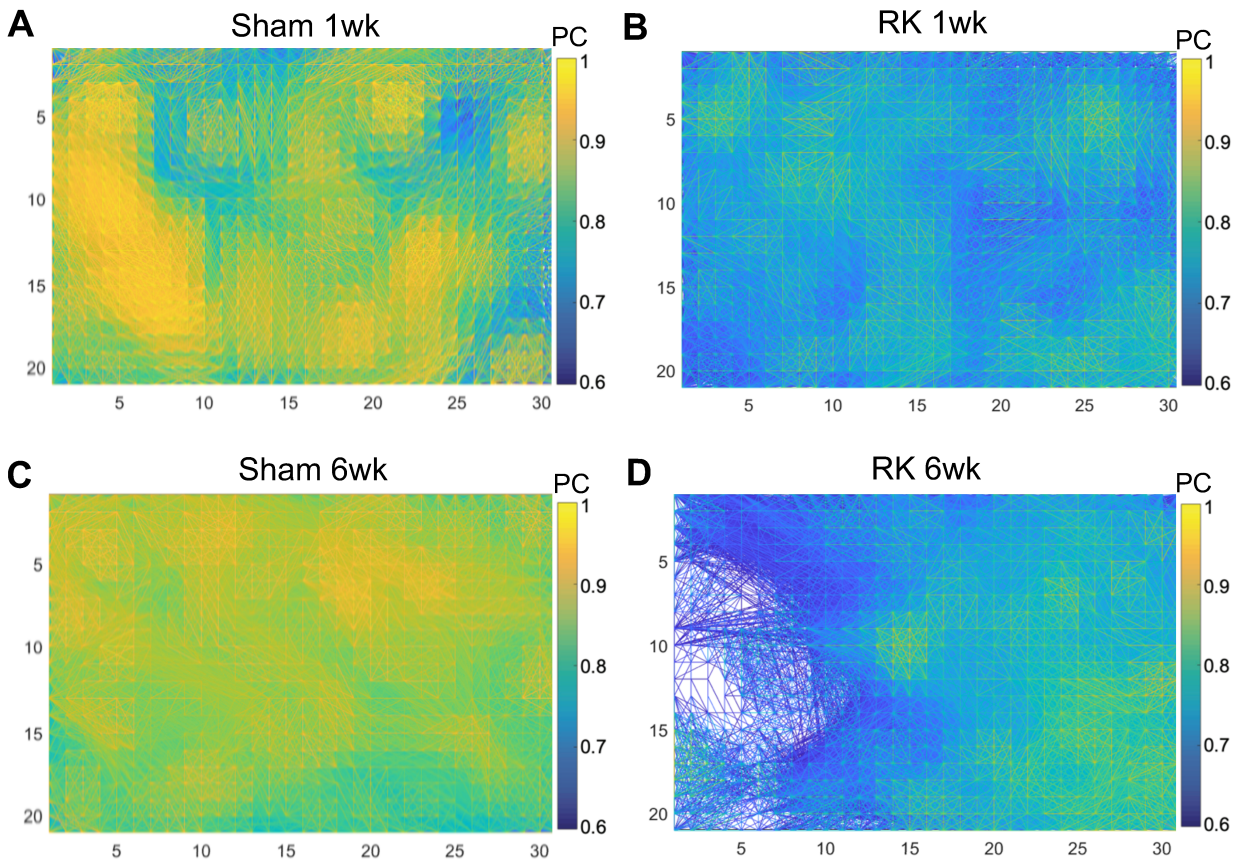

Figure 4.5. Graph representation of the phase coherence of tubuloglomerular feedback synchronization at the kidney surface in RK 1wk, RK 6wk and their sham controls. These results are from spatial speckle from individual rats. LSCI pixels are depicted as nodes (orange dots), each of which is connected to every other node with an edge that has significant PC. The color of the edge corresponds to the strength of PC between the pair of connected nodes. *A:* The sham 1wk rat which had a $PC_{TGF(S)}$ of 0.64, $CV_{PC,TGF(S)}$ of 19% and 85475 TGF edges, in contrast to *B:* the RK 1wk rat which had lower $PC_{TGF(S)}$ of 0.55 and equivalent $CV_{PC,TGF(S)}$ (17%), and a low number of TGF edges (61941). *C:* The sham 6wk rat had $PC_{TGF(S)}$ of 0.75, $CV_{PC,TGF(S)}$ of 11%, and 197707 edges, while *D:* the RK 6wk rat had a lower $PC_{TGF(S)}$ of 0.54, a higher $CV_{PC,TGF(S)}$ of 22% and lower TGF edges (71961). The left side of the graph also depicts areas of scant edges between nodes, indicating reduced strength and extent of synchronization in RK 6wk.

Table 4.6 summarizes changes in synchronization after dapagliflozin intervention. Dapagliflozin did not affect MR synchronization in either group. TGF synchronization was unaltered after intervention in the sham controls, but dapagliflozin increased the strength of TGF synchronization, reflected by increased $PC_{TGF(S)}$, in the RK group (Figure 4.6).

Table 4.6. Assessment of the strength and heterogeneity in synchronization in RK and sham controls administered dapagliflozin.

	Sham Controls		RK	
	Baseline	Dapagliflozin	Baseline	Dapagliflozin
MR				
PC_{MR}	0.39 ± 0.05	0.37 ± 0.03	0.31 ± 0.05	0.34 ± 0.03
$CV_{PC,MR}$, %	21.2 ± 4.6	20.3 ± 4.3	21.4 ± 3.9	20.2 ± 2.4
#Edges for high PC (>0.6)	9344 ± 6094	5558 ± 2932	1805 ± 1019	2116 ± 706
Length, high PC, mm	0.11 ± 0.03	0.10 ± 0.02	0.08 ± 0.01	0.08 ± 0.00
TGF (Spatial speckle)				
$PC_{TGF(S)}$	0.66 ± 0.02	0.68 ± 0.01	0.60 ± 0.05	0.68 ± 0.03*
$CV_{PC,TGF(S)}$, %	12.3 ± 1.3	12.2 ± 1.2	14.1 ± 2.2	11.6 ± 1.4
#Edges for high PC (>0.6)	160138 ± 18245	163579 ± 16499	120138 ± 31842	163579 ± 16499
Length, high PC, mm	0.45 ± 0.03	0.47 ± 0.01	0.40 ± 0.07	0.46 ± 0.03
TGF (Temporal speckle)				
$PC_{TGF(T)}$	0.74 ± 0.02	0.72 ± 0.03	0.70 ± 0.04	0.64 ± 0.07
$CV_{PC,TGF(T)}$, %	10.0 ± 1.5	12.6 ± 1.9	10.5 ± 2.0	14.8 ± 3.5
#Edges for high PC (>0.6)	194836 ± 11563	176273 ± 12707	175376 ± 12707	121426 ± 35905
Length, high PC, mm	0.57 ± 0.02	0.54 ± 0.03	0.54 ± 0.05	0.44 ± 0.08

Values are presented as mean ± SEM; n = 6 sham controls; n = 6 RK. Shown is a summary of cluster and graph analysis to assess the strength and variability of synchronization. RK, remnant kidney; MR, myogenic response; TGF, tubuloglomerular feedback; PC, phase coherence; PC_{MR} and PC_{TGF}, average PC of edges in MR and TGF frequency bands; $CV_{PC,MR}$ and $CV_{PC,TGF}$, coefficients of variation of PC in MR and TGF frequency bands; length, mean length of edges detected in the field of view; S, spatial speckle; T, temporal speckle. Dapagliflozin administration in the RK group increased $PC_{TGF(S)}$ (*p = 0.014). (Two Way RM ANOVA).

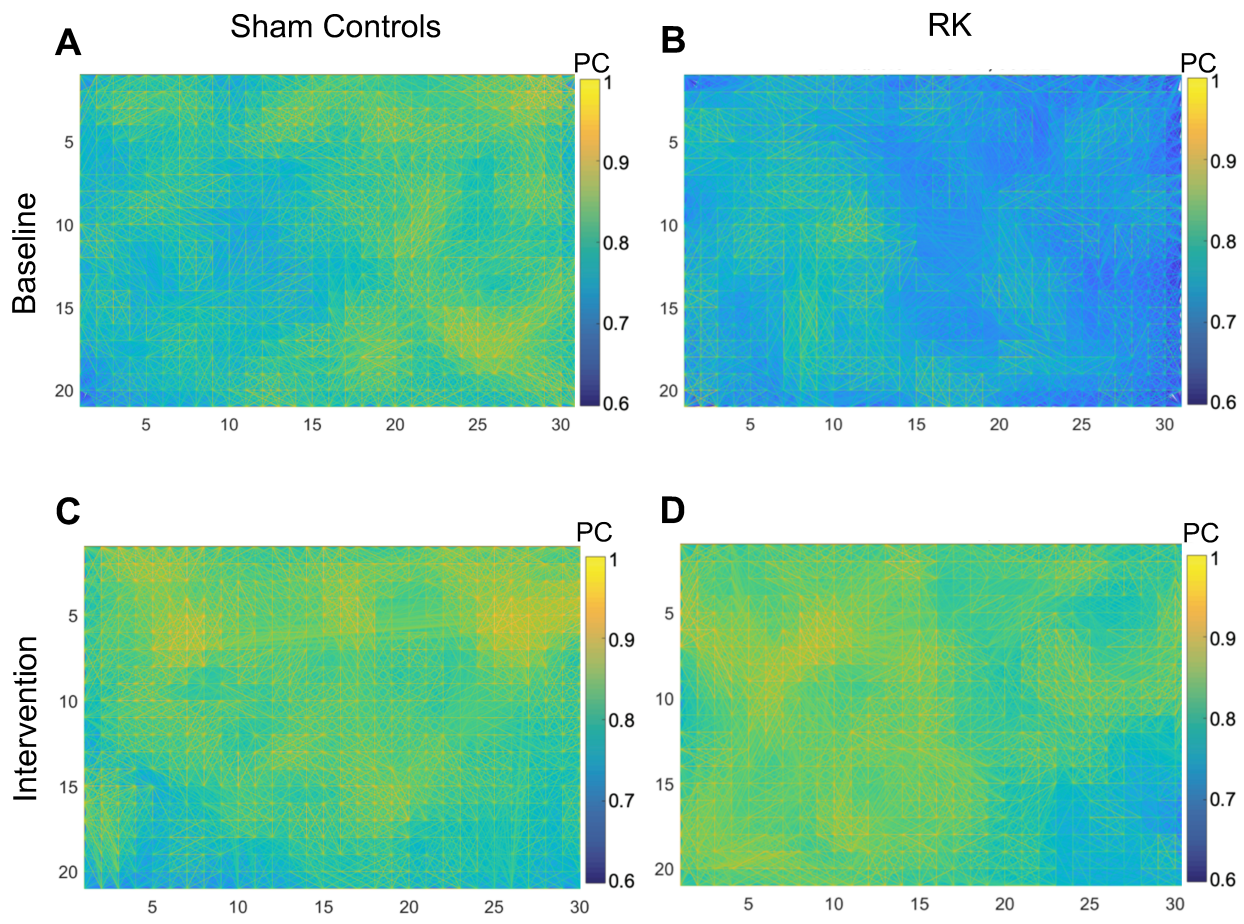

Figure 4.6. Graph representation of the phase coherence of tubuloglomerular feedback (PC_{TGF}) synchronization at the kidney surface in RK and sham controls administered dapagliflozin. These results are from spatial speckle from individual rats. LSCI pixels are depicted as nodes (orange dots), each of which is connected to every other node with an edge that has significant PC. The color of the edge corresponds to the strength of PC between the pair of connected nodes. $PC_{TGF(S)}$ was increased in the RK rat after dapagliflozin administration. Dapagliflozin in the sham control did not alter $PC_{TGF(S)}$ (0.67 to 0.71), $CV_{PC,TGF(S)}$ (11% to 9%), or the number of TGF edges (172655 to 199091). In this RK rat, dapagliflozin increased $PC_{TGF(S)}$ (0.59 to 0.73), reduced $CV_{PC,TGF(S)}$ (15% to 8%), and increased the number of TGF edges (99172 to 207319).

Decay of TGF synchronization with distance.

Figure 4.7 shows a heatmap of the decay of PC associated with TGF (PC_{TGF}) over edge length in one rat at baseline and after furosemide and in a second rat at baseline and after dapagliflozin, which is summarized in Table 4.7. The sum of exponentials equation that was used to describe this decay had two exponential decay equations. The first equation, associated with the first length constant, describes the initial decline of PC_{TGF} over short edge lengths; these occur in the same region of the kidney that the TGF signal originates from. The second decay is associated with the second length constant and describes the decline of PC_{TGF} at longer edge lengths, which occur in different regions of the kidney some distance away from where the signal source was. Spatial speckle showed that furosemide did not affect the decay of PC_{TGF} over short edge lengths, but decreased the distance synchronization travels over long edge lengths. Temporal speckle showed a significant decrease in k_1 compared to the dapagliflozin group after intervention, indicating a more rapid decay of PC_{TGF} at short edge lengths. Dapagliflozin administration did not affect the magnitude of decay of the fast process nor the length constants.

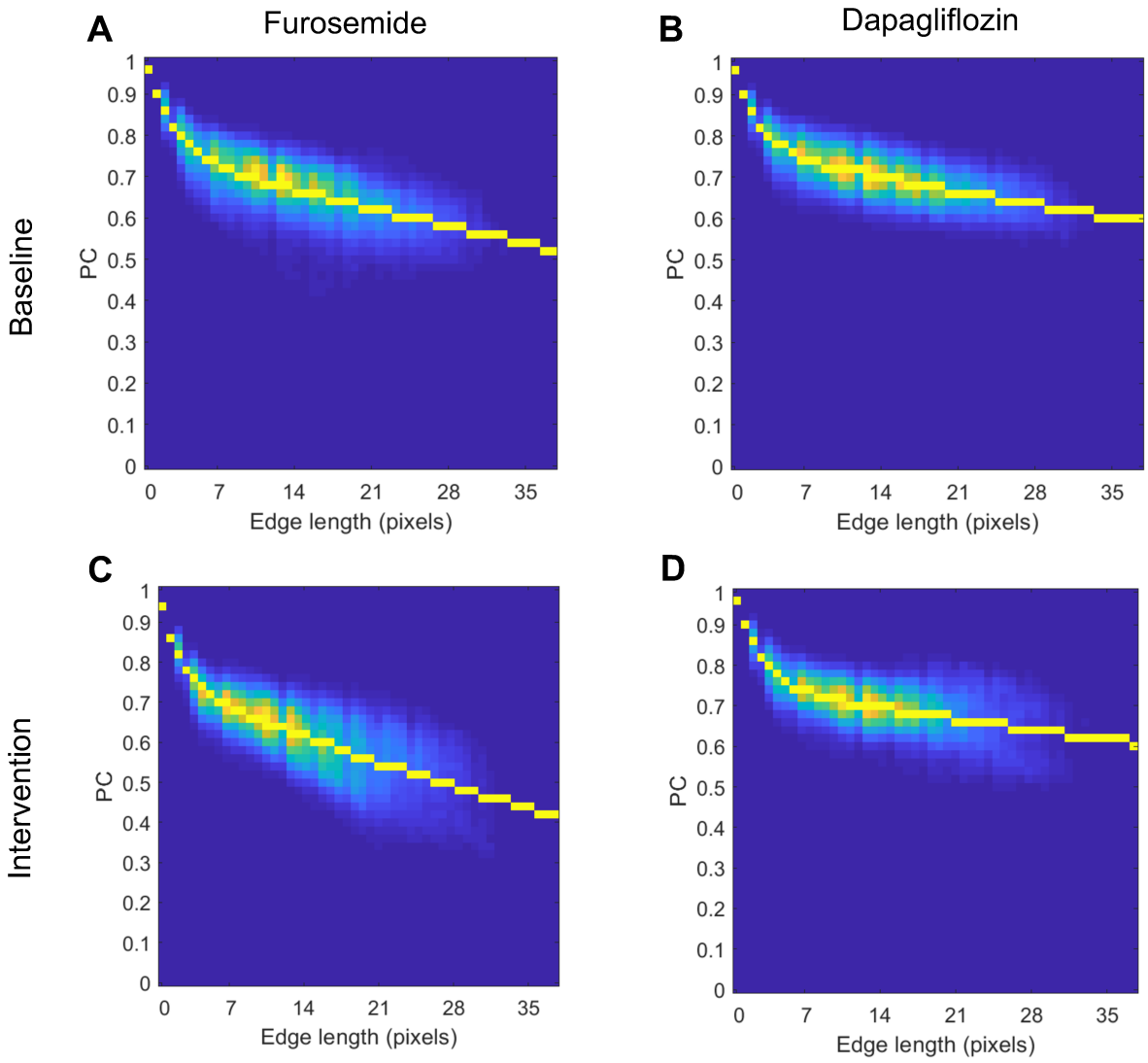

Figure 4.7. Heatmap of the decay of tubuloglomerular feedback phase coherence (PC_{TGF}) with edge length after acute furosemide and dapagliflozin interventions. These results are from spatial speckle. The best-fit curve is overlaid in yellow. Areas of yellow represent a greater number of nodes whereas blue represents a decreased number of nodes. *A* and *C:* In the rat given furosemide, the magnitude of decay *A* (0.23 to 0.24) was unchanged, k_1 (-0.41 to -0.55) decreased and k_2 (-7.28E-03 to -1.10E-02) increased. *B* and *D:* The rat given dapagliflozin showed no significant changes in the magnitude of decay, *A* (0.22 to 0.24), k_1 (-0.43 to -0.42) or k_2 (-5.3E-03 to -4.13E-03).

Table 4.7: Non-linear regression analysis of the decay in tubuloglomerular feedback phase coherence (PC_{TGF}) with edge length after acute furosemide and dapagliflozin administration.

	Furosemide		Dapagliflozin	
	Baseline	Intervention	Baseline	Intervention
Spatial speckle				
A	0.22 ± 0.06	0.26 ± 0.03	0.25 ± 0.02	0.21 ± 0.01
k1	-0.34 ± 0.04	-0.51 ± 0.05	-0.43 ± 0.05	-0.46 ± 0.03
k2	-6.59E-03 ± 2.07E-03	-6.68E-03 ± 9.55E-04*	-7.57E-03 ± 9.58E-04	-8.91E-03 ± 1.30E-03
MSE	4.07E-03 ± 1.31E-03	4.18E-03 ± 1.35E-03	2.87E-03 ± 4.93E-04	3.00E-03 ± 5.30E-04
$Length_{max}$,mm	16.60 ± 5.84	8.58 ± 1.41	7.42 ± 0.82	7.49 ± 1.13
Temporal speckle				
A	0.38 ± 0.14	0.20 ± 0.05	0.17 ± 0.02	0.20 ± 0.03
k1	-0.26 ± 0.07	-0.57 ± 0.07†	-0.36 ± 0.03	-0.35 ± 0.08
k2	-3.94E-03 ± 3.17E-03	-8.17E-03 ± 9.04E-04	-7.02E-03 ± 1.59E-03	-7.99E-03 ± 8.70E-04
MSE	5.64E-03 ± 1.25E-03	3.52E-03 ± 8.29E-04	2.37E-03 ± 3.85E-04	3.71E-03 ± 1.10E-03
$Length_{max}$,mm	11.72 ± 2.50	9.60 ± 1.64	12.94 ± 2.04	10.03 ± 2.26

Values are presented as mean ± SEM; n = 6 furosemide; n = 6 dapagliflozin. Shown is a summary of non-linear regression analysis. RK, remnant kidney; PC, phase coherence; TGF, tubuloglomerular feedback; *A*, magnitude of decay of PC_{TGF}, k_1, length constant associated with initial decay; *k2,* length constant associated with second decay; MSE, mean squared error; $length_{max}$, the maximum distance that TGF synchronization occurs over. Rank-deficient trials were excluded from calculating $length_{max}$. One temporal speckle trial in the furosemide group was rank-deficient. This means that multiple set of parameters could fit the data equally well and the trial is not as reliable as others. From spatial speckle, furosemide increased k_2 (*p = 0.002). From temporal speckle, furosemide had a higher k_1 after intervention compared to the dapagliflozin group (†p = 0.016) (Two Way RM ANOVA).

Figure 4.8 illustrates the decay of PC_{TGF} with edge length in the remnant kidney groups, which is summarized in Table 4.8. Temporal speckle shows that both RK 1wk and 6wk increased the speed of decay of synchronization at short edge lengths so that the signal travels a shorter distance before declining.

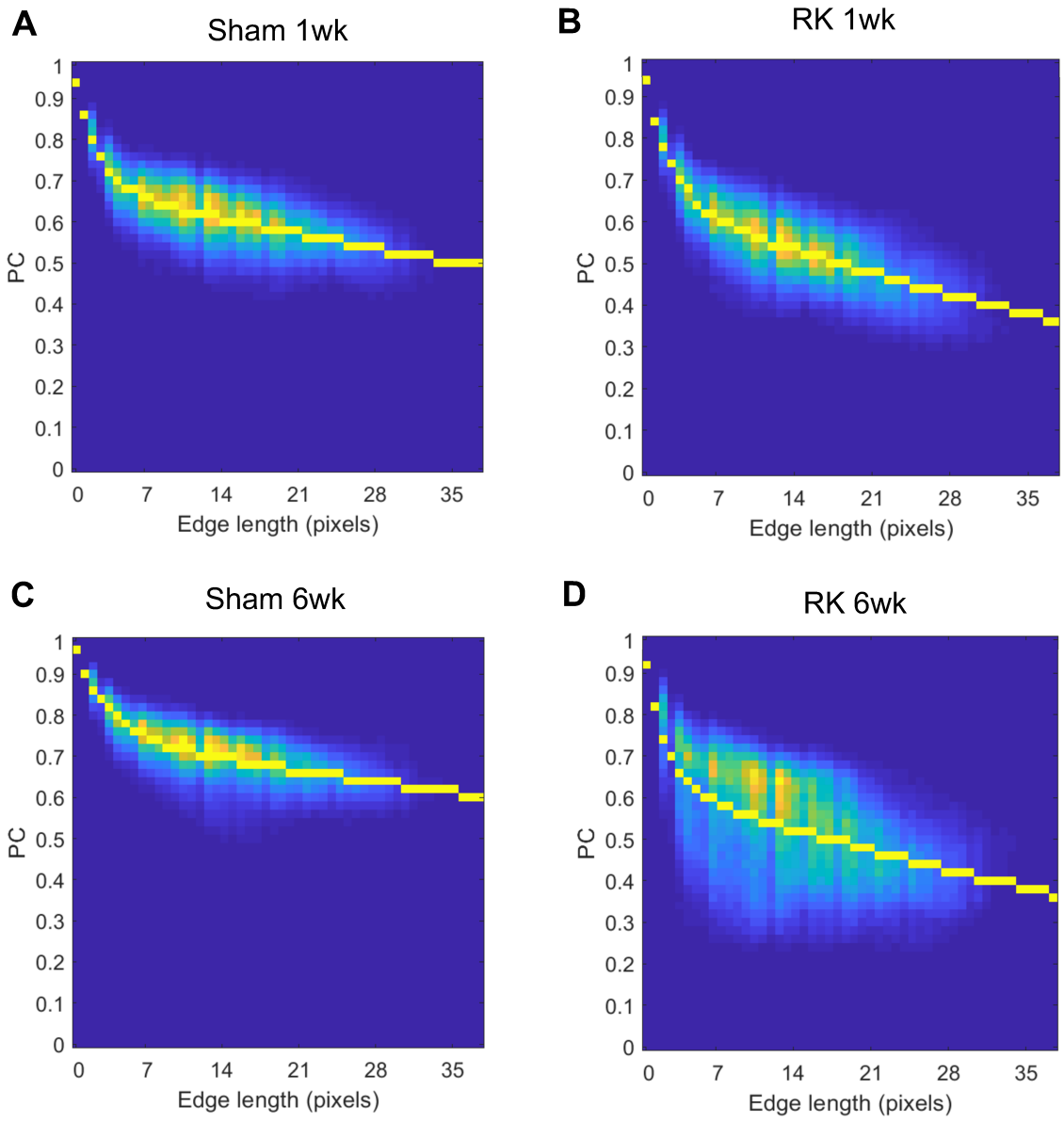

Figure 4.8. Heatmap of the decay of tubuloglomerular feedback phase coherence (PC_{TGF}) with edge length in RK 1wk, RK 6wk and their sham controls. These results are from spatial speckle from individual rats. The best-fit curve is overlaid in yellow. Areas of yellow represent a greater number of nodes (LSCI pixels) whereas blue represents a decreased number of nodes. In these rats, RK 1wk (0.34) and 6wk (0.36) have a greater magnitude of decay, A, than sham 1wk (0.31) and 6wk (0.24). The speed of decay, k_1, was higher in RK 6wk (-0.52) than RK 1wk (-0.42), sham 1wk (-0.32) or sham 6wk (-0.34).

Table 4.8. Summary of non-linear regression analysis of the decay in tubuloglomerular feedback phase coherence (PC_{TGF}) with edge length in RK 1wk, RK 6wk and sham controls.

	Sham 1wk	RK 1wk	Sham 6wk	RK 6wk
Spatial speckle				
A	0.31 ± 0.07	0.30 ± 0.09	0.21 ± 0.04	0.34 ± 0.05
k1	-0.38 ± 0.06	-0.49 ± 0.07	-0.48 ± 0.09	-0.57 ± 0.04
k2	-4.92E-03 ± 1.01E-03	-5.65E-03 ± 1.36E-03	-7.85E-03 ± 1.89E-03	-8.49E-03 ± 6.00E+03
MSE	4.03E-03 ± 8.88E-04	2.88E-03 ± 8.30E-04	3.64E-03 ± 7.58E-04	5.13E-03 ± 1.00E-03
$Length_{max}$,mm	13.42 ± 2.58	10.47 ± 1.81	9.77 ± 1.57	6.82 ± 1.19
Temporal speckle				
A	0.27 ± 0.06	0.31 ± 0.09	0.16 ± 0.02	0.26 ± 0.03
k1	-0.35 ± 0.14	-0.52 ± 0.11*	-0.42 ± 0.07	-0.54 ± 0.04†
k2	-5.65E-03 ± 1.24E-03	-6.65E-03 ± 2.06E-03	-8.61E-03 ± 2.08E-03	-9.29E-03 ± 1.35E-03
MSE	4.20E-03 ± 8.11E-04	3.24E-03 ± 4.00E+00	2.66E-03 ± 6.76E-04	5.46E-03 ± 1.68E-03
$Length_{max}$,mm	13.08 ± 2.66	9.87 ± 2.03	16.56 ± 3.75	7.96 ± 1.28‡

Values are presented as mean ± SEM; n = 7 sham 1wk; n = 4 RK 1wk; n = 7 sham 6wk; n = 6 RK 6wk. Shown is a summary of non-linear regression analysis of the decay in PC_{TGF} with edge length. RK, remnant kidney; PC, phase coherence; TGF, tubuloglomerular feedback; *A*, magnitude of decay of PC_{TGF}, k_1, length constant associated with initial decay; *k2,* length constant associated with second decay; MSE, mean squared error; $length_{max}$, the maximum distance that TGF synchronization occurs over. Rank-deficient trials were excluded from calculating $length_{max}$. k_1 from temporal speckle was higher in RK 1wk and RK 6wk than sham 1wk (*p = 0.026 and †p = 0.016, respectively). RK 6wk had a significantly lower $length_{max}$ than its sham counterpart from temporal speckle (‡p = 0.031) (Two Way RM ANOVA).

Figure 4.9 demonstrates the decay of PC_{TGF} with edge length after dapagliflozin intervention in the remnant kidney, which is summarized in Table 4.9. The sham controls showed no change after dapagliflozin. In contrast, spatial speckle shows that dapagliflozin induced a decline in the magnitude of decay of PC_{TGF} at shorter edge lengths in the RK group. Temporal speckle showed that the remnant kidney induced a rapid decline in synchronization at short edge lengths overall compared to sham controls.

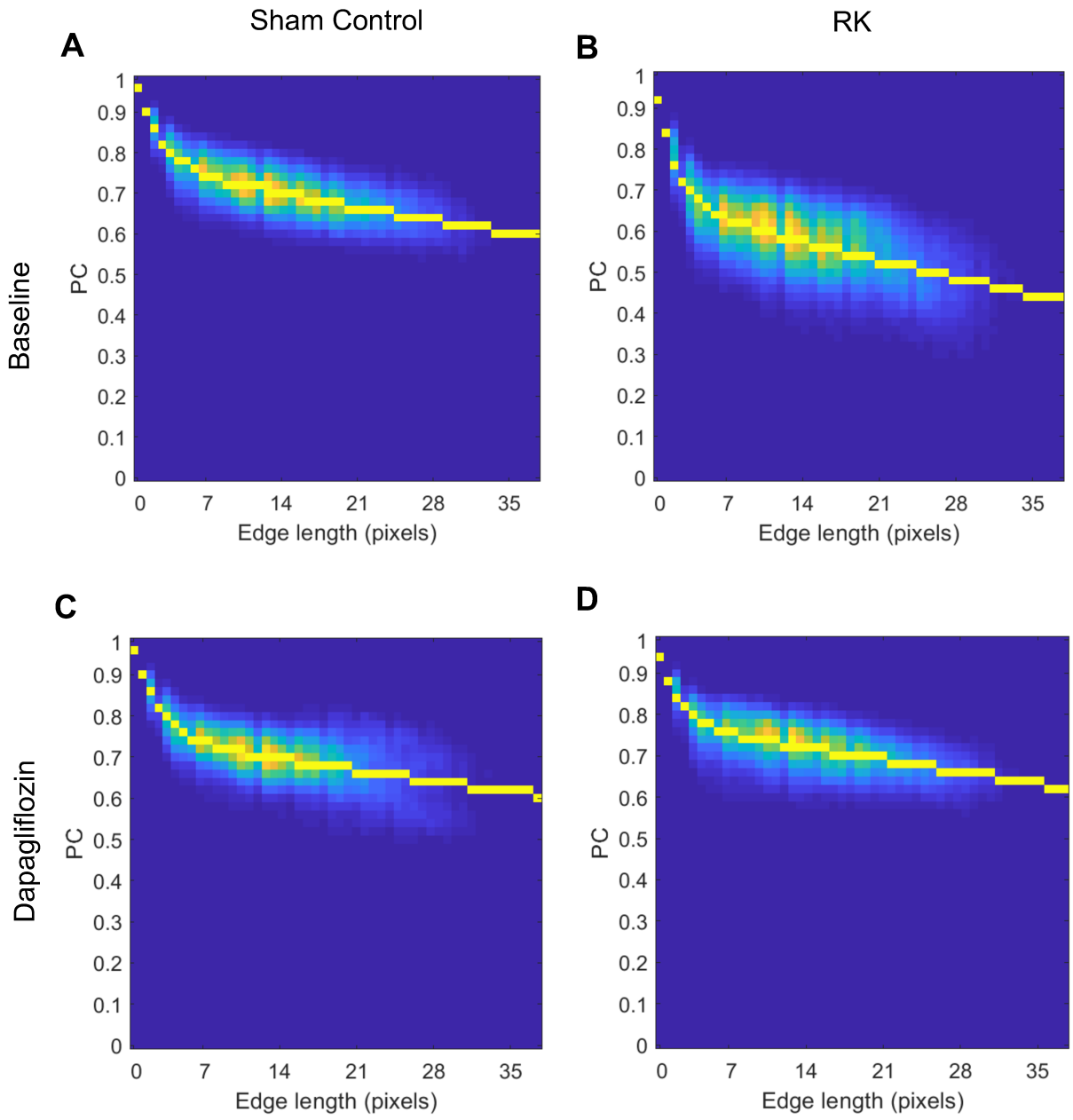

Figure 4.9. Heatmap of the decay of tubuloglomerular feedback phase coherence (PC_{TGF}) with edge length in RK and sham controls administered dapagliflozin. These results are from spatial speckle from individual rats. The best-fit curve is overlaid in yellow. Areas of yellow represent a greater number of nodes whereas blue represents a decreased number of nodes. The sham control rat showed no significant changes in the magnitude of decay, A (0.22 to 0.24), k_1 (-0.43 to -0.42)

or k_2 (-5.3E-03 to -4.13E-03) between *A:* baseline and *C:* after dapagliflozin. *D:* The magnitude of the decay of PC_{TGF} was decreased significantly after dapagliflozin administration in the RK rat (0.32 to 0.21), but changes in k_1 (-0.57 to -0.60) or k_2 (-7.33E-03 to -4.63E-03) were not significant.

Table 4.9. Summary of non-linear regression analysis of the decay in tubuloglomerular feedback phase coherence (PC_{TGF}) with edge length in RK and sham controls administered dapagliflozin.

	Sham Controls		RK	
	Baseline	Dapagliflozin	Baseline	Dapagliflozin
Spatial speckle				
A	0.25 ± 0.02	0.21 ± 0.01	0.33 ± 0.06	0.22 ± 0.03*
k1	-0.43 ± 0.05	-0.46 ± 0.03	-0.58 ± 0.06	-0.59 ± 0.06
k2	-7.57E-03 ± 9.58E-04	-8.91E-03 ± 1.30E-03	-5.82E-03 ± 1.18E-03	-8.55E-03 ± 1.77E-03
MSE	2.87E-03 ± 4.93E-04	3.00E-03 ± 5.30E-04	3.83E-03 ± 5.37E-04	2.72E-03 ± 3.28E-04
$Length_{max}$, mm	7.42 ± 0.82	7.49 ± 1.13	8.08 ± 0.88	8.30 ± 1.47
Temporal speckle				
A	0.17 ± 0.02	0.20 ± 0.03	0.21 ± 0.04	0.24 ± 0.06
k1	-0.36 ± 0.03	-0.35 ± 0.08	-0.58 ± 0.04†	-0.57 ± 0.05†
k2	-7.02E-03 ± 1.59E-03	-7.99E-03 ± 8.70E-04	-7.09E-03 ± 1.10E-03	-9.98E-03 ± 2.90E-03
MSE	2.37E-03 ± 3.85E-04	3.71E-03 ± 1.10E-03	2.38E-03 ± 5.65E-04	3.24E-03 ± 7.45E-04
$Length_{max}$, mm	12.94 ± 2.04	10.03 ± 2.26	11.18 ± 1.96	12.40 ± 6.04

Values are presented as mean ± SEM; n = 6 sham controls; n = 6 RK. Shown is a summary of non-linear regression analysis of the decay in PC_{TGF} with edge length. RK, remnant kidney; PC, phase coherence; TGF, tubuloglomerular feedback; *A*, magnitude of decay of PC_{TGF}, k_1, length constant associated with initial decay; *k2,* length constant associated with second decay; MSE, mean squared error; $length_{max}$, the maximum distance that TGF synchronization occurs over. Rank-deficient trials were excluded from calculating $length_{max}$. Intervention with dapagliflozin decreased *A* from spatial speckle in RK (*$p = 0.023$). k_1 from temporal speckle was higher in RK overall than sham controls (†$p = 0.009$) (Two Way RM ANOVA).

Heterogeneity in cortical perfusion.

Table 4.10 summarizes variables that assess the heterogeneity in cortical perfusion after TGF manipulation. The dominant operating frequencies of each autoregulatory mechanism indicates the frequency range that MR or TGF operate at maximally. f_{MR} and f_{TGF} were unchanged within each group after furosemide and dapagliflozin administration. The coefficient of variation in the dominant operating frequency of MR and TGF indicate variability in the frequency coupling at the renal surface, which suggests altered entrainment across kidney regions. $CV_{f,MR}$ was increased after furosemide. Variation in TGF's operating frequency from temporal speckle decreased significantly after dapagliflozin, indicating dapagliflozin increased entrainment of regions across the kidney. Figure 4.10 shows changes in spatiotemporal heterogeneity of surface perfusion before and after furosemide and dapagliflozin, determined by spatial and temporal coefficients of variation ($CV_{spatial}$ and $CV_{temporal}$) of LSCI speckle. Figure 4.10A and 4.10B show no significant changes in $CV_{spatial}$ after furosemide or dapagliflozin intervention, indicating neither drug altered perfusion across the kidney surface. $CV_{temporal(S)}$ reflects the fluctuations in how steady surface blood flow is and was reduced after dapagliflozin (Figure 4.10C), while $CV_{temporal(T)}$ was unchanged.

Table 4.10. Assessment of the heterogeneity in cortical perfusion after acute furosemide and dapagliflozin administration.

	Furosemide		Dapagliflozin	
	Baseline	Intervention	Baseline	Intervention
MR				
f_{MR}, Hz	0.104 ± 0.003	0.106 ± 0.002	0.108 ± 0.002	0.110 ± 0.005
$CV_{f,MR}$, %	10.1 ± 2.1	16.7 ± 1.4*	13.0 ± 2.3	14.5 ± 1.1
TGF (Spatial speckle)				
$f_{TGF(S)}$, Hz	0.021 ± 0.001	0.021 ± 0.001	0.019 ± 0.002	0.019 ± 0.001
$CV_{f,TGF(S)}$, %	10.1 ± 3.1	15.5 ± 3.8	10.9 ± 2.9	10.0 ± 2.5
TGF (Temporal speckle)				
$f_{TGF(T)}$, Hz	0.022 ± 0.002	0.022 ± 0.003	0.021 ± 0.001	0.020 ± 0.001
$CV_{f,TGF(T)}$, %	6.5 ± 1.7	12.7 ± 4.1	21.0 ± 3.7†	10.4 ± 2.6‡

Values are presented as mean ± SEM; n = 6 furosemide; n = 6 dapagliflozin. Shown is a summary of the analysis of heterogeneity in cortical perfusion after furosemide and dapagliflozin interventions. MR, myogenic response; TGF, tubuloglomerular feedback; f_{MR} and f_{TGF}, dominant MR and TGF operating frequencies; $CV_{f,MR}$ and $CV_{f,TGF}$, coefficient of spatial variation of dominant MR and TGF frequencies; S, spatial speckle; T, temporal speckle. $CV_{f,MR}$ increased after FUR (*p = 0.019). $CV_{f,TGF(T)}$ was significantly higher at baseline in the dapagliflozin group than furosemide group (†p = 0.004) and decreased after intervention (‡p = 0.030) (Two Way RM ANOVA).

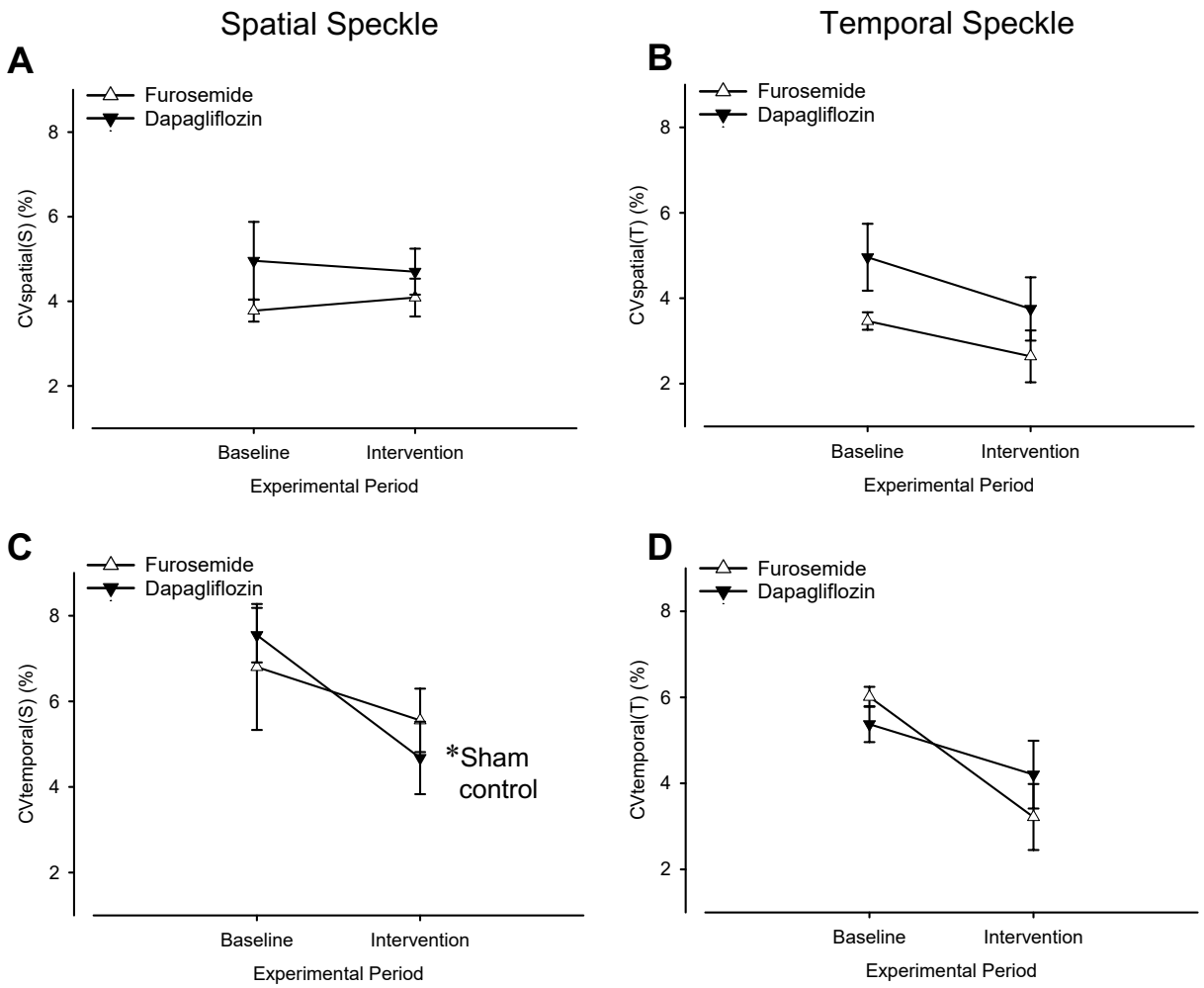

Figure 4.10. Assessment of spatiotemporal heterogeneity in cortical perfusion after acute furosemide (△) and dapagliflozin (▼) interventions, quantified by spatial and temporal coefficients of variation ($CV_{spatial}$ and $CV_{temporal}$). *A* and *C* shows data calculated from spatial speckle and *B* and *D* show data from temporal speckle (denoted by S and T in parentheses in the Y-axes). Neither intervention altered *A:* $CV_{spatial(S)}$ ($p = 0.186$) or *B:* $CV_{spatial(T)}$ ($p = 0.826$). Dapagliflozin decreased *C:* $CV_{temporal(S)}$ (*$p = 0.021$), and *D:* $CV_{temporal(T)}$ ($p = 0.053$) was unaltered after both. There were no significant differences between spatial and temporal speckle (Two Way RM ANOVA). $CV_{spatial}$ and $CV_{temporal}$ are shown as mean ± SEM; n = 6 furosemide; n = 6 dapagliflozin.

The dominant operating frequencies of MR (f_{MR}) and TGF ($f_{TGF(S)}$) were higher in RK 1wk only (Table 4.11). The variation in the operating frequency of TGF measured by spatial speckle was increased significantly in both RK 1wk and RK 6wk groups, demonstrating decreased entrainment of regions across the kidney. Figure 4.11 shows that both RK 1 and 6wk groups comparably increased $CV_{spatial(S)}$ and $CV_{spatial(T)}$ compared to their sham counterparts (Figure 4.11A and 4.11B), indicating that the remnant kidney induces dispersion in perfusion, or in other words the blood flow is heterogenous across the kidney surface. There was no change in $CV_{temporal}$, suggesting that minimal fluctuations in how variable surface blood flow is over time.

Table 4.11. Assessment of the heterogeneity in cortical perfusion in RK 1wk, RK 6wk and sham controls.

	Sham 1wk	RK 1wk	Sham 6wk	RK 6wk
MR				
f_{MR}, Hz	0.105 ± 0.002	0.159 ± 0.019*	0.108 ± 0.003	0.110 ± 0.003
$CV_{f,MR}$, %	12.2 ± 0.9	17.6 ± 4.2	13.7 ± 1.6	15.2 ± 1.6
TGF (Spatial speckle)				
$f_{TGF(S)}$, Hz	0.020 ± 0.001	0.027 ± 0.004†	0.019 ± 0.000	0.020 ± 0.001
$CV_{f,TGF(S)}$, %	10.4 ± 2.3	20.7 ± 5.1	12.6 ± 1.9	25.6 ± 3.8‡
TGF (Temporal speckle)				
$f_{TGF(T)}$, Hz	0.020 ± 0.001	0.024 ± 0.003	0.019 ± 0.001	0.021 ± 0.001
$CV_{f,TGF(T)}$, %	7.8 ± 1.0	21.5 ± 5.8§	12.6 ± 2.4	16.6 ± 4.8

Values are presented as mean ± SEM; n = 7 sham 1wk; n = 4 RK 1wk; n = 7 sham 6wk; n = 6 RK 6wk. Shown is a summary of the analysis of heterogeneity in cortical perfusion. RK, remnant kidney; MR, myogenic response; TGF, tubuloglomerular feedback; f_{MR} and f_{TGF}, dominant MR and TGF operating frequencies; $CV_{f,MR}$ and $CV_{f,TGF}$, coefficient of spatial variation of dominant MR and TGF frequencies; S, spatial speckle; T, temporal speckle. RK 1wk increased f_{MR} (*$p < 0.001$) and $f_{TGF(S)}$ (†$p = 0.019$) compared to RK 6wk and sham controls, and had no change in $CV_{f,TGF(S)}$ compared to sham controls ($p = 0.073$). RK 6wk had increased $CV_{f,TGF(S)}$ compared to sham controls (‡$p = 0.010$). $CV_{f,TGF(T)}$ was increased in RK 1wk compared to sham 1wk (§$p = 0.007$) (One Way RM ANOVA).

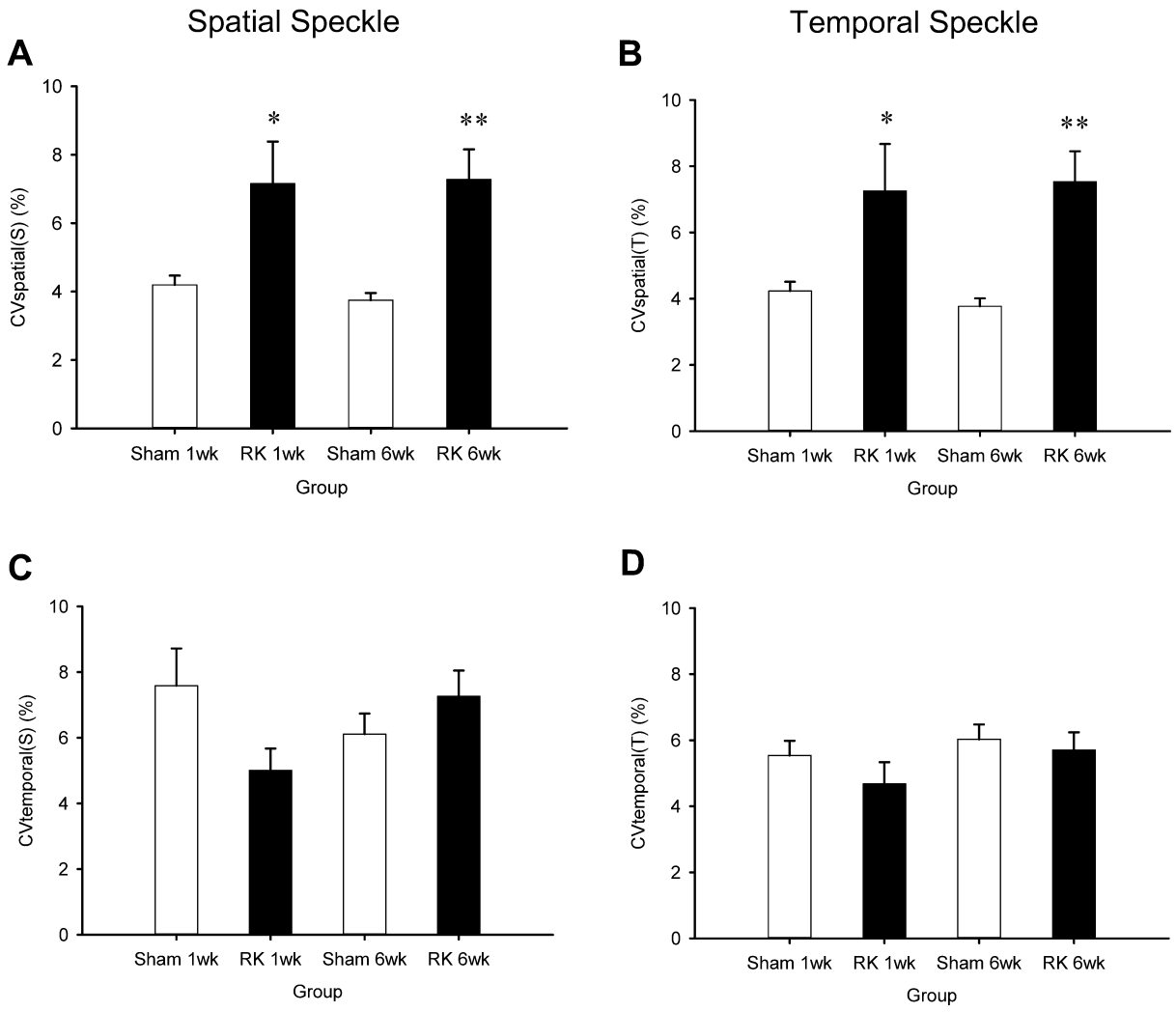

Figure 4.11. Assessment of spatiotemporal heterogeneity in cortical perfusion in RK 1wk, RK 6wk and their sham controls, quantified by spatial and temporal coefficients of variation ($CV_{spatial}$ and $CV_{temporal}$). *A* and *C* show data calculated from spatial speckle and *B* and *D* show data from temporal speckle (denoted by S and T in parentheses). *A:* RK 1 and 6wk increased $CV_{spatial(S)}$ (*$p = 0.004$ and **$p < 0.001$, respectively) and *B:* $CV_{spatial(T)}$ (*$p = 0.007$ and **$p = 0.001$, respectively) compared to sham controls. There were no significant differences between values from spatial and temporal speckle (One Way RM ANOVA). Data are shown as mean ± SEM; n = 7 sham 1wk; n = 4 RK 1wk; n = 7 sham 6wk; n = 6 RK 6wk.

Table 4.12 summarizes the analysis of perfusion heterogeneity after intervention in the remnant kidney. A decrease in the variation of TGF's dominant frequency from spatial speckle in the remnant kidney after intervention shows increased frequency coupling of TGF across kidney regions.

Figure 4.12 shows that $CV_{spatial}$ was unaffected by dapagliflozin (Figure 4.12A and 4.12B). Baseline $CV_{temporal}$ from spatial speckle decreased in sham controls after dapagliflozin (Figure 4.12C), indicating improved homogeneity in the spatial variability of surface blood flow. $CV_{temporal}$ from temporal speckle showed no change in either group.

Table 4.12. Assessment of the heterogeneity in cortical perfusion in RK and sham controls administered dapagliflozin.

	Sham Controls		RK	
	Baseline	Dapagliflozin	Baseline	Dapagliflozin
MR				
f_{MR}, Hz	0.109 ± 0.002	0.110 ± 0.005	0.112 ± 0.002	0.107 ± 0.005
$CV_{f,MR}$, %	13.0 ± 2.3	14.5 ± 1.1	13.4 ± 3.0	13.4 ± 3.0
TGF (Spatial speckle)				
$f_{TGF(S)}$, Hz	0.019 ± 0.002	0.019 ± 0.001	0.023 ± 0.002	0.023 ± 0.004
$CV_{f,TGF(S)}$, %	10.9 ± 2.9	10.0 ± 2.5	28.5 ± 3.1*	13.7 ± 3.1†
TGF (Temporal speckle)				
$f_{TGF(T)}$, Hz	0.021 ± 0.001	0.020 ± 0.001	0.027 ± 0.004	0.024 ± 0.003
$CV_{f,TGF(T)}$, %	21.0 ± 3.7	10.4 ± 2.6†	35.4 ± 4.8‡	32.0 ± 8.2§

Values are presented as mean ± SEM; n = 6 sham controls; n = 6 RK. Shown is a summary of the analysis of heterogeneity in cortical perfusion. RK, remnant kidney; MR, myogenic response; TGF, tubuloglomerular feedback; f_{MR} and f_{TGF}, dominant MR and TGF operating frequencies; $CV_{f,MR}$ and $CV_{f,TGF}$, coefficient of spatial variation of dominant MR and TGF frequencies; S, spatial speckle; T, temporal speckle. $CV_{f,TGF(S)}$ was higher at baseline in RK than sham controls (*p = 0.002) and decreased in RK significantly after intervention (†$p < 0.05$). Dapagliflozin intervention decreased $CV_{f,TGF(T)}$ in sham controls (†$p < 0.05$). $CV_{f,TGF(T)}$ was higher at baseline (‡p = 0.028) and after intervention (§p = 0.019) in RK compared to sham controls. (Two Way RM ANOVA).

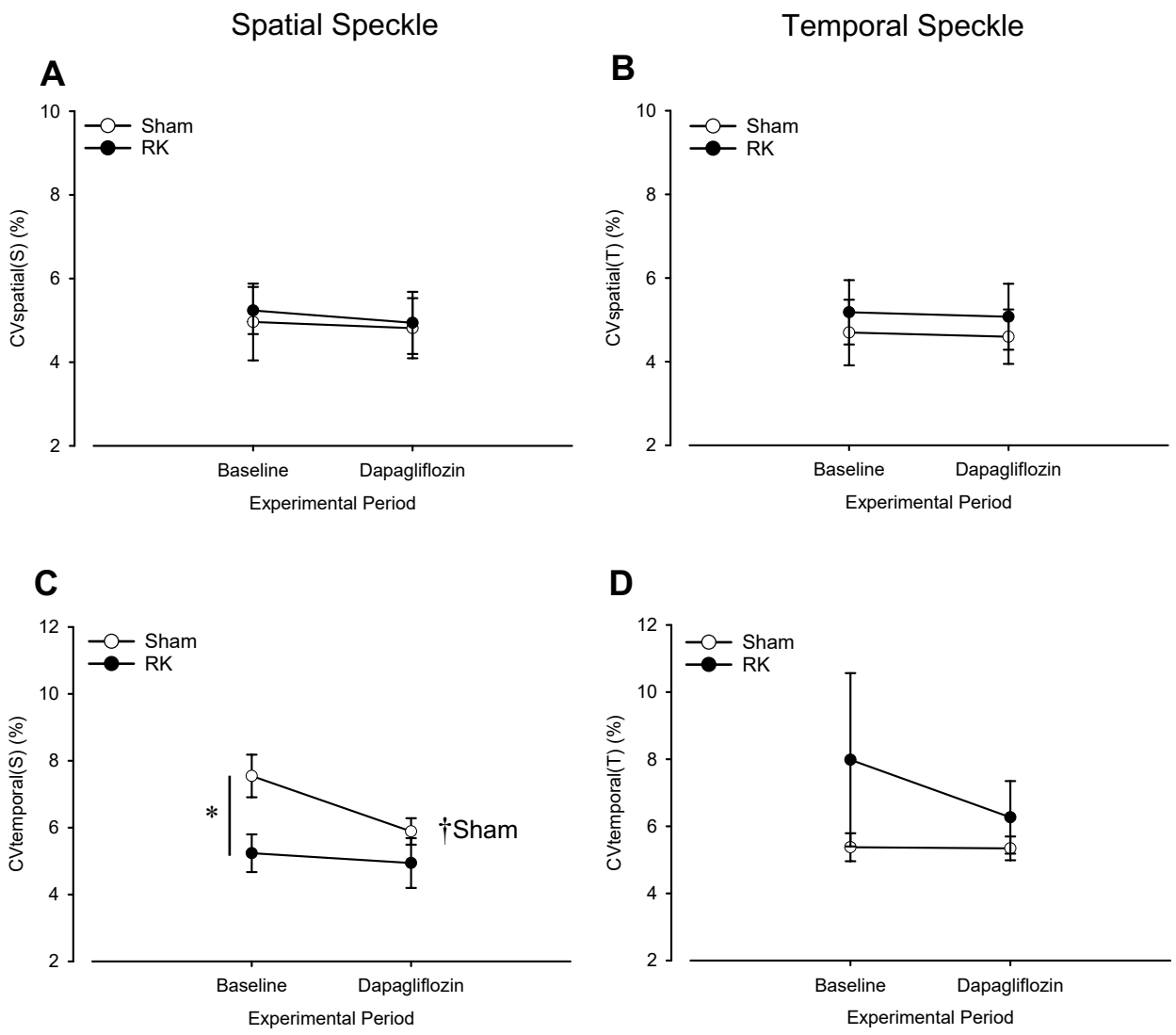

Figure 4.12. Assessment of spatiotemporal heterogeneity in cortical perfusion in RK (●) and sham (○) controls administered dapagliflozin, quantified by spatial and temporal coefficients of variation ($CV_{spatial}$ and $CV_{temporal}$). A and *C* show data calculated from spatial speckle, and *B* and *D* show data from temporal speckle (denoted by S and T in parentheses). *A* and *B:* There were no changes in $CV_{spatial}$. *C:* $CV_{temporal(S)}$ was higher at baseline in sham controls than RK (*p = 0.015), and reduced after dapagliflozin (†p = 0.021). *D*: $CV_{temporal(T)}$ did not change after intervention for either group. There were no significant differences between spatial and temporal

speckle (Two Way RM ANOVA). Data are shown as mean ± SEM; n = 6 sham controls; n = 6 RK.

For all LSCI variables that were measured, spatial speckle and temporal speckle results yielded similar values, none of which differed significantly. The only exception to this was RK 6wk results from Table 4.6, where PC, #edges and length associated with TGF were significantly different between spatial and temporal speckle.

Cx40 expression.

Immunofluorescence results show Cx40 localization obtained from one sham rat that was administered dapagliflozin. Figure 4.13A shows a glomerulus and its associated afferent arteriole. CD31 highlights the endothelium in red and Cx40 expression in green is evident in the endothelium of the afferent arteriole as well as in the glomerulus. Figure 4.13B also shows a glomerulus and its associated afferent arteriole, with CD31 expression highlighting the endothelium along the vessel and the Cx40 signal appearing where CD31's signal does. Figure 4.13C shows a cross sectional view of the lumen of a smaller vessel; the lumen of the vessel, where the endothelium is, is lined with Cx40 signals. Figure 4.13D shows a cross sectional view of a larger vessel, namely the cortical radial artery, with Cx40 signals illuminated in the endothelium.

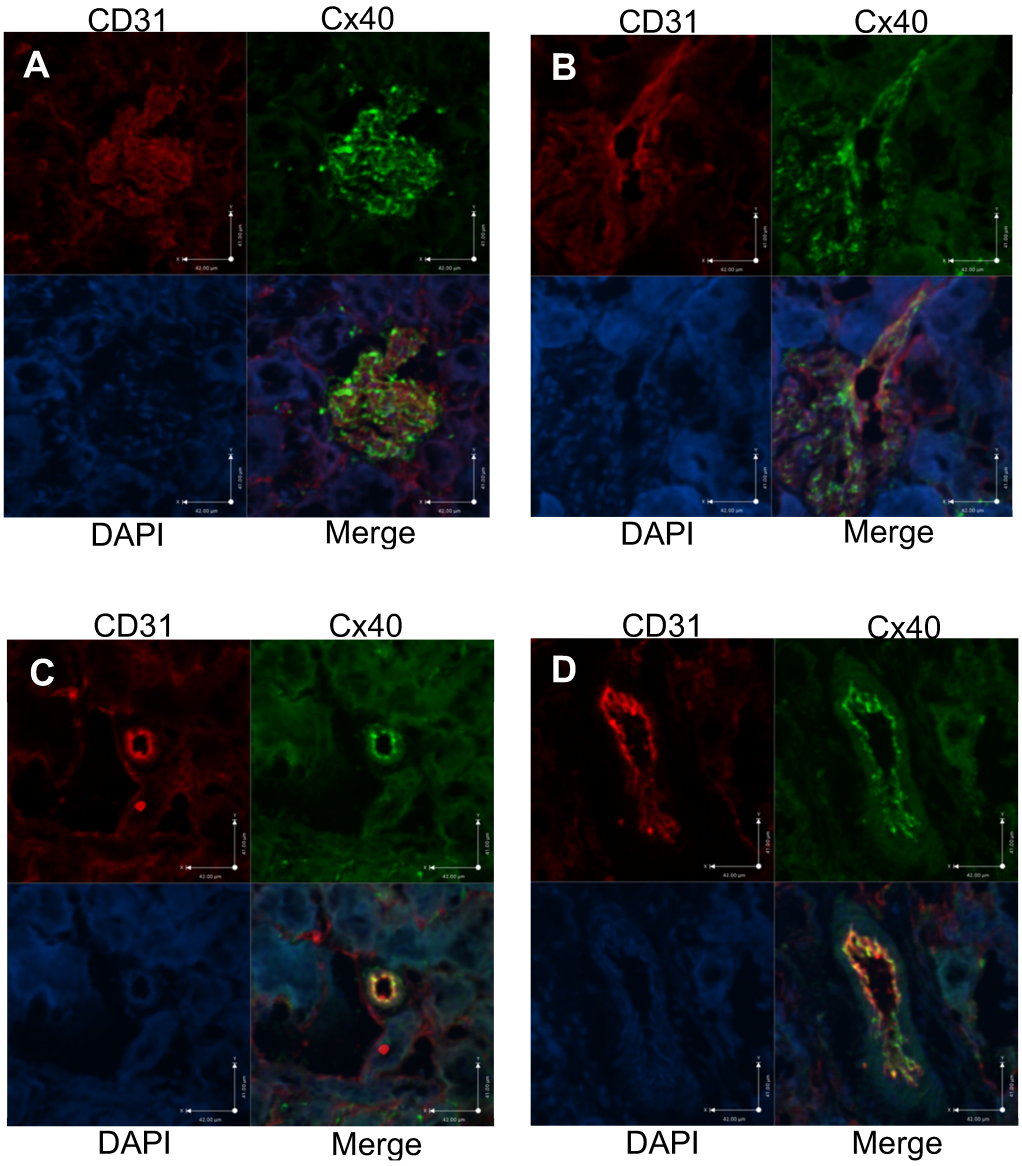

Figure 4.13. Endothelial Cx40 expression detected with immunofluorescence. *A - D* show endothelial Cx40 expression from a sham control rat given dapagliflozin. *A and B:* Cx40 signal (green) and CD31 signal (red) are positive in the endothelium of the glomerulus and its associated afferent arteriole. *C:* A cross-sectional view of a smaller vessel, presumably an artery because of the appearance of a thicker wall, shows the inside of the lumen lined with CD31 signal which indicates the endothelium. Cx40 signal colocalizes with the CD31 signal. *D:* Cx40

and CD31 signal colocalize in the endothelium of a cortical radial vessel. DAPI signal (blue) stains the nucleus. Presence of Cx40 in the afferent arteriole and the cortical radial vessel reflects their participation in propagating TGF-induced VCRs to coordinate resistance changes.

CHAPTER 5: DISCUSSION, CONCLUSION & PERSPECTIVES

5.1 General Discussion

The purpose of this study was to first gain an understanding of synchronization in the nephrovascular network in physiology, hypothesizing that inhibiting and enhancing TGF signalling would decrease and increase synchronization, respectively. The second hypothesis was that functional and structural changes that occur in the remnant kidney model of CKD would impair TGF synchronization by disrupting the nephrovascular network. In the third hypothesis we tested whether intervention in CKD with an SGLT2 inhibitor, known for their cardioprotective and renoprotective effects, would enhance synchronization. The main findings of the first aim are that furosemide had a weak and rather variable effect on TGF and it only induced a rapid decay in TGF synchronization across longer distances in the kidney. Dapagliflozin exerted minimal effect on TGF synchronization in intact rats, whose baseline TGF activity was appropriate. In the second aim, we found that the early remnant kidney had increased strength and extent of MR synchronization only, while after 6 weeks the strength of TGF synchronization was diminished. Both induced a rapid decay in the transmission of TGF signals, decreased coupling of kidney regions and increased the heterogeneity of perfusion. The second aim also allowed us to explore modularity, a common feature of biological networks, of the nephrovascular network in pathophysiology [6]. We found in the third aim that dapagliflozin enhanced TGF synchronization in the remnant kidney, reduced the magnitude of its decay over distance, and enhanced entrainment amongst regions at the kidney surface.

The results of this investigation provide novel insights into distributed network behavior in pathophysiology as well as the extent to which TGF-induced VCRs are able to travel in the kidney. The use of LSCI is a recent advancement for assessing renal cortical perfusion and provides information into the distributed nature of blood flow in the cortex [7,8,27,64,70,83,90]. This is

the first description of large-scale synchronization assessment after furosemide and dapagliflozin administration and in a 5/6th nephrectomy model.

Urine excretion.

Aim 1: The hemodynamic actions of furosemide induced by 1) vasodilation caused by NKCC1 inhibition and 2) removal of TGF's vasoconstriction at the afferent arteriole by NKCC2 inhibition would suggest that its effect should be to increase renal vascular conductance (RVC, the inverse of renal vascular resistance), RBF and GFR [91]. However, most studies performed in mice and rats consistently indicate decreased RVC and parallel reductions in RBF and GFR despite inhibition of afferent arteriolar constriction [92–97], indicating the complexity and inconsistency of furosemide's hemodynamic effects [91,95,98]. In our study, we found that RVC was unchanged, a finding also reported by Blantz et al [99]. The decrease in RBF in our study was also very slight, appearing consistent with the unaltered RVC because a decrease in the latter would presumably decrease RBF significantly. We also observed increased GFR, which has been reported by others (Figure 4.1) [100,101]. Increased GFR may explained by a rise in glomerular capillary pressure (P_{GC}) induced by furosemide that was not neutralized by other determinants of glomerular ultrafiltration, such as increased tubular hydrostatic pressure and peritubular capillary compression, nor by renin and vasoconstrictor prostaglandin activity. This is likely a result of variable inhibition of the NKCC2 by furosemide.

Dapagliflozin inhibits sodium-coupled glucose reabsorption by inhibiting SGLT2 at the proximal tubule, leading to glucosuria and natriuresis. Our results support dapagliflozin-induced afferent arteriole constriction and the subsequent reduction in intraglomerular pressure because

we observed a decrease in GFR in intact rats as well as in the remnant kidney group, in accordance with numerous studies (Figure 4.1 and 4.3) [102,103].

Aim 2 & 3: The remnant kidney at 6 weeks had elevated blood pressure compared to the early remnant kidney. Hypertension is a characteristic finding of the remnant kidney model of CKD [104,105] and is suggested to be a result of increased angiotensin II levels [106,107]. Increased intrarenal ANG II activity in particular has been shown to be increased after renal ablation [108,109]. The pathogenesis of glomerular injury in renal disease has been attributed to systemic hypertension that transmits to glomeruli and causes intraglomerular hypertension [104,107,110]. Intact autoregulatory responses would be expected to contribute to proportionate afferent arteriolar vasoconstriction and it would be assumed that hypertensive injury to preglomerular capillaries and glomeruli would precede impairment of autoregulatory mechanisms. However, Bidani et al reported that impairment of autoregulation in the remnant kidney actually precedes hypertensive injury to the microvasculature [104]. This early impairment contributes to the progressive nature of renal disease.

When renal mass is initially reduced, the remaining NVUs undergo functional changes resulting in an increase in single-nephron GFR (SNGFR). This adaptive hyperfiltration compensates for the function of lost NVUs and mitigates the reduction in GFR that would otherwise ensue [111]. Despite the fact that hyperfiltration is "costly" because it places a heightened metabolic stress on the tubules to reabsorb filtered sodium, the remnant kidney may prioritize maintaining salt homeostasis over the advantages conveyed by TGF [112]. Thus, while TGF has the capacity to minimize extensive increases in SNGFR, TGF-mediated suppression of SNGFR fails after a 5/6th ablation of renal mass and TGF is reset rightward so that P_{GC} is maintained at elevated levels, requiring a higher tubular flow rate to elicit the same level of activity [113–115]. In

addition to a suppressed TGF signal, Thomson et al have shown that in response to a high salt diet, the remnant kidney will convert its TGF from a negative feedback signal to a positive feedback [112,116]. This can occur because in response to salt-sensing at the macula densa, vasoconstrictor adenosine (which has constrictor and dilator receptors) and vasodilatory nitric oxide is released. The remnant kidney has highly anomalous TGF whereby nitric oxide release or increased abundance of dilatory adenosine receptors may tip the balance to promote a positive feedback response so that increased distal delivery would result in increased SNGFR [112,116,117]. Our results cannot confirm whether positive feedback resetting occurred of TGF. Nonetheless, while we did not measure SNGFR, we observed no changes in GFR in the early remnant kidney which may be explained by increased SNGFR in the remaining NVUs offsetting the decrease in total GFR (Figure 4.2). More progressed disease after 6 weeks caused a decline in GFR, consistent with clinical observations that show a link between worsening kidney function and lower eGFR [118].

Strength and variability of synchronization.

Aim 1: That furosemide and dapagliflozin did not affect the strength or variability of TGF synchronization in intact rats was an unexpected finding (Table 4.4). We expected furosemide to decrease TGF synchronization because it abolishes TGF signalling. Additionally, when TGF is inhibited, MR becomes the predominant autoregulatory mechanism for providing protection against hypertensive injury [119]. Therefore, we expected an increase in the strength of MR synchronization. However, these changes were not observed likely owing to weak NKCC2 inhibition by furosemide. In contrast, dapagliflozin enhances TGF activity so increased strength of TGF synchronization was anticipated but also not seen. An explanation for this finding may

be that in healthy normoglycemic animals with intact TGF signalling, SGLT2 inhibition would not enhance TGF activity beyond an appropriate level.

Aim 2: The remnant kidney at 1 week did not affect TGF synchronization but enhanced the strength and extent of MR synchronization (Table 4.5). After 6 weeks, the remnant kidney had reduced strength of TGF synchronization, reduced number of TGF edges, and a lower average edge length between two points on the renal surface. Graph analysis of PC in both RK 1wk and 6wk groups shows that shorter edge lengths (two nodes closer to each other) are coupled with edges with higher $PC_{TGF,}$ forming clusters with stronger synchronization, versus two points farther from each other coupled with lower PC_{TGF} edges, pointing to a modular structure of synchronization (Figure 4.5). These results illustrate the scale and modularity of TGF synchronization that is significantly disrupted with advancing kidney disease.

Aim 3: Dapagliflozin increased the strength of TGF synchronization in the remnant kidney. Sham control rats showed a negligible effect (Table 4.6). In the remnant kidney, hyperfiltration is associated with a decreased activity of TGF that would not be present in sham controls [112,116]. In a healthy, euglycemic animal without hyperfiltration, SGLT2 inhibition may not exert large effects on TGF because baseline TGF activity is appropriate [120]; it was shown in humans that dapagliflozin did not significantly increase urine glucose excretion in normo-filtering healthy subjects, but it did in diabetic patients with hyperfiltering NVUs [121].

Decay of TGF synchronization with distance.

Examination of the relationship between PC_{TGF} and edge length provides a unique insight into its decay over short and long edge lengths within the context of renal anatomy. The TGF-induced VCR is a non-regenerative electrotonic signal that is expected to decay with

distance. Previous studies have modeled the transmission of TGF signals along afferent arterioles as exponential decays with single length constants [48–50]. Our finding of two mechanical length constants arises from the observation apparent in Figures 4.7-4.9 that the decay in PC_{TGF} was modelled by as a sum of exponentials. However, it is important to emphasize that there are other parameters and equations that could fit the data equally well. The first decay could represent the initial rapid decline in PC_{TGF} that occurs over shorter edge lengths within a lobule (CRA and associated afferent arterioles) where the TGF signal originates, and the second equation could represent the slower decay occurring over longer edge lengths. To our knowledge, the only other study that reported a biphasic TGF process was Oppermann et al who reported an initial rapid fall in stop flow pressure that continues at a slower speed [122]. Increasing the expression of A1AR, the adenosine receptor responsible for TGF signal transduction, was found to prolong the response. They concluded, similar to our findings, that TGF is comprised of two mechanisms with different temporal characteristics [122].

Furosemide caused a steeper decay in TGF synchronization at longer edge lengths which reflects reduced involvement of other lobules in synchronization (Table 4.7). This suggests furosemide caused TGF inhibition to some degree that curtailed the spread of conducting VCRs. Dapagliflozin in intact rats induced no changes in the decay of PC_{TGF}. The remnant kidney at both 1 and 6 weeks showed a rapid initial decay in TGF synchronization, prominently at short edge lengths (Table 4.8). This is likely a result of structural changes to the conduction pathway along which TGF signals travel as well reduced network components in the remnant kidney which reduces the number of TGF-signal generators, because intervention with dapagliflozin did not restore either length constant. However, intervention with dapagliflozin in the remnant kidney did decrease the magnitude of decay of TGF synchronization, consistent with SGLT2

inhibition enhancing the strength of PC_{TGF} (Table 4.9). The finding that temporal speckle showed greater decay in the remnant kidney but not in sham controls, whereas spatial speckle did not, might indicate that temporal trends are stronger than spatial differences.

The sum of exponentials equation allowed us to estimate the maximum distance that TGF synchronization occurs over, with striking results that reveal lengths as long as 16.6 mm between two nodes (Table 4.7). This is a greater distance of synchronization than previous reports that predict TGF constriction conducts distances around 0.3 mm to 1.5 mm [48–50]. For perspective, an intact rat kidney has dimensions of approximately 20 x 10 x 7 mm [72]. The maximum distance a VCR conducts would likely be from a surface NVU in one lobule into the CRA, along the arcuate artery and back up to the surface of another lobule. Although there is no experimental evidence that shows VCRs taking this route, it is consistent with 1) the dimensions of the renal vasculature and 2) previous studies suggesting that synchronization occurs across many lobules [8,70]. While the depiction of a renal lobule is well known, its dimensions are not. We use an approximation provided by Prof. Wilhelm Kriz (personal communication) that the diameter of a lobule is about 0.7 mm. Our results show average edge lengths less than 0.7 mm and maximum edge lengths as long as 16.6 mm. This is because we constrained our analysis to $PC > 0.6$ and edge lengths with high PC are likely to be shorter, more numerous and linking NVUs closest to each other (i.e. within lobules), whereas those that are farther away are less common, with weaker PC (≤ 0.6) but have not been accounted for by our analysis.

A caveat when considering $length_{max}$ is that synchronization analysis is based on frequency detection. Detection of coupling at long edge lengths where PC_{TGF} approaches zero may actually be an epiphenomenon, where the frequency that is being detected is actually the TGF frequency times an integer, influenced by other frequencies it encountered in the signal

pathway. We have no evidence to suggest this is typically the case in the kidney and there may be limits to cluster sizes based on the organization of the arterial tree or other phenomena associated with oscillating systems such as oscillation quenching [123]. Knowledge about what limits the size of clusters warrants further study.

The mechanism behind the rapid transmission of VCRs at short edge length involves myoendothelial gap junctions (MEGJs) that enable radial communication between endothelial cells and vascular smooth muscle cells. As discussed in chapter 2, optimal conduction of vasoconstriction occurs through endothelial gap junction (particularly Cx40) mediated communication (Figure 4.13) which requires an optimal distribution of MEGJs. The slower decay of VCRs over long edge lengths may be explained by the reduced abundance of MEGJs in larger vessels like mid-sized CRA and arcuate arteries, which prevents current leakage from the endothelium and can enable long-distance VCR transmission. The RK 6wk group had reduced $length_{max}$, probably a result of the additional structural changes that accrue as kidney disease progresses (Table 4.8).

Heterogeneity in cortical perfusion.

Aim 1: Furosemide increased the variability in the degree of MR frequency coupling (Table 4.10) at the renal surface, contrary to expectation because in the face of TGF inhibition, MR strength increases and variability in f_{MR} is expected to decrease. MR handles the smaller, frequent fluctuations arising from MAP while TGF predominates in the face of larger fluctuations and modulates MR. Inhibition of TGF with furosemide increases the magnitude of the MR response [16], and when TGF is abolished using a hydronephrotic rat kidney preparation, the oscillation frequency of MR is free to respond to blood pressure fluctuations [124]. Our results

may reflect a differential distribution of f_{MR} values at the renal surface so that there are localized regions of higher frequency coupling reflecting enhanced MR activity, and other regions with weak f_{MR} [64]. The variability in the dominant operating frequency of TGF gives insight into the degree of TGF-frequency coupling among kidney regions at the surface. That $CV_{f,TGF}$ did not increase after furosemide administration is unexpected since TGF-inhibition should theoretically reduce the degree of TGF-frequency coupling, yet is consistent with our findings because we observed no significant decrease in the strength of TGF synchronization in Table 4.4. Dapagliflozin, on the other hand, increased entrainment amongst kidney regions indicated by lower variability in the degree of TGF-frequency coupling.

Further investigation of the variability in cortical perfusion showed that neither furosemide nor dapagliflozin administration altered the pattern of blood flow across the kidney surface (Figure 4.10). $CV_{temporal}$ did not indicate differences after furosemide, which means that fluctuations in $CV_{spatial}$ are constant. Dapagliflozin did not enhance the strength of TGF synchronization, but it decreased $CV_{temporal}$ in the dapagliflozin group which reflects enhanced entrainment of kidney regions and decreased fluctuations in the variability of surface blood flow over time. This finding may be explained by increased coordination of TGF signals induced by dapagliflozin so that more TGF signals are in phase with each other and therefore more likely to synchronize.

Aim 2: Increased dominant operating frequency of MR in the early remnant kidney (Table 4.11) reflects alterations in the kinetics of the myosin light chain kinase, myosin light chain phosphatase, and actin-myosin interactions, which underlie the MR [125]. Because the strength of MR synchronization was increased in RK 1wk, increased f_{MR} might be compensation for diminished TGF activity or perhaps caused by increased flow past the afferent arteriole in the

remnant NVUs that the vascular smooth muscle layers are responding to. Increased dominant frequency of TGF in the early remnant kidney was unexpected; hypertrophy occurs relatively early in the remnant kidney and would be expected to reduce f_{TGF} because it lengthens the tubules. The increase in f_{TGF} at 1 week suggests hypertrophy may not yet have occurred, and could be related to faster transmission of the fluid wave from the Bowman's capsule to the macula densa and increased SNGFR and tubular reabsorption that affect transit time of the fluid wave [23,126]. These changes are influenced by blood flow alterations in the remnant kidney related to the increase in SNGFR. Another explanation for increased f_{TGF} may be the erratic TGF activity which has been reported in the remnant kidney [117].

The remnant kidney at 1 and 6 weeks induced greater variability in TGF's operating frequency (Table 4.11), reflecting reduced entrainment between NVUs across the kidney. Heightened variability in TGF in the remnant kidney have been reported by others, albeit using micropuncture [108,112,113,116,117]. Reduced entrainment is likely a result of the variability in TGF signalling that makes it difficult for multiple signals to synchronize, as well as a result of structural changes such as loss of NVUs and the onset of progressive structural deterioration in the remnant kidney that prevent TGF signals from conducting. Loss of NVUs have an impact on the modularity of the nephrovascular network [6,89]. Mitrou et al demonstrated this characteristic by altering the small-world dynamics of the nephrovascular network through administration of L-NAME [70]. While small-world networks are considered fault-tolerant, this quality is dependent upon intact elements being present within a cluster to contain any perturbations experienced by that cluster. First, the physical loss of elements (NVUs) in the network, whether by a direct effect of renal ablation or because of progressive damage like lesions, may increase the difficulty for the remaining NVUs, which may be prioritizing sodium balance over TGF, to synchronize [112].

Loss of NVUs also reduces the amount of TGF-signal generation required for coupling and increases the average distance between NVUs, which hinders VCRs from spreading effectively. These changes compromise coupling and therefore synchronization across the cortical surface, and reduce the modularity of the overall network.

The remnant kidney induced the development of spatial heterogeneity in cortical perfusion after both 1 and 6 weeks that appears to be perpetually heterogenous, as indicated by unchanged $CV_{temporal}$ (Figure 4.11). The physical loss of NVUs and spatially heterogeneous vascular injury sustained by tubules and glomeruli is expected to impair synchronization by altering topology and/or geometry of the microcirculation [111,127]. Breaking of the nephrovascular network in this way is predicted to increase variation of capillary flow and pressure which disperses tissue P_{O2}, thus enhancing perfusion heterogeneity [4]. The heightened variability in perfusion may reflect dysregulated vasomotor activity because of abrogated gap junction mediated endothelial communication. This is consistent with the effect of blocking gap junctions using CBX, which results in increased dispersion of renal cortical perfusion because of dysregulated vasomotor activity [8]. In other tissue beds like the hindlimb, mice who have defective upstream perfusion concurrently have impaired vasomotor activity [128]. These findings reflect the importance of intact synchronization to ensure homogenous perfusion.

Aim 3: Decreased TGF-entrainment amongst kidney regions before dapagliflozin intervention is consistent with the pathological changes sustained by the remnant kidney as previously discussed (Table 4.12). Dapagliflozin increased the entrainment of regions across the kidney, consistent with enhanced PC_{TGF} after intervention in the remnant kidney shown in Table 4.6.

Dapagliflozin did not affect the variability of cortical perfusion (Figure 4.12). The nature of disease in the remnant kidney did not appear very progressed because increased spatial heterogeneity of surface blood flow was expected at baseline as seen in the RK 1wk and 6wk groups in Aim 2. In sham controls, dapagliflozin decreased the variability in surface blood flow over time, but this effect was not seen in the remnant kidney (Figure 4.12C). Studies with SGLT2 inhibition have shown improved P_{O2} in the cortex in conditions like diabetes mellitus which have reduced cortical P_{O2} [129]. The lack of change in $CV_{spatial}$ might be because perfusion was appropriate at baseline since the remnant kidney group did not appear to have progressed disease.

A multitude of clinical data has demonstrated that SGLT2 inhibitors improve renal outcomes in diabetic nephropathy [130–132]. The mechanism has been attributed to increased TGF activation causing afferent arteriole vasoconstriction. We observed that TGF's strength was enhanced after dapagliflozin, suggesting an alternate mechanism by which this therapy imparts renoprotective effects. As mentioned previously, majority of renal oxygen consumption feeds the active proximal sodium transport. Hyperglycemia in diabetes arising from proximal tubular and kidney growth, and hyperfiltration as a compensatory mechanism for NVU loss in the remnant kidney, lead to increased SNGFR and subsequently, increased proximal tubular reabsorption which generates a greater oxygen demand [133]. Hyperfiltration and intraglomerular hypertension, a significant determinant of glomerular injury, go hand in hand. As the disease progresses and NVUs start to become non-functional, the remaining NVUs hyperfilter more to compensate. Not only does this result in a disrupted network which jeopardizes synchronization and consequently oxygenation-perfusion matching, but the remaining NVUs progressively increase GFR, increasing their oxygen demand. SGLT2 blockade decreases proximal hyper-reabsorption and

restores the TGF signal by increasing afferent arteriolar tone. This mitigates hyperfiltration and reduces metabolic demand and lowers the risk of hypertensive injury which would otherwise lead to lesions, thus preserving the network. Zhang et al reported an absence of renoprotection in rats with a remnant kidney who were given dapagliflozin, contrary to our findings [134]. However, no reduction in MAP or GFR were observed by us which may be related to the smaller dosage used (0.5 mg/kg twice/day for 12 weeks). It also appears that the chronic SGLT blockade used by Zhang et al may not have fully saturated the TGF response, leading to a more muted effect compared to acute administration of SGLT2 inhibitors [120].

A few limitations of this study exist. When considering the results of furosemide, the negligible effect on RVC and on TGF synchronization suggests highly variable inhibition of NKCC2 which may be related to the pharmacokinetics of furosemide. It is difficult for an inhibitor to reliably block a transporter, and more so if the inhibitor travels bound to the plasma protein albumin and must be secreted into the tubule to exert its effect [135,136]. Furosemide has a high affinity for binding albumin and at physiological concentrations of this protein, the rate of secretion of furosemide into the tubule depends on the concentration of the drug that is not bound to albumin. Additionally, response to the same dosage of furosemide results in variable degrees of inhibition for the reason that it is modulated by the fluid and electrolyte balance as well as the initial renal vascular resistance of each subject [136]. Scully et al also reported significant differences in autoregulation dynamics between animals after infusion of the nitric-oxide synthase inhibitor L-NAME [64]. In general, larger sample sizes are need for all experiments to generate more conclusive results. Second, the remnant kidney group given dapagliflozin intervention in Aim 3 did not appear to have disease as progressed as the RK 6wk group in Aim 2, so interpretation of those data must be done carefully. Third, we fit the decay of TGF

synchronization with a sum of exponentials equation with a few trials being rank-deficient, which suggests that other equations and parameters exist that could represent our data equally well. Finally, any conclusions made in this work regarding the scale of TGF synchronization are strictly dependent upon frequency detection at the renal surface and are therefore prone to overinterpretation. This is because LSCI analysis could detect what appears to be PC_{TGF} at very long distances that may actually be the TGF frequency multiplied by an integer because of other oscillatory influences on the original signal. There is no direct experimental evidence to support the extent of TGF synchronization our analysis suggests so we cannot confirm whether the signal truly travels such long distances or whether it is phenomenon associated with frequency detection.

5.2 Conclusion

This investigation showed in the first aim that

- furosemide caused a rapid decay in TGF synchronization at longer edge lengths, and
- dapagliflozin administration in intact rats increased entrainment of regions across the kidney.

We demonstrated for the first time the consequences of breaking the nephrovascular network in the remnant kidney in Aim 2. These consequences included

- enhanced MR synchronization at 1 week and diminished TGF synchronization at 6 weeks,
- a rapid decay in TGF synchronization at short edges, reduced entrainment across the kidney, and heightened cortical perfusion heterogeneity after both 1 and 6 weeks, and
- reduction in the maximum distance over which synchronization occurs after 6 weeks.

An intact, dynamic small-world network that provides a communication pathway is important in many biological systems, and in the kidney, it serves to enable homogenously distributed perfusion. Intervention with dapagliflozin in the remnant kidney in Aim 3 showed

- increased strength of TGF synchronization, and
- reduced magnitude of decay in synchronization.

Finally, we showed that VCRs are capable of conducting long distances in the kidney to enable information exchange. Such extensive, long-distance synchronization argues that despite individual NVUs being the source of TGF signals, renal autoregulation is best considered a distributed network process that optimizes perfusion over space and time to minimize dispersion in blood flow and pressure.

5.3 Perspectives

This study argues that large-scale synchronization occurs across the kidney and is enabled by the presence of functioning elements (NVUs) in the nephrovascular network. We demonstrated that synchronization can be manipulated by prevalent therapies such as loop diuretics and SGLT2 inhibitors, and that loss of renal mass leads to failure of synchronization which is improved after SGLT2 inhibition. This concept advances the understanding of network behavior in the etiology and progression of renal disease and provides value in using interventions that can restore the coordinated regulation of vascular responses among NVUs and improve disease outcomes as a consequence of preventing renal injury and oxygenation-perfusion mismatch.

References

1. Bello AK, Ronksley PE, Tangri N, et al. Prevalence and Demographics of CKD in Canadian Primary Care Practices: A Cross-sectional Study. *Kidney Int Reports*. 2019;4(4):561-570.
2. Beeuwkes R. Efferent vascular patterns and early vascular-tubular relations in the dog kidney. *Am J Physiol*. 1971;221(5);1361-74.
3. Beeuwkes R. Vascular-tubular relationships in the human kidney. A. Leaf, G. Giebisch L. Bolis, and S. Gorini, eds. *Int Symp Ren Pathophysiology* New York Raven Press. 1980;155-163.
4. Tran CHT, Vigmond EJ, Goldman D, Plane F, Welsh DG. Electrical communication in branching arterial networks. *Am J Physiol Heart Circ Physiol*. 2012;303(6):H680-92.
5. Pikovsky A, Rosenblum M, Kurths J, Hilborn RC. Synchronization: A Universal Concept in Nonlinear Science. Cambridge: Cambridge University Press; 2003.
6. Newman MEJ. Modularity and community structure in networks. *Proc Natl Acad Sci*. 2006;103(23):8577-82.
7. Mitrou N, Scully CG, Braam B, Chon KH, Cupples WA. Laser speckle contrast imaging reveals large-scale synchronization of cortical autoregulation dynamics influenced by nitric oxide. *Am J Physiol Ren Physiol*. 2015;308(7):F661-70.
8. Mitrou N, Braam B, Cupples WA. A gap junction inhibitor, carbenoxolone, induces spatiotemporal dispersion of renal cortical perfusion and impairs autoregulation. *Am J Physiol Heart Circ Physiol*. 2016;311(3):H582-H591.
9. Beeuwkes R, Bonventre J. Tubular organization and vascular-tubular relations in the dog
   a. kidney. *Am J Physiol Content.* 1975;229(3):695-713.

10. Moore DH, Ruska H. The fine structure of capillaries and small arteries. *J Biophys Biochem Cytol.* 1957;3(3):457-462.

11. Hosoyamada Y, Ichimura K, Sakai T. Organ specificity and functional relevance of the arterial structure: A comparative study in the kidney and the skeletal muscle with electron microscopy. *J Vasc Res*. 2016;52(4):265-72.

12. Marsh DJ, Postnov DD, Rowland DJ, Wexler AS, Sosnovtseva OV., Holstein-Rathlou NH. Architecture of the rat nephron-arterial network: analysis with micro-computed tomography. *Am J Physiol Ren Physiol*. 2017;313(2):F351-F360.

13. Postnov DD, Marsh DJ, Postnov DE, et al. Modeling of Kidney Hemodynamics: Probability-Based Topology of an Arterial Network. *PLoS Comput Biol.* 2016;12(7):1-28.

14. Casellas D, Dupont M, Bouriquet N, Moore LC, Artuso A, Mimran A. Anatomic pairing of afferent arterioles and renin cell distribution in rat kidneys. *Am J Physiol Ren Physiol*. 1994;267(6 Pt 2):F931-6.

15. Braus H. Anatomie des Menschen: Zweiter Band Eingeweide. Berlin: Springer. 1924.

16. Yip KP, Holstein-Rathlou NH, Marsh DJ. Dynamics of TGF-initiated nephron-nephron interactions in normotensive rats and SHR. *Am J Physiol*. 1992;262(6 Pt 2):F980-8.

17. Holstein-Rathlou NH. Synchronization of proximal intratubular pressure oscillations: evidence for interaction between nephrons. *Pflugers Arch Eur J Physiol*. 1987;408(5):438-443.

18. Leyssac PP, Baumbach L. An oscillating intratubular pressure response to alterations in Henle loop flow in the rat kidney. *Acta Physiol Scand.* 1983;117(3):415-419.

19. Holstein-Rathlou NH, Marsh DJ. A dynamic model of the tubuloglomerular feedback mechanism. *Am J Physiol Ren Fluid Electrolyte Physiol*. 1990; 258(5 Pt 2):F1448-59.

20. Marsh DJ, Wexler AS, Brazhe A, Postnov DE, Sosnovtseva OV., Holstein-Rathlou NH. Multinephron dynamics on the renal vascular network. *Am J Physiol Ren Physiol*. 2012;304(1):F88-F102.

21. Källskog O, Marsh DJ. TGF-initiated vascular interactions between adjacent nephrons in the rat kidney. *Am J Physiol*. 1990;259(1 Pt 2):F60-4.

22. Sosnovtseva OV., Pavlov AN, Mosekilde E, Holstein-Rathlou NH, Marsh DJ. Double-wavelet approach to study frequency and amplitude modulation in renal autoregulation. *Phys Rev E - Stat Physics, Plasmas, Fluids, Relat Interdiscip Top.* 2004;70(3):8.

23. Yip KP, Holstein-Rathlou NH, Marsh DJ. Mechanisms of temporal variation in single-nephron blood flow in rats. *Am J Physiol Ren Physiol*. 1993;264(3):F427-F434.

24. Chon KH, Raghavan R, Chen YM, Marsh DJ, Yip KP. Interactions of TGF-dependent and myogenic oscillations in tubular pressure. *Am J Physiol Ren Physiol*. 2004;288(2):F298-F307.

25. Sosnovtseva OV., Pavlov AN, Mosekilde E, Yip KP, Holstein-Rathlou NH, Marsh DJ. Synchronization among mechanisms of renal autoregulation is reduced in hypertensive rats. *Am J Physiol Ren Physiol*. 2007;293(5):F1545-F1555.

26. Sosnovtseva OV., Pavlov AN, Mosekilde E, Holstein-Rathlou NH. Bimodal oscillations in nephron autoregulation. *Phys Rev E - Stat Physics, Plasmas, Fluids, Relat Interdiscip Top.* 2002;66(6 Pt 1):061909.

27. Holstein-Rathlou NH, Sosnovtseva OV., Pavlov AN, Cupples WA, Sorensen CM, Marsh DJ. Nephron blood flow dynamics measured by laser speckle contrast imaging. *Am J Physiol Ren Physiol.* 2010;300(2):5319-29.

28. Arendshorst WJ. Connexin 40 mediates tubuloglomerular feedback paracrine signaling by coupling tubular and vascular cells in the renal juxtaglomerular apparatus. A*m J Physiol Ren Physiol.* 2012;303(10):F1409-F1411.

29. Hanner F, Sorensen CM, Holstein-Rathlou NH, Peti-Peterdi J. Connexins and the kidney. *Am J Physiol Regul Integr Comp Physiol.* 2010;298(5):R1143-55.

30. Just A, Kurtz L, de Wit C, Wagner C, Kurtz A, Arendshorst WJ. Connexin 40 Mediates the Tubuloglomerular Feedback Contribution to Renal Blood Flow Autoregulation. *J Am Soc Nephrol.* 2009;20(7):1577-1585.

31. Machura K, Neubauer B, Müller H, Tauber P, Kurtz A, Kurtz L. Connexin 40 is dispensable for vascular renin cell recruitment but is indispensable for vascular baroreceptor control of renin secretion. *Pflugers Arch Eur J Physiol*. 2015;467(8):1825-34.

32. de Wit C, Roos F, Bolz SS, Pohl U. Lack of vascular connexin 40 is associated with hypertension and irregular arteriolar vasomotion. *Physiol Genomics*. 2003;13(2):169-177.

33. Abed AB, Kavvadas P, Chadjichristos CE. Functional roles of connexins and pannexins in the kidney. *Cell Mol Life Sci*. 2015;72(15):2869-2877.

34. Zhang J, Hill CE. Differential connexin expression in preglomerular and postglomerular vasculature: Accentuation during diabetes. *Kidney Int.* 2005;68(3):1171-1185.

35. Sorensen CM, Holstein-Rathlou NH. Cell-Cell Communication in the Kidney Microcirculation. *Microcirculation*. 2012;19(5):451-460.

36. Kurtz L, Janssen-Bienhold U, Kurtz A, Wagner C. Connexin Expression in Renin-Producing Cells. *J Am Soc Nephrol*. 2008;20(3):506-12.

37. Kurt B, Kurtz L, Sequeira-Lopez ML, et al. Reciprocal expression of connexin 40 and 45 during phenotypical changes in renin-secreting cells. *Am J Physiol Ren Physiol*. 2011;300(3):F743-8.

38. Heberlein KR, Straub AC, Isakson BE. The myoendothelial junction: Breaking through the matrix? *Microcirculation*. 2009;16(4):307-322.

39. Sandow SL, Hill CE. Incidence of myoendothelial gap junctions in the proximal and distal mesenteric arteries of the rat is suggestive of a role in endothelium-derived hyperpolarizing factor-mediated responses. *Circ Res.* 2000;86(3):341-346.

40. Gustafsson F, Holstein-Rathlou NH. Conducted vasomotor responses in arterioles: Characteristics, mechanisms and physiological significance. *Acta Physiol Scand.* 1999;167(1):11-21.

41. Pogoda K, Kameritsch P. Molecular regulation of myoendothelial gap junctions. *Curr Opin Pharmacol.* 2019;45:16-22.

42. Pogoda K, Mannell H, Blodow S, et al. NO augments endothelial reactivity by reducing myoendothelial calcium signal spreading: A novel role for C×37 (Connexin 37) and the protein tyrosine phosphatase SHP-2. *Arterioscler Thromb Vasc Biol*. 2017;37(12):2280-2290.

43. Sorensen CM, Cupples WA. Myoendothelial communication in the renal vasculature and the impact of drugs used clinically to treat hypertension. *Curr Opin Pharmacol*. 2019;45:49-56.

44. Krattinger N, Capponi A, Mazzolai L, et al. Connexin40 regulates renin production and blood pressure. *Kidney Int*. 2007;72(7):814-22.

45. Wagner C, Jobs A, Schweda F, et al. Selective deletion of Connexin 40 in renin-producing cells impairs renal baroreceptor function and is associated with arterial hypertension. *Kidney Int.* 2010. doi:10.1038/ki.2010.257

46. Kurtz L, Schweda F, De Wit C, et al. Lack of connexin 40 causes displacement of renin-producing cells from afferent arterioles to the extraglomerular mesangium. *J Am Soc Nephrol.* 2010;78(8):762-8.

47. Lübkemeier I, Machura K, Kurtz L, et al. The connexin40 A96S mutation causes renin-dependent hypertension. *J Am Soc Nephrol*. 2011;22(6):1031-40.

48. Chen YM, Yip KP, Marsh DJ, Holstein-Rathlou NH. Magnitude of TGF-initiated nephron-nephron interactions is increased in SHR. *Am J Physiol*. 1995;269(2 Pt 2):F198-204.

49. Wagner AJ, Holstein-Rathlou NH, Marsh DJ. Internephron coupling by conducted vasomotor responses in normotensive and spontaneously hypertensive rats. *Am J Physiol.* 1997;272(3 Pt 2):F372-9.

50. Steinhausen M, Endlich K, Nobiling R, Parekh N, Schütt F. Electrically induced vasomotor responses and their propagation in rat renal vessels in vivo. *J Physiol*. 1997;505(2):493-501.

51. Welsh DG, Tran CHT, Hald BO, Sancho M. The Conducted Vasomotor Response: Function, Biophysical Basis, and Pharmacological Control. *Annu Rev Pharmacol Toxicol*. 2018;58(1):391-410.

52. Peti-Peterdi J. Calcium wave of tubuloglomerular feedback. *Am J Physiol Ren Physiol*. 2006;291(2):F473-F480.

53. Ren YL, Carretero OA, Garvin JL. Role of mesangial cells and gap junctions in tubuloglomerular feedback. *Kidney Int.* 2002;62(2):525-531.

54. Hald BO, Welsh DG, Holstein-Rathlou NH, Jacobsen JCB. Gap junctions suppress electrical but not [Ca2+] heterogeneity in resistance arteries. *Biophys J.* 2014;107(10):2467-2476.

55. Diep HK, Vigmond EJ, Segal SS, Welsh DG. Defining electrical communication in skeletal muscle resistance arteries: A computational approach. *J Physiol*. 2005;568(1):267-281.

56. Hald BO, Jacobsen JCB, Sandow SL, Holstein-Rathlou NH, Welsh DG. Less is more: Minimal expression of myoendothelial gap junctions optimizes cell-cell communication in virtual arterioles. *J Physiol*. 2014;592(15):3243-3255.

57. Little TL, Xia J, Duling BR. Dye tracers define differential endothelial and smooth muscle coupling patterns within the arteriolar wall. *Circ Res*. 1995;76(3):498-504.

58. Rhodin JAG. The ultrastructure of mammalian arterioles and precapillary sphincters. *J Ultrasructure Res*. 1967;18(1):181-223.

59. Taugner R, Kirchheim H, Forssmann WG. Myoendothelial contacts in glomerular arterioles and in renal interlobular arteries of rat, mouse and Tupaia belangeri. *Cell Tissue Res.* 1984;235(2):319-25.

60. Ushiyama A, Kataoka H, Iijima T. Glycocalyx and its involvement in clinical pathophysiologies. *J Intensive Care*. 2016;8;4(1):59.

61. Hald BO, Welsh DG, Holstein-Rathlou NH, Jacobsen JCB. Origins of variation in conducted vasomotor responses. *Pflugers Arch Eur J Physiol*. 2015;467(10):2055-2067.

62. Marsh DJ, Toma I, Sosnovtseva OV., Peti-Peterdi J, Holstein-Rathlou NH. Electrotonic vascular signal conduction and nephron synchronization. *Am J Physiol Ren Physiol.* 2008;296(4):F751-F761.

63. Laugesen JL, Sosnovtseva OV., Mosekilde E, Holstein-Rathlou NH, Marsh DJ. Coupling-induced complexity in nephron models of renal blood flow regulation. *Am J Physiol Regul Integr Comp Physiol.* 2010;298(4):R997-R1006.

64. Scully CG, Mitrou N, Braam B, Cupples WA, Chon KH. Segmentation of renal perfusion signals from laser speckle imaging into clusters with phase synchronized dynamics. *IEEE Trans Biomed Eng.* 2014;61(7):1989-1997.

65. Meunier D, Lambiotte R, Bullmore ET. Modular and hierarchically modular organization of brain networks. *Front Neurosci*. 2010;4:(200).

66. Sales-Pardo M. The importance of being modular. *Science*. 2017;357(6347):128-129.

67. Hilgetag CC, Goulas A. Is the brain really a small-world network? *Brain Struct Funct.* 2016;221:(4):2361-2366.

68. Legrand M, Bezemer R, Kandil A, Demirci C, Payen D, Ince C. The role of renal hypoperfusion in development of renal microcirculatory dysfunction in endotoxemic rats. *Intensive Care Med.* 2011;37(9):1534-42.

69. Konukoglu D, Uzun H. Endothelial dysfunction and hypertension. *Advances in Experimental Medicine and Biology.* 2016;965:511-540.

70. Mitrou N, Morrison S, Mousavi P, Braam B, Cupples WA. Transient impairment of dynamic renal autoregulation in early diabetes mellitus in rats. *Am J Physiol Regul Integr Comp Physiol.* 2015;309(8):R892-R901.

71. Clark DP, Badea CT. Micro-CT of rodents: State-of-the-art and future perspectives. *Phys Medica.* 2014;30(6):619-34.

72. Cupples WA. At last! quantitative cortical vascular anatomy. *Am J Physiol Ren Physiol.* 2018;314(5):F928-F929.

73. Lorenz JN. Micropuncture of the Kidney: A primer on techniques. *Compr Physiol.* 2012;2(1):621-37.

74. Dunn AK. Laser speckle contrast imaging of cerebral blood flow. *Ann Biomed Eng.* 2012;40(2):367-77.

75. Venugopal K, Unni SN, Bach A, Conzen C, Lindauer U. Assessment of cerebral hemodynamics during neurosurgical procedures using laser speckle image analysis. *J Biophotonics.* 2019;12(9):e201800408.

76. Rauh A, Henn D, Nagel SS, Bigdeli AK, Kneser U, Hirche C. Continuous Video-Rate Laser Speckle Imaging for Intra- and Postoperative Cutaneous Perfusion Imaging of Free Flaps. *J Reconstr Microsurg.* 2019;35(7):489-498.

77. Neganova AY, Postnov DD, Sosnovtseva OV, Jacobsen JCB. Rat retinal vasomotion assessed by laser speckle imaging. *PLoS One.* 2017;12(3):e0173805.

78. Postnov DD, Tang J, Erdener SE, Kılıç K, Boas DA. Dynamic Laser Speckle Imaging. *bioRxiv*. 2019;2:626515.

79. Vaz PG, Humeau-Heurtier A, Figueiras E, Correia C, Cardoso J. Laser Speckle Imaging to Monitor Microvascular Blood Flow: A Review. *IEEE Rev Biomed Eng*. 2016;9:106-20.

80. Allen J, Howell K. Microvascular imaging: Techniques and opportunities for clinical physiological measurements. *Physiol Meas.* 2014;35(7):R91-R141.

81. Brazhe AR, Marsh DJ, Holstein-Rathlou NH, Sosnovtseva OV. Synchronized renal blood flow dynamics mapped with wavelet analysis of laser speckle flowmetry data. *PLoS One.* 2014;9(9):e105879.

82. O'Doherty J, McNamara P, Clancy NT, Enfield JG, Leahy MJ. Comparison of instruments for investigation of microcirculatory blood flow and red blood cell concentration. *J Biomed Opt.* 2009;14(3):034025.

83. Scully CG, Mitrou N, Braam B, Cupples WA, Chon KH. Detecting physiological systems with laser speckle perfusion imaging of the renal cortex. *Am J Physiol Regul Integr Comp Physiol*. 2013;304(11):R929-R939.

84. Detre JA, Wang J. Technical aspects and utility of fMRI using BOLD and ASL. *Clin Neurophysiol.* 2002; 113(5):621-34.

85. Hernandez-Garcia L, Lahiri A, Schollenberger J. Recent progress in ASL. *Neuroimage.* 2019;187:3-16.

86. Chen F, Li S, Sun D. Methods of blood oxygen level-dependent magnetic resonance imaging analysis for evaluating renal oxygenation. *Kidney Blood Press Res.* 2018;43(2):378-388.

87. Schmithorst VJ, Hernandez-Garcia L, Vannest J, Rajagopal A, Lee G, Holland SK. Optimized simultaneous ASL and BOLD functional imaging of the whole brain. *J Magn Reson Imaging*. 2014;39(5):1104-17.

88. Prasad PV. Evaluation of intra-renal oxygenation by BOLD MRI. *Nephron - Clin Pract.* 2006;103(2):c58-65.

89. Bryden J, Funk S, Geard N, Bullock S, Jansen VAA. Stability in flux: Community structure in dynamic networks. *J R Soc Interface*. 2011;8(60):1031-40

90. Scully CG, Mitrou N, Braam B, Cupples WA, Chon KH. Detecting physiological systems with laser speckle perfusion imaging of the renal cortex. *Am J Physiol Regul Integr Comp Physiol*. 2013;304(11):R929-R939.

91. Huang X, Dorhout Mees E, Vos P, Hamza S, Braam B. Everything we always wanted to know about furosemide but were afraid to ask. *Am J Physiol Ren Physiol.* 2016;310(10):F958-71.

92. Araujo M, Welch WJ, Zhou X, et al. Inhibition of ROMK blocks macula densa tubuloglomerular feedback yet causes renal vasoconstriction in anesthetized rats. *Am J Physiol Ren Physiol*. 2017;312(6):F1120-F1127.

93. Pedersen M, Vajda Z, Stødkilde-Jørgensen H, Nielsen S, Frøkiær J. Furosemide increases water content in renal tissue. *Am J Physiol Ren Physiol*. 2007;292(5):F1645-51.

94. Dobrowolski L, Badzynska B, Sadowski J. Differential effect of frusemide on renal medullary and cortical blood flow in the anaesthetised rat. *Exp Physiol*. 2000;85(6):783-9.

95. Oppermann M, Hansen PB, Castrop H, Schnermann J. Vasodilatation of afferent arterioles and paradoxical increase of renal vascular resistance by furosemide in mice. *Am J Physiol Ren Physiol.* 2007;293(1):F279-87.

96. Janssen BJA, Eerdmans PHA, Smits JFM. Mechanisms of renal vasoconstriction following furosemide in conscious rats. *Naunyn Schmiedebergs Arch Pharmacol*. 1994;349(5):528-37.

97. Araujo M, Solis G, Welch WJ, Wilcox CS. Renal nerve deafferentation attenuates the fall in GFR during intravenous infusion of furosemide in anesthetized rats. *Kidney Blood Press Res*. 2020;45(1):70-83.

98. Castrop H, Lorenz JN, Hansen PB, et al. Contribution of the basolateral isoform of the Na-K-2Cl- cotransporter (NKCC1/BSC2) to renin secretion. *Am J Physiol Ren Physiol.* 2005;289(6):F1185-92.

99. Tucker BJ, Blantz RC. Effect of furosemide administration on glomerular and tubular dynamics in the rat. *Kidney Int*. 1984;26(2):112-21.

100. Woods LL, DeYoung DR, Smith BE. Regulation of renal hemodynamics after protein feeding: Effects of loop diuretics. *Am J Physiol Ren Physiol.* 1991;261(5 Pt 2):F815-23.

101. Nishiyama A, Majid DSA, Walker M, Miyatake A, Navar LG. Renal interstitial ATP responses to changes in arterial pressure during alterations in tubuloglomerular feedback activity. *Hypertension*. 2001;37(2 Pt 2):753-9.

102. Takakura S, Takasu T. Acute and direct effects of sodium-glucose cotransporter 2 inhibition on glomerular filtration rate in spontaneously diabetic torii fatty rats. *Biol Pharm Bull.* 2019;42(10):1707-1712.

103. Lambers Heerspink HJ, De Zeeuw D, Wie L, Leslie B, List J. Dapagliflozin a glucose-regulating drug with diuretic properties in subjects with type 2 diabetes. *Diabetes Obes Metab.* 2013;15(9):853-62.

104. Bidani AK, Schwartz MM, Lewis EJ. Renal autoregulation and vulnerability to hypertensive injury in remnant kidney. *Am J Physiol Ren Physiol*. 1987;252(6):F1003-F1010.

105. Griffin KA, Bidani AK. Hypertensive renal damage: Insights from animal models and clinical relevance. *Curr Hypertens Rep*. 2004;6(2):145-153.

106. Rosenberg ME, Smith LJ, Correa-Rotter R, Hostetter TH. The paradox of the renin-angiotensin system in chronic renal disease. *Kidney Int*. 1994;45(2):403-10.

107. Anderson S, Meyer TW, Rennke HG, Brenner BM. Control of glomerular hypertension limits glomerular injury in rats with reduced renal mass. *J Clin Invest*. 1985;76(2):612-9.

108. Wilke WL, Persson AEG. Captopril and tubuloglomerular feedback in remnant kidneys of prehypertensive rats. *J Am Soc Nephrol*. 1992;3(1):73-9.

109. Gilbert RE, Wu LL, Kelly DJ, et al. Pathological expression of renin and angiotensin II in the renal tubule after subtotal nephrectomy: Implications for the pathogenesis of tubulointerstitial fibrosis. *Am J Pathol*. 1999;155(2):429-40.

110. Griffin KA, Bidani AK. Progression of renal disease: renoprotective specificity of renin-angiotensin system blockade. *Clin J Am Soc Nephrol*. 2006;1(5):1054-65.

111. Brenner BM. Hemodynamically mediated glomerular injury and the progressive nature of kidney disease. *Kidney Int*. 1983;23(4):647-55.

112. Singh P, Thomson SC. Salt sensitivity of tubuloglomerular feedback in the early remnant kidney. *Am J Physiol Ren Physiol.* 2014;306(2):F172-80.

113. Salmond R, Seney FD. Reset tubuloglomerular feedback permits and sustains glomerular hyperfunction after extensive renal ablation. *Am J Physiol Ren Physiol*. 1991;260(3 Pt 2):F395-401.

114. Thomson SC, Vallon V, Blantz RC. Resetting protects efficiency of tubuloglomerular feedback. *Kidney Int Suppl.* 1998;54(67):65-70.

115. Braam B, Mitchell KD, Koomans HA, Gabriel Navar L. Relevance of the tubuloglomerular feedback mechanism in pathophysiology. *J Am Soc Nephrol.* 1993; 4(6):1257-74.

116. Thomson SC. Nitric oxide mediates anomalous tubuloglomerular feedback in rats fed high- NaCl diet after subtotal nephrectomy. *Am J Physiol Ren Physiol*. 2019;316(2):F223-F230.

117. Singh P, Deng A, Blantz RC, Thomson SC. Unexpected effect of angiotensin AT1 receptor blockade on tubuloglomerular feedback in early subtotal nephrectomy. *Am J Physiol Ren Physiol.* 2009;296(5):F1158-65.

118. Perez-Gomez MV, Bartsch LA, Castillo-Rodriguez E, et al. Clarifying the concept of chronic kidney disease for non-nephrologists. *Clin Kidney J.* 2018;12(2):258-261.

119. Bidani AK, Griffin KA, Williamson G, Wang X, Loutzenhiser R. Protective Importance of the Myogenic Response in the Renal Circulation. *Hypertension*. 2009;54(2):393-398.

120. Thomson SC, Rieg T, Miracle C, et al. Acute and chronic effects of SGLT2 blockade on glomerular and tubular function in the early diabetic rat. *Am J Physiol Regul Integr Comp Physiol*. 2012;302(1):R75-83.

121. Komoroski B, Vachharajani N, Boulton D, et al. Dapagliflozin, a novel SGLT2 inhibitor, induces dose-dependent glucosuria in healthy subjects. *Clin Pharmacol Ther.* 2009;85(5):520-6.

122. Oppermann M, Qin Y, Lai EY, et al. Enhanced tubuloglomerular feedback in mice with vascular overexpression of A1 adenosine receptors. *Am J Physiol Ren Physiol*. 2009;297(5):F1256-64.

123. Marsh DJ, Postnov DD, Sosnovtseva OV., Holstein-Rathlou NH. The nephron-arterial network and its interactions. *Am J Physiol Ren Physiol*. 2019;316(5):F769-F784.

124. Wang X, Loutzenhiser RD, Cupples WA. Frequency modulation of renal myogenic autoregulation by perfusion pressure. *Am J Physiol Regul Integr Comp Physiol.* 2007;293(3):R1199-204.

125. Cole WC, Welsh DG. Role of myosin light chain kinase and myosin light chain phosphatase in the resistance arterial myogenic response to intravascular pressure. *Arch Biochem Biophys.* 2011;510(2):160-73.

126. Holstein-Rathlou NH, Marsh DJ. Oscillations of tubular pressure, flow, and distal chloride concentration in rats. *Am J Physiol.* 1989;256(6 Pt 2):F1007-14.

127. Fine LG, Orphanides C, Norman JT. Progressive renal disease: The chronic hypoxia hypothesis. *Kidney Int, Supplement*. 1998;65:S74-8.

128. Fang JS, Angelov SN, Simon AM, Burt JM. Compromised regulation of tissue perfusion and arteriogenesis limit, in an AT1R-independent fashion, recovery of ischemic tissue in Cx40-/- mice. *Am J Physiol Heart Circ Physiol*. 2013;304(6):H816-27.

129. O'Neill J, Fasching A, Pihl L, Patinha D, Franzén S, Palm F. Acute SGLT inhibition normalizes O2 tension in the renal cortex but causes hypoxia in the renal medulla in anaesthetized control and diabetic rats. *Am J Physiol Ren Physiol*. 2015;309(3):F227-34.

130. Perkovic V, Jardine MJ, Neal B, et al. Canagliflozin and renal outcomes in type 2 diabetes and nephropathy. *N Engl J Med.* 2019;380(24):2295-2306.

131. Mahaffey KW, Jardine MJ, Bompoint S, et al. Canagliflozin and Cardiovascular and Renal Outcomes in Type 2 Diabetes Mellitus and Chronic Kidney Disease in Primary and Secondary Cardiovascular Prevention Groups: Results from the Randomized CREDENCE Trial. *Circulation*. 2019;140(9):739-750.

132. Wanner C, Inzucchi SE, Lachin JM, et al. Empagliflozin and progression of kidney disease in type 2 diabetes. *N Engl J Med.* 2016;375(4):323-34.

133. Layton AT, Vallon V, Edwards A. Predicted consequences of diabetes and SGLT inhibition on transport and oxygen consumption along a rat nephron. *Am J Physiol Ren Physiol*. 2016;310(11):F1269-83.

134. Zhang Y, Thai K, Kepecs DM, Gilbert RE. Sodium-glucose linked cotransporter-2 inhibition does not attenuate disease progression in the rat remnant kidney model of chronic kidney disease. *PLoS One*. 2016;11(1):1-17.

135. Bowman RH. Renal secretion of [32S]furosemide and its depression by albumin binding. *Am J Physiol*. 1975;229(1):93-8.

136. Boles Ponto LL, Schoenwald RD. Furosemide (Frusemide) A Pharmacokinetic/Pharmacodynamic Review (Part I). *Clin Pharmacokinet.* 1990;18(5):381-408.